Silesian University of Technology
Faculty of Civil Engineering
Department of Mechanics and Bridges

DOCTORAL DISSERTATION

Bridge health monitoring using automated FE model updating, signal processing, and machine learning

NGUYEN CONG DUC

Dissertation supervisor: Marek Salamak
Full Professor, Ph.D., D.Sc. Eng.
Silesian University of Technology, Gliwice
Faculty of Civil Engineering
Department of Mechanics and Bridges

Dissertation supervisor: Andrzej Katunin
Associate Professor, Ph.D., D.Sc. Eng.
Silesian University of Technology, Gliwice
Faculty of Mechanical Engineering
Department of Fundamentals of Machinery Design

Gliwice, May 2024

Acknowledgements

I would like to thank my supervisors: Prof. Marek Salamak and Prof. Andrzej Katunin for their excellent guidance, encouragement, and patience throughout these studies.

I would like to express my deepest thanks and sincere appreciation to Dr. Grzegorz Poprawa for sharing and supporting field experimental data sets from the long-term vibration-based structural health monitoring system of Dębica railway steel arch bridge in Poland, and for his assistance and contributions in my conferences and papers as co-author.

I also would like to thank all the technicians in SUT's Lab and CADmost for their industrial projects of some bridge diagnostic load tests in Poland. I wish to extend my thanks to the whole "family" of the Department of Mechanics and Bridges (RB5), for having made my degree research journey.

I would like to thank accredited national laboratory LASXD-162 of the MienTrung University of Civil Engineering managed by the Ministry of Construction of Vietnam for providing data sets from field diagnostic load testing of some bridges, where I have been working as a lecturer and field engineer since 2010.

My gratitude is extended to Doctoral School of Silesian University of Technology; NAWA-Polish Government under PPN/FRC/2020/1/00034 for Polish language course at Cracow University of Technology and BPN/FRC/2021/1/00048 for the doctoral program at Silesian University of Technology; as part of bilateral agreements and cooperation with Vietnamese Government for more financial support given to this work under 3416/QĐ-BGDĐT 04/11/2020; 4534/QĐ-BGDĐT 30/11/2021; Nr145/21-NG-LHS 21/6/2021; MienTrung University of Civil Engineering for salary support of lecturer resource training program given to my study abroad.

Finally, a special thanks is extended to my wife, Nguyen Thi Ai Nuong, whose patience has remained steadfast for four years of my research work. Therefore, this Ph.D. thesis is dedicated to her; to my children: Nguyen Minh Phu and Nguyen Minh Nhat, who received less attention and love than they deserve; to my wife's mother Le Thi Xuan and father Nguyen Ngoc Anh, who have been taking care of my two sons; particularly to my mother Nguyen Thi Hoang and father Nguyen Van Hong, who are Vietnamese rice farmers with no scientific background but have always encouraged me, as well as my young sister and brother.

Summary

Bridge health monitoring plays an important role in ensuring the safety, reliability, and longevity of the road and railway bridges. This thesis investigates bridge health monitoring using automated FE model updating, signal processing, and machine learning, which can be categorized as the following main points.

Intelligent data processing algorithms based on ANN and ANFIS are proposed to predict the dynamic behavior of Dębica railway steel arch bridge produced from dynamic responses of steel hangers during the passage of trains. Field data sets were collected from the vibration-based SHM system of the hangers and bridge deck over a nine-month period from December 2019 to September 2020. The input variables of the ANN and ANFIS models consist of RMS values of vibration signals installed on hangers, and the output is RMS values of dynamic responses on each of the two bridge spans. The optimization of the ANN architecture based on the genetic algorithm is implemented to determine the number of neurons in the hidden layers of the ANN regression models. Optimized ANN prediction models have been shown to outperform ANFIS regression models among the six proposed strategies.

Data-driven applications of wavelet transforms, orbit-shaped analysis and CNN using GoogLeNet are proposed for Dębica railway bridge health monitoring in Poland. Training and validation data sets are the dynamic behavior of the bridge deck recorded through an IEPE vibration sensor with a sampling frequency of 100 Hz from vibration-based SHM system during a nine-month period. Utilizing Morse, Morlet, and Bump wavelet, the vibration signal scalogram images are produced in the time-frequency domain as the input for CNN classification models, while the output is to predict health states based on the experimental tension force of eight hangers using label thresholds developed by calibrated finite element model. Moreover, the vibration-based orbit-shaped image patterns, acquired through a bidirectional sensor on each hanger are processed with CNN classification models for automated hanger health diagnostic.

Diagnostic load testing refers to the use of the historical measured responses of the structure in field data to better understand its dynamic and static structural behaviors. The calibration of the full-scale FE model of the existing bridges plays an important role, in which the representative FE model of the actual structure is determined from the optimization procedures. The optimization variables are applied, including the cross-sectional and material properties calibrated through the GA and PSO methods in the MATLAB software, which interfaces with the FE modeling in the scripting of the SOFISTIK TEDDY and ANSYS APDL softwares automatically using static and dynamic responses in the field tests. The final updated FE modeling is used to apply truck or train load configurations according to bridge design standards, specifications, or codes, which can predict the load limits and overloads of the existing bridge structure more accurately and reliably. These proposed approaches can be applied to the RC bridge, steel-concrete composite bridge as well as the railway steel arch bridge.

The developed approaches of the bridge FE model calibration using field load testing and monitoring can equip the engineer with a useful tool to make evaluation decisions that require less time and improve its cost effectiveness. The SHM system of the complex heavy bridges would be tested in a more reliable way when the updated FE models are applied. The machine learning algorithms integrated into the data-driven vibration-based SHM system are useful solutions to analyze intelligent data processing as well as to predict the structural behavior under the different load events. It can keep a “remote eye” on bridge structures with the smart alarm system.

Contents

List of Figures

List of Tables

List of Nomenclature and Abbreviation

AASHTO	American Association of State Highway and Transportation Officials
AI	Artificial Intelligence
ANFIS	Adaptive Neuro-Fuzzy Inference Systems
ANN	Artificial Neural Networks
BDI	Bridge Diagnostics, Inc. in the USA
BHM	Bridge Health Monitoring
BIM	Building Information Modeling
BrIM	Bridge Information Modeling
CAD	Computer-Aided Design
CAE	Computer-Aided Engineering
CNN	Convolutional Neural Network
DAQ	Data Acquisition
DL	Deep Learning
DNN	Deep Neural Networks
FE	Finite Element
FEA	Finite Element Analysis
FEM	Finite Element Method
FFT	Fast Fourier transform
GA	Genetic Algorithm

IoT	Internet of Things
LVDT	Linear Variable Differential Transformer
MAE	Mean Absolute Error
MAPE	Mean Absolute Percentage Error
MEMS	Micro-electromechanical Systems
ML	Machine Learning
NN	Neural Network
NSE	Nash-Sutcliffe efficiency
OMA	Operational Modal Analysis
PCA	Principal Component Analysis
PSO	Particle Swarm Optimization
QML	Quantum Machine Learning
RF	Random Forest
RMS	Root Mean Square
RMSE	Root Mean Squared Error
SHM	Structural Health Monitoring
SSI	Stochastic Subspace Identification
STS-WiFi	Wireless Structural Testing System
SVM	Support Vector Machines
XGBoost	eXtreme Gradient Boosting

Chapter 1

Introduction

1.1 Overview

The transport infrastructure system is the lifeblood of every country. The construction, maintenance and management of transport networks are beneficial for economic, social, political and military purposes. Sustainable transportation improves connectivity between local regions, transport modes, and countries. It can be seen that well-managed transportation facilitates various activities. On the other hand, when the transportation is not well developed, everything is delayed. Infrastructure asset operators, managers and owners have not been well functioning the cost-effective, real-time reliable and onsite safe solutions for intelligent civil infrastructure data processing and management to enhance smarter decision-making information.

SHM systems with embedded advanced signal processing algorithms is one of the comprehensive and systematic ways in tracking the health condition of different civil structures including: aerospace, offshore oil platforms, docks, rotating machinery, wind turbines, tunnels, bridges, buildings, railways, hydroelectric dams, pavements, deep foundations, geotechnical construction, etc. There are many research challenges and potential applications of SHM technologies for the civil sectors, specifically complex and heavy bridges during traffic loading events, environmental conditions, flood hazards, earthquakes, etc.

Bridge health monitoring is combined with machine learning-based approaches to predict the health conditions of structural members under various load events and wind excitation. The use of FE model updating will be useful for practical and industrial data-driven SHM, because FE modeling is a standardized procedure for designing the bridge structure, when calibrating the measured and computed responses to reproduce data used in machine learning-assisted classification and regression models.

1.2 Motivations for undertaking research

The motivations for engaging in research studies on bridge health monitoring approaches can be either one or more of the following reasons:

- Why the structural diagnostic load test need to be performed? Why the SHM of the existing heavy bridge is needed?
- There are many structural health monitoring systems on the market. What is the right technology for bridge monitoring?
- There are so many structural members and so many sensors. Why collect structural parameters?
- How to reduce the duration and costs of monitoring maintaining high detectability level of possible events?
- What are the best technologies and algorithms for field bridge data processing and management? How to acquire and process data effectively?

1.3 Aim and scope of the current work

The performed research studies within this thesis allowed providing some answers to above questions and formulate the aims of the study on their basis. The objective of the research topic is to propose the automated FE model updating, signal processing, and machine learning approaches that can be used for bridge health monitoring. The topic covers issues related to automated bridge FE model calibration using field testing, advanced signal processing for vibration signals collected from a long-term vibration-based SHM system of railway steel arch bridge, and machine learning techniques to predict railway bridge health conditions.

The bridge diagnostic load test consists of the load evaluation and the load test (or proof-load test). The purpose is to use field data to calibrate the FE model for load rating. The final calibrated FE model is proposed to integrate into the SHM system of the existing bridge.

Bridge SHM is used to track changes over time under the various load events and weather conditions. The vibration-based SHM system installed on the railway steel arch bridge is to record the dynamic behavior of the hangers and the spans under train events. The vibration measurement is useful to analyze the experimental natural frequencies of hangers, and then determine tension forces and stresses. The objective of the development of the the long-term SHM system is proposed to monitor on-line and remote alarms.

The structural parameters collected in the field tests are the strains, deflections and natural frequencies of the real bridges. These measured parameters can be used for the FE model updating to calibrate the material and stiffness properties. The right technology for bridge testing and monitoring is the innovative solution which makes it possible to connect the experimental parameters with the current bridge design guide specifications and standards.

The duration and costs of bridge testing and monitoring depend more on data processing and management than the use of many sensors in the field. Sensors can be reused in the various bridge structures, while the data processing needs and requirements may vary depending on the behavior of each bridge under load events.

The data processing approaches comprise FFT algorithms, wavelet transforms and machine learning, including deep learning. The advanced signal processing technologies are implemented for the vibration signals recorded from the SHM system to analyze the field data patterns as well as to predict the structural behavior under the different load events.

The primary contributions of the study can be summarized as the following main issues:

- Automated FE model calibrations were proposed to update the stiffness and material properties of bridge structures using measured static strains and natural frequencies. Case studies consist of the highway bridges in Vietnam to demonstrate the applicability and effectiveness of the proposed FE model updating algorithms.

- Machine learning-assisted regression models were performed to predict the dynamic behavior of the railway bridge span under various train events. Data sets used in prediction models that were collected from the vibration-based SHM system of the Dębica railway steel arch bridge in Poland over a period of nine months from December 2019 to September 2020.

- GoogLeNet CNN classification models were developed to predict the hanger health conditions of the existing railway bridge using wavelet-based and orbit-shaped signal images.

1.4 Outline of the dissertation

The dissertation is divided into 7 chapters, which present an overview on the current state-of-the-art in the topic of BHM, measurement setups, and developed procedures for processing the acquired measurement signals. Finally, real-world examples are described in detail to demonstrate the performance of the developed procedures. The chapters of this thesis are organized as follows:

Chapter 2 discusses the current status and development trends of bridge health monitoring systems. The latest trends and growing needs in bridge health monitoring are reviewed. Market demands and needs for bridge health monitoring in Vietnam and Poland are reported. In this chapter, advanced signal processing techniques in bridge health monitoring are discussed. The framework of digital twins for data-driven bridge health monitoring is proposed.

Chapter 3 describes the data acquisition instruments and advanced signal processing. It presents the bridge diagnostic load testing apparatus. The chapter also emphasizes advanced signal processing approaches including wavelet transforms and machine learning algorithms.

Chapter 4 focuses on the railway bridge health monitoring using machine learning. In this thesis, the object of the research is the Dębica railway steel arch bridge. Herein, the SHM system used for Dębica bridge is described. The optimized ANN and ANFIS regression models are developed for the vibration-based SHM of Dębica railway steel arch bridge in Poland.

Chapter 5 presents the railway bridge health diagnosis using wavelet analysis and deep learning. Data collections from the vibration-based SHM system of the existing Dębica railway bridge are used for developing deep learning-based classification models. GoogLeNet CNN classification models are performed to predict structural health conditions using wavelet scalograms achieved from vibration signals from the tested bridge. Orbit-shaped CNN classification models are performed to assess hanger health status.

Chapter 6 describes the bridge diagnostic load ratings using automated FE model updating. This approach is proposed to apply for the two road bridges in Vietnam. The calibrations of the FE models are conducted for two case studies, namely, reinforced concrete and steel-concrete composite bridges.

Chapter 7 summarizing this thesis and makes recommendations for further studies.

Chapter 2

Current status and development trends of bridge health monitoring systems

2.1 Introduction

This chapter provides an overview of the current status and development trends of state-of-the-art bridge health monitoring systems. In Poland and Vietnam, where the civil infrastructure has developed rapidly, the demands and needs of the SHM market are expected to grow significantly. All-in-one comprehensive solutions for intelligent data processing and management of data-driven SHM systems are to implement machine learning techniques designed with the smart alert system in real time to ensure the safety, reliability, and integrity of bridge structures during major load events, natural hazards, and weather change risks. Bridge SHM data management is not only intelligent data processing, but also integrating bridge information management, referred to as virtual digital twins. Furthermore, national guidelines and regulations for SHM of civil structures and bridges could be continuously updated to meet international standards, codes, and specifications.

2.2 A review of the latest trends and growing needs in bridge health monitoring

Bridge structural health monitoring, which has attracted significant attention in recent decades, plays an important role in transportation infrastructure networks to ensure integrity and safety operation, identify potential structural risks to prevent accidents, and allow proactive decision-making in asset management and maintenance schedules [1], [2].

The advantages of the long-term (live-load) SHM system are to keep a “remote eye” on troubled structures with an alarm feature; to track changes or “dead load effects” over time such as crack growth or tilting (rotations) of piers; to capture truck passages at highway speed; to understand fatigue stress magnitudes and cycles; to use a smaller number of sensors [3], [4], [5]. The objectives of the diagnostic bridge test are to understand the distribution of the live load; use data to calibrate the simplified finite element model under a truck of known load to cross the bridge slowly; predict the stresses induced by the permit or overloaded vehicles through the final calibrated model [6], [7].

There are many technologies for SHM systems of existing bridges depending on the types of structure sensors, intelligent data processing and management, communications and intelligent early warning system [8], [9]. Furthermore, the key application of the vibration-based SHM has been designed to record dynamic responses of bridges analyzed using OMA techniques, SSI methods, FFT algorithms, FE model updating, which associated benefits can provide useful information to better understand the measured live-load behavior of structure [10], [11], [12], [13], [14]. Bridge diagnostic load testing is used to measure actual responses of the structure against known loads so that realistic calibrated FE models can be developed for critical load ratings and service load limits [15], [16]; while bridge structural health monitoring automatically records field data during days, months, and years to keep a remote eye focusing on potential health problems of critical structure for the smart alert system, as well as to upload multiple field data sources in real time to validate and adjust digital twin models for the operation, safety, and maintenance of bridge cost-effectively [17], [18], [19], [20], [21], [22]. Bridge data management is one of the most crucial and complex aspects of smart SHM solutions.

Although these research studies have demonstrated the effectiveness of the FE model calibration for bridges, they were also limited by the need for large data sets and complex railway bridge structures. The limitation is that FE simulation software, sensors and data acquisition systems were not originally designed for updating FE model. Furthermore, the integration of advanced signal processing into the SHM system might be limited. The users of industrial SHM applications rely on the hardware and software configurations provided by the manufacturer. The communication and transmission of sensor data between instruments, hardware, SHM systems, and IoT devices may vary among different manufacturers for bridge data management. Therefore, it is essential to explore additional solutions for signal processing and the integration of machine learning algorithms into the SHM system.

2.3 Market demands and needs for bridge health monitoring in Poland and Vietnam

The economic benefits and challenges of studies on SHM for bridges using automated FE model updating, vibration signal processing, and machine learning algorithms include: the demands of bridge diagnostic load testing in both Poland and Vietnam; the markets of long-term SHM in Poland and Vietnam; the potential opportunities for investments in advanced signal processing of big data through the use of AI and machine learning algorithms in the field.

In Poland, the development and investment in transport infrastructure have increased significantly in recent years. In 2022, 19.394 thousand km of railway lines were operated in Poland, 54.0% of which were single-track lines [23]. In 2022, there were more than 317.5 thousand km of hard surfaced public roads in Poland, consisting of communal roads: 48.2% and district roads: 36.4%; Voivodship roads: 9.3% of public roads; national roads: 6.1%; Motorways and expressways: 1.5% of public roads [23]. It can be seen that bridge testing is essential when considering the existing well-defined and established Polish standards, such as: PN–S–10040:1999 for reinforced and prestressed bridges; PN-89/S-10050 for steel bridges [24]. Numerous studies have discussed the advantages and effectiveness of implementing the SHM systems for bridges in Poland [25], [26], [27], [28], [29], [30], [31], [32], [33], [34], [35]. SHM systems have been installed for some bridges in Poland, as shown in Figure 2.1.

Vietnam has 570.448 thousand km of roads, of which national highways 24.136 thousand km; expressways 816 km; provincial roads 25.741 thousand km; district roads 58.347 thousand km; urban roads 26.953 thousand km; commune roads 144.670 thousand km; village roads 181.188 thousand km; and inner field roads 108.597 thousand km [36]. Urban railway metro systems were building and developing in Ha Noi capital and Ho Chi Minh city (before 1975 year: Sai Gon city) [37]. A feasibility study of the large north-south high-speed railway project (200-350 km/h trains) is currently underway to replace the existing century-old north-south single track railway system [37]. SHM systems have been installed on large complex bridges in Vietnam, for example: My Thuan cable-stayed bridge [38], [39]; Sai Gon bridge [40], [41], Phu My cable-stayed bridge [42], [43], [43]; Bai Chay bridge [39]; three bridges: Thuan Phuoc, Dragon and Tran Thi Ly bridge [44]. SHM systems have been installed for bridges in Vietnam, as shown in Figure 2.2

Figure 2.1: SHM systems for bridges in Poland informed by Dr. Grzegorz Poprawa (images of bridges collected from Google Maps).

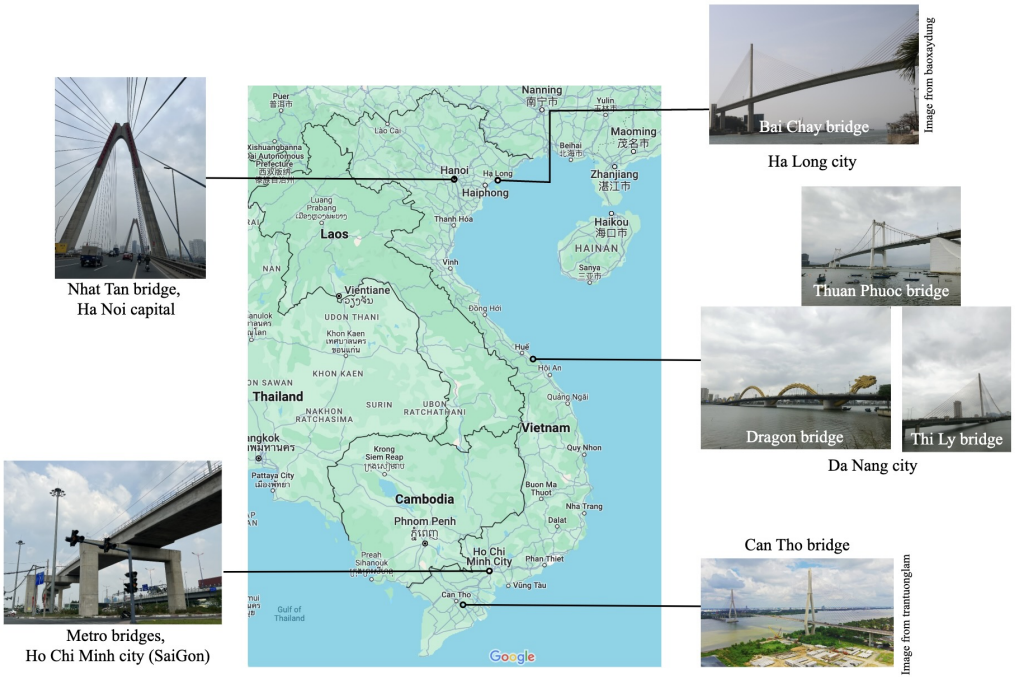

Figure 2.2: SHM systems for bridges in Vietnam informed by the Bridge Diagnostics Inc in the USA and the Scientific Technical Supplies limited company in Vietnam.

2.4 A review of advanced signal processing and machine learning for SHM

The future of AI in SHM applications has received considerable attention for intelligent data processing and management of various civil infrastructure sectors such as: bridges, railways, pavements, tunnels, buildings, hydraulic structures, foundations, and construction [45], [46]. One of the major subfields of AI is machine learning in which artificial neural networks and deep learning have presented challenges to integrate intelligent data processing and automation into SHM systems of infrastructure [47]. The important benefits of SHM tasks are for the evaluation, assessment, and monitoring of civil structures [48] for which machine learning-based SHM technologies of existing bridges have recently been developed [49]. Therefore, the application of machine learning-based algorithms for data sets of the SHM system equipped with various types of sensors is a useful solution that could obtain valuable insights into historical responses and predict the health status of the structure. As discussed studies, intelligent data processing is one of important requirements for the emerging technology implemented in machine learning approaches. The benefits of vibration measurement of structures related to all of the above topics could bring new opportunities for researchers who are interested in the applications of AI and machine learning for bridge structures, especially in a smart vibration-enhanced SHM system for bridge data management.

In the context of bridge health monitoring, operational modal analysis techniques using only accelerometers with no hammer or shaker excitation, were proposed for bridges to determine modal parameters (natural frequencies, damping ratios and mode shapes) of structures to be used for automatic FE model updating [50], [51], [52], [53], [54]. Cable (or hanger) force testing and analysis were performed for cable-stayed bridges or arch bridge structures using vibration frequencies based on the fundamental principle of the Taut cable vibration method [55], [56].

Furthermore, data-driven SHM methods with neuro-fuzzy classifier can be used to monitor bridge health conditions in real-time and automatically without the need to develop an FE model [57]. For example, supervised and unsupervised ML algorithms were introduced to predict vortex-induced vibrations and other events of the long-span twin-cable stayed bridge through RMS acceleration of the SHM system for three months [58]. In addition, machine learning algorithms such as artificial neural networks, support vector machines, decision trees, random forest, etc., were proposed for the prediction and early warning of excessive wind-induced vibration of the long-span cable-supported bridge using RMS values of vertical and lateral vibrations recorded from the SHM system [59].

In addition, having explored the benefits of wavelet techniques have been used for analyzing advanced vibration signal processing of bridge structural health monitoring such as: meaningful informative feature extraction, structural damage identification, anomaly pattern detection, scalogram image processing, signal filters, and data compression [60], [61], [62], [63], [64], [65], [66], [67]. Supervised and semi-supervised CNN models incorporating the wavelet transform were performed to classify anomalous or novelty data collected from acceleration measurements of the railway bridge under train-induced loads [68]. The proposed bridge damage identification approach combines synchrosqueezing continuous wavelet transform with MobileNet v1 and ResNet50 models to analyze benchmark vibration data from vibration-based SHM of the Z24 bridge [69]. The wavelet-based AlexNet classification model for structural damage detection was discussed using acceleration responses recorded from the old ADA bridge [70].

For the vibration signals recorded from the bridge SHM system, the wavelet transforms are powerful tools for analyzing the data features in the time-frequency domain [71]. The CWT can visualize the 2D color scalograms of the 1D vibration signals to generate the 2D images with the time–frequency localization representations used for the CNN classification models[72]. Wavelet scalograms can provide the local time-frequency energy distribution (or density) for each coefficient with the time as the horizontal axis and the scale (or frequency) as the vertical axis [73]. Wavelet analysis has the time-frequency localization and offers spectral decomposition of the short-period events [74]. Additionally, the wavelet scalograms can reveal the time–frequency features of the vibration signal while also highlighting the components of low energy [75]. The above studies show that the wavelet transforms have been applied to convert vibration signals to obtain the time–frequency representations of the energy density of the signals at different time intervals and frequency bands.

2.5 The proposed framework of digital twins for data-driven bridge health monitoring

Intelligent bridge data management is the use of digital twin technologies to collect, process, analyze and manage data from the field bridge infrastructure to BrIM and SHM. The Taiji (Tai Chi) model used to describe the integration of smart SHM digital twins for bridges, as shown in Figure 2.3, according to the Yin and Yang principle in ancient Chinese philosophy, has been applied in many areas of daily life. Depending on various aspects, the application and explanation of the Yin-Yang law will be different. However, the Yin-Yang principle from traditional Chinese philosophy and cosmology is that Yin represents black, female, moon and night; while Yang represents white, male, sun, and light.

The smart SHM framework for the bridge includes physical and virtual assets. The physical asset (Yang) consists of the bridge health monitoring system, the Internet of Things, machine learning, signal processing, and data management, while the virtual asset (Yin) contains the finite element model, the 3D bridge information model, and simulation. According to the Yin-Yang theory, it describes opposition but interdependence. This is the main reason chosen to illustrate the concept of smart bridge health monitoring. If either asset is missing, the bridge health monitoring system will not work effectively and reliably.

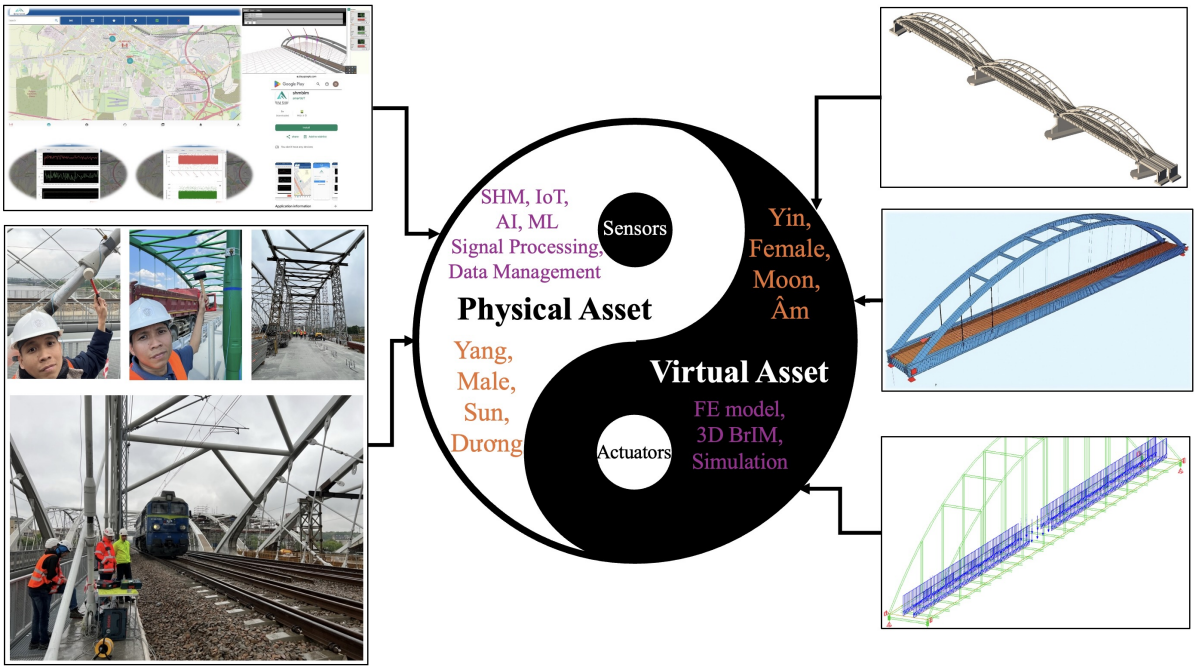

Figure 2.3: The Taiji model for smart SHM digital twins.

SHM technologies have been widely applied in numerous interdisciplinary research areas devoted to the monitoring and evaluation of structural health state and life cycle assessment for civil structures and infrastructures with potential industrial applications, as well as latest advances and innovations in both the intelligent data management of real-time emergency situations and maintenance needs in recent trends, especially in the high-tech strategies of Virtual BrIM, Internet of Things, Web of Things, Industry 4.0. Sensor data sets are managed and transferred to the Web server for interactive display of real-time data information and event-structural historical behaviors in the Web mapping service, in which the positions of sensors and structures are integrated into the virtual digital twin Lab with all-in-one solution to interface with viewers to monitor the health state of the structure. The smart alert system sets the machine learning-based threshold values of the vibration signals to implement in the SHM system that can send SMS messages via Telegram online, as shown in Figure 2.4 [35], [76].

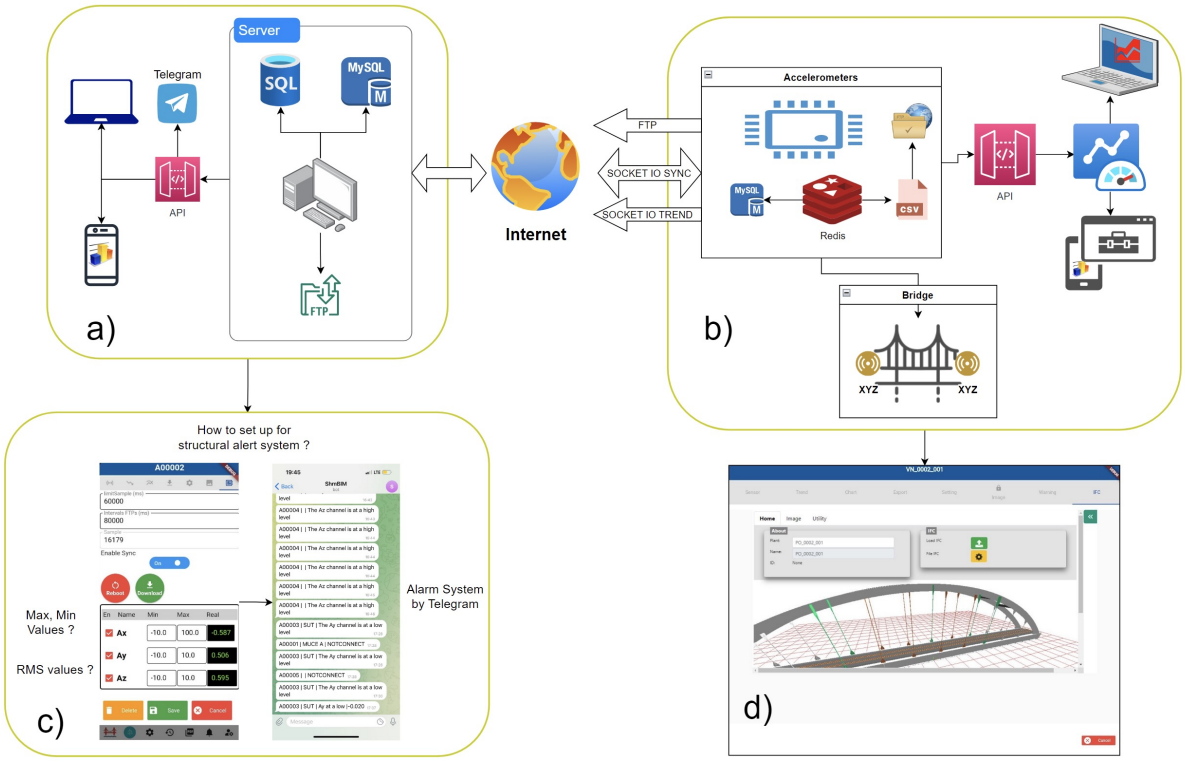

Figure 2.4: Digital twin-based intelligent SHM data management: a) Integration of machine learning algorithms for SHM system; b) Vibration-based SHM system; c) Smart alert system using Telegram; d) BrIM data management [35].

2.6 Concluding remarks

This chapter provided a systematic overview of the state-of-the-art SHM used for bridges. The presentation of the latest trends and growing needs in bridge health monitoring. It will work towards developing innovative solutions in the experimental data processing for both bridge load testing and health monitoring. The discussion of the market demands and needs for bridge health monitoring in Poland and Vietnam has been performed. It presented both market opportunities and challenges to seek and recognize cutting-edge solutions to commercialize bridge health monitoring studies.

A comprehensive overview of advanced signal processing techniques in bridge health monitoring was provided. These ideas will help provide machine learning techniques for the field data processing applied in the SHM system. A framework of digital twins for data-driven bridge health monitoring was proposed. The proposed digital twin technology is demonstrated through the integration of the visual 3D BIM models with the SHM system.

The current study is complementing ongoing research activities in the data processing and management for the bridge testing and monitoring in the field.

Chapter 3

Data acquisition instruments and advanced signal processing

3.1 Introduction

This chapter presents instruments for the field bridge load testing and the long-term vibration-based SHM system used for this study. Diagnostic load tests used for the bridges in Poland and Vietnam are introduced. The advanced signal processing methods are performed using the Morse, Morlet, and Bump wavelet transforms to convert vibration signals into 2D scalogram images as the input for CNN classification models to predict structural potential problems. The GoogLeNet architecture is used to classify the feature maps for recognizing the analyzed and collected vibration signal images. In addition, ANN, ANFIS, and random forest are also proposed to extract the field data feature, as well as to develop regression models to predict bridge health conditions. The input variables of the optimized ANN and ANFIS models consist of RMS values of vibration signals installed on the hangers, and the output is RMS values of dynamic responses on each of the two bridge spans. Additionally, evaluation metrics are introduced for classification and regression models. R^2, RMSE, MAE, MAPE, and NSE metrics are utilized for assessing the accuracy of the regression models. F1-score, macro F1-score, and weighted F1-score metrics are used to evaluate the performance of the classification models addressing with imbalanced data sets.

3.2 Bridge diagnostic load testing apparatus

3.2.1 In Poland

Bridge diagnostic load testing refers to the use of measured static and dynamic responses in field tests to understand the distribution of static and live loads throughout the bridge structures. There are two main types of field bridge load tests: static load testing and dynamic testing. The main objective of static tests is to measure the vertical deflections of the span, the displacements of the pier, and the abutment in various loading cases, as shown in Figures 3.1 and 3.2.

The load testing vehicle is a loaded dump truck, where the number of trucks depends on different types of structure. The positions of the load testing vehicle on the bridges consist of three common cases: left and right eccentric positions, as well as a centric location of the section of the bridge span. The number of train tractors used for static load testing on the railway bridge depends on the type of structure. The dynamic tests of road and railway bridges include two main scenarios: traveling at different speeds, and applying impact loads. The primary purpose of dynamic testing is to determine the modal frequencies of the structure through accelerometers installed at different locations (1/2 and 1/4 of the span length). Some common instruments used in bridge load testing include: LVDT displacement sensors (see Figures 3.3a, b, c, d); strain gauges (see Figures 3.3e); the telescope instrument to measure the deflection of the bridge span and the displacement of the abutment (or pier) (see Figures 3.3f); accelerometers to record the dynamic behavior of the bridge (see Figures 3.3g, h, i).

Figure 3.1: Field bridge diagnostic tests in Poland.

Figure 3.2: Diagnostic load testing for steel arch bridges: a), b), c), d) Vistula railway steel arch bridge in Kraków city; e), f) Steel arch bridge on the Kędzierzyn-Koźle (DK40).

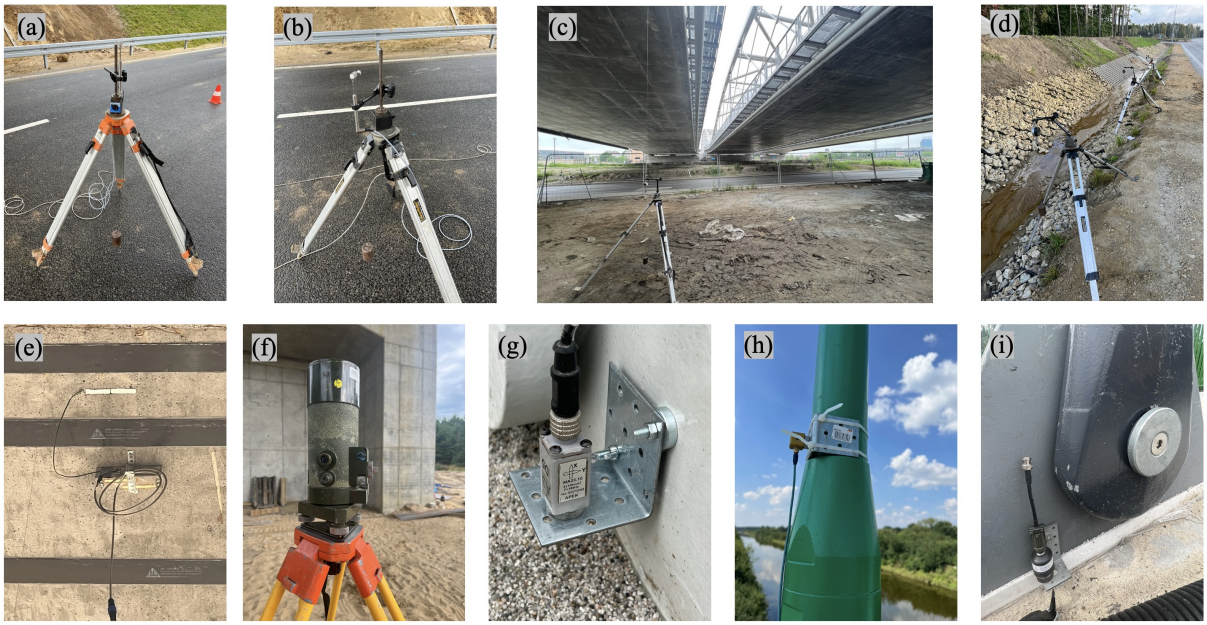

Figure 3.3: Instruments for bridge diagnostic testing in the field: a), b), c), d) deflection measurement; e) strain gauge sensor; f) Jenoptik Koni 007 for measuring span deflection and abutment displacement; g), h), i) vibration measurement.

3.2.2 In Vietnam

The wireless structural testing system (STS-WiFi) of Bridge Diagnostics Inc. from the USA has been widely used for field load testing of different types of existing structures to implement various sensors, including: intelligent strain transducers, accelerometers, strain gauges, LVDT displacement sensors, and auto-clicker as shown in Figure 3.4.

- The WinSTS data acquisition software can control the WiFi data acquisition hardware nodes and the WiFi mobile-based station to record field data from the sensors. It can display the state of every node, such as power, signal strength, name, standby mode, or 'sleep' function. The monitoring sensors in real-time window that can set up the zero sensors and access the calibrated sensor file. The sampling rate, test duration, and data file name can be assigned to collect data.
- The mobile-based battery-powered WiFi hardware station can be directly communicated with WinSTS data acquisition software that can control more than one WiFi data acquisition hardware node, also connected by an Internet ethernet cable through four ethernet ports and WiFi (see Figure 3.4b).
- The four-channel WiFi data acquisition hardware node is powered by a rechargeable battery using wireless technology to communicate with the WiFi mobile-based hardware station, which communicates wirelessly with a laptop and iPad for a signal range of more than one km. This WiFi node system can implement a wide variety of sensors (see Figure 3.4c).
- Intelligent strain transducers are installed in steel members and reinforced concrete structures (see Figure 3.4d).
- Accelerometers record the dynamic behavior of structures and concrete piers (see Figure 3.4e).
- The micro-strain measurements are integrated by the re-usable quarter bridge foil strain gages which can measure strain of the different materials: fibre reinforced polymer, reinforced steel bars (see Figure 3.4f).
- The LVDT displacement sensors are used to determine the deflection of structural members and spans (see Figure 3.4g).
- The auto-clicker is used to track the position of moving trucks at every wheel revolution, which is placed on the driver side front wheel (see Figure 3.4h).

Figure 3.4: The wireless structural testing system (STS-WiFi) for diagnostic load testing of existing bridge structures [8].

3.3 Signal processing and data evaluation for railway bridge health monitoring

3.3.1 Wavelet transforms used for vibration signals

Wavelet transforms have various applications in advanced signal processing analysis, image analysis, many other disciplines, including biomedical signal processing applications. The CWT, although the one of the oldest transforms, has numerous advantages, especially in selection of wavalet functions. The analysis of signals and images of vibration signals offers powerful and versatile techniques for practical SHM applications related to accelerometers when performing and interpreting the time-frequency analysis of signals. The selection of mother wavelet functions and parameters should be carefully tuned to suit the specific needs and signal characteristics of each practical application.

The continuous wavelet transform creates possibilities of comprehensive multi-respolution analysis of diagnostic signals, which of the 1D input signal with real-valued wavelets is defined as [77], [78], [79]:

$$\mathrm{CWT}(a,b;s(t),\psi(t)) = \frac{1}{\sqrt{a}}\int_{-\infty}^{\infty} s(t)\psi^*_{a,b}(\frac{t-b}{a})\mathrm{d}t, \tag{3.1}$$

where: $\mathrm{CWT}(a,b;s(t),\psi(t))$ is the resulting wavelet coefficients; $s(t)$ is the continuous-time signal; ψ^* is is the complex conjugate of ψ mother wavelet function; a and b are the scale and shift parameters of the wavelet, respectively; dt is time steps.

The CWT offers application of a variety of wavelet functions with only little limitations. This makes it possible to adjust specific wavelet functions to the investigated problem and analyzed signals. In the following study, we selected three wavelets: Morse, Morlet, and Bump. These functions have an analytic form (except for Morse, which is not exactly analytic), which is important from the point of view of parametrization and possible hardware implementation. Moreover, analyticity of mentioned wavelets results in decrease of the number of artifacts and time-frequency interferences, which, in turn, resulting in correct representation of amplitude and phase estimates. These wavelets are characterized by an advantageous ratio of the number of vanishing moments and the effective length of the support [80]. This was also confirmed in previous tests using these wavelets [73], where the authors demonstrated that the selected wavelets demonstrate the best time-frequency resolution and sensitivity to damage signatures.

The generalized Morse wavelet is defined as [81], [82]:

$$\Psi_{P,\gamma} = \int_{-\infty}^{\infty} \psi_{P,\gamma}(t)e^{-i\omega t}\mathrm{d}t = U(\omega)a_{P,\gamma}\omega^{\frac{P^2}{\gamma}}e^{-\omega^\gamma}, \tag{3.2}$$

where: $\Psi_{P,\gamma}$ is the frequency domain representation; $\psi_{P,\gamma}(t)$ is the time domain wavelet function; $U(\omega)$ is the unit step function; $a_{\beta,\gamma}$ is a normalizing constant; P^2 is the time-bandwidth product; γ controls the time domain decay of the wavelet; while β controls the wavelet frequency domain decay.

The Morse wavelet parameterized by β and γ is defined as [83]:

$$\Psi_{\beta,\gamma} = \int_{-\infty}^{\infty} \psi_{\beta,\gamma}(t)e^{-i\omega t}\mathrm{d}t = U(\omega)a_{\beta,\gamma}\omega^{\beta}e^{-\omega^\gamma}, \tag{3.3}$$

The fourier transform of analytic Morlet (Gabor) wavelet corresponds to the following definition [84], [85]:

$$\hat{\Psi}(\omega) = \sqrt{2}\pi^{\frac{1}{4}} \left[e^{\frac{-1}{2}(\omega-k)^2} - e^{\frac{-1}{2}(\omega^2+k^2)} \right], \tag{3.4}$$

where: ω is the angular frequency; k is parameter to determine the shape of the wavelet.

The Bump wavelet is defined as [86], [87]:

$$\hat{\Psi}(sw) = e^{\Theta} \cdot I_{\left\lceil \frac{\mu-\sigma}{s}, \frac{\mu+\sigma}{s} \right\rceil}; \; \Theta = \left(1 - \frac{1}{1 - \frac{(s\omega-\mu)^2 1}{\rho^2}} \right), \tag{3.5}$$

where: ω is the angular frequency; μ is parameter in the range of (3, 6); σ is parameter in the range of (0.1, 1.2); $I_{\left\lceil \frac{\mu-\sigma}{s}, \frac{\mu+\sigma}{s} \right\rceil}$ is the indicator function for the interval.

The CWT function in the MATLAB software was used to extract individual vibration signal segments with N length samples each, in the form of 2D scalogram graphs.

3.3.2 Feature analysis and machine learning approaches

3.3.2.1 Optimization of neural network architecture

Artificial neural networks that contain multiple hidden layers, namely deep neural networks, are computational deep learning technologies that utilize complex and non-linear mappings, clusterings, and intelligent data analysis in big data consisting of several input and output variables [88], [89]. In addition, there are many considerations in a wide spectrum of classification and recognition applications, where the trained ANN output can represent categories, predictions, simulations, and continuous variables in examples of civil infrastructure, as well as bridge structures [90], [91], [92], [93], [94], [95].

The main purpose of optimizing the ANN architecture is to improve the performance of training and testing the ANN model [96], where the number of neurons in hidden layers is one of the important parameters as a way to investigate the effect of the capacity and precision of neural networks [97], [98]. The characteristics, attitudes, and relationships of the data sets in various systems contain different information, so the ANN architecture for the prediction models could be distinct. Optimization of neural network architectures such as ANN, ANFIS, and CNN models based on the GA and PSO algorithms can be found in numerous studies of different applications [99], [100], [101].

Furthermore, several recent studies have proposed robust optimization algorithms to optimize the number of nodes in the hidden layers of the ANN structure [102], [103], [104], [105]. Optimization of the ANN architecture has brought new opportunities to improve the results of training and testing data sets in optimal ANN models, making them more efficient and reliable. In the proposed approach, ANN models have been carried out for training and testing data sets with input parameters of experimental dynamic responses of eight steel hangers and one output of dynamic behavior from the structural vibration signal on each span of the bridge. ANN could more effectively predict the RMS of the vibration signal in the steel span based on the input variables of the historical dynamic responses of eight steel hangers. ANN could be used to describe the relationship between the input components and the prediction of the output, as shown in Figure 3.5.

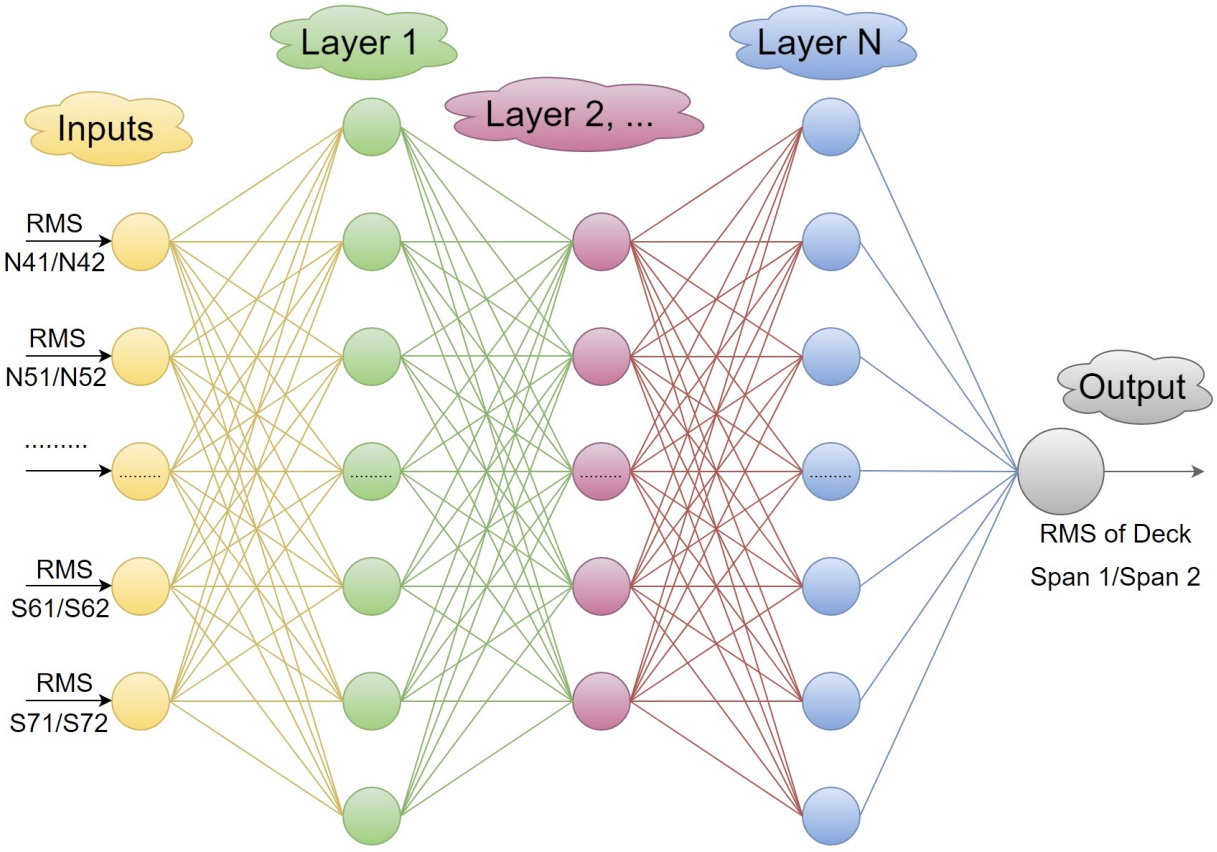

Figure 3.5: ANN architecture with RMS input and output variables [35].

There are two main strategies for the input variables including: 16 inputs for the RMS values of MEMS-based accelerations on the x-axis (A_x) and y-axis (A_y) directions; 8 inputs for the RMS vector sums of two accelerations ($A = \sqrt{A_x^2 + A_y^2}$). The ANN architecture utilized tangent sigmoid functions in hidden layers, which the ANN structure optimization algorithm has developed to find the best ANN models based on the objective function of the root mean squared error in the regression analysis, as shown in Figure 3.6. Multilayer deep neural network regression models have been trained using Levenberg-Marquardt backpropagation [106], [107]. The optimization procedure of the ANN architecture as follows:

- Data sets of accelerometers that are installed on hangers of the steel structure are collected from the long-term SHM system of the steel bridge of the railway system. The RMS values of dynamic responses of eight hangers from each steel span are used to forecast the RMS values of vertical dynamic behavior of the deck during the passage of the train.
- The data sets in the ANN models are randomly split into two separate parts, including: training (70%) and testing (30%) sets. The RMSE values of the training and testing data sets corresponding to the number of neurons in each hidden layer are calculated to obtain a minimum value as a criterion to evaluate the updated ANN model performance.
- Training data sets in the ANN model using the Levenberg-Marquardt algorithm in the MATLAB software. The ANN architecture consists of hidden neurons and hidden layers that optimizing the number of hidden neurons in the ANN structure has been conducted to find the best models corresponding to the objective function of the lowest RMSE values. The GA method is used to optimize these hidden neurons as parameters in the optimization procedure. The parameters of hidden neurons are positive integers that are set integer values of variables in the GA function.
- Testing data sets in the adjusted ANN model after each iteration step. The different evaluation metrics of the prediction ANN model for testing data sets are calculated with the updated hidden neurons in each hidden layer. The main goal of GA optimization solutions is to obtain the best ANN model with the highest coefficient of determination and the Nash-Sutcliffe efficiency values of testing data sets.

Pre-processing data sets are used to understand the characteristics of input and output data in a structural system by statistical analysis before training and prediction. For example, a correlation coefficient matrix could produce a pairwise comparison of multivariate data sets. Furthermore, the random forest algorithm could be used for classification and regression problems that are used to understand the important features and interactions of variables by ranking.

ANN algorithm [108] is implemented in the MATLAB functions as follows: the **train** function is used for multiple inputs and outputs; the **newff** function in the MATLAB simulation is to design a multilayer feedforward backpropagation neutral network and create hyperbolic tangent and sigmoid transfer function; the **sim** function runs the simulation configuration of a MATLAB Simulink model to predict the outputs from the corresponding input values. In addition, the **gamultiobj** function from the MATLAB software based on a genetic algorithm is used for the optimization problem of the ANN architecture, in which the parameters of hidden layers are the number of neurons configured as positive integers.

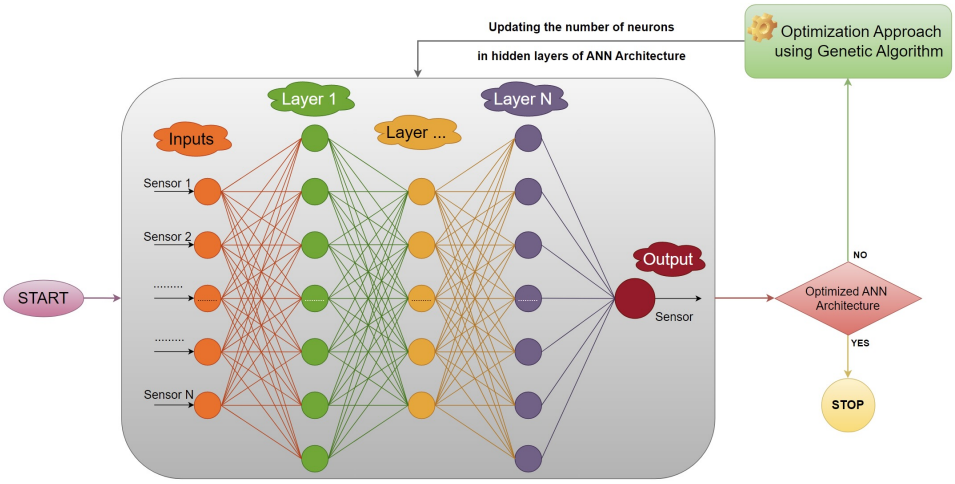

Figure 3.6: Optimization approach of the ANN architecture [35].

3.3.2.2 Adaptive neuro-fuzzy inference system approach

ANFIS has emerged as a powerful data processing technique for forecasting problems of civil structures that could provide robust learning tools for engineers and researchers with in-depth methodologies in order to build models, make predictions, mine data and process intelligent information across a broad range of bridge applications [109], [110], [111]. For aspects of the current and future SHM system, ANFIS is used to model a system that could receive input and produce output. The inputs are RMS values of the dynamic responses of eight hangers, and the outputs are RMS values of the dynamic behavior of the bridge span. The relationships between inputs and outputs and the representation parameters are important issues in the design of the ANFIS architecture for diagnosing and determining dynamic behavior of the steel bridge structure. The ANFIS models consist of (70%) training data sets and (30%) testing data sets using the ANFIS algorithm in the MATLAB software as shown in Figure 3.7. The values of parameters of the ANFIS architecture are well chosen in the MATLAB software using the fuzzy C-Means (FCM) clustering algorithm [112] as shown in Table 3.1.

Table 3.1: The parameters of the ANFIS architecture.

ANFIS parameters	Value
Maximum number of training epochs	200
Training error goal	0
Initial training step size	0.01
Step-size decrease rate	0.9
Step-size increase rate	1.1
Number of clusters	15
Maximum number of iterations	200
Minimum improvement in the objective function	1e-5

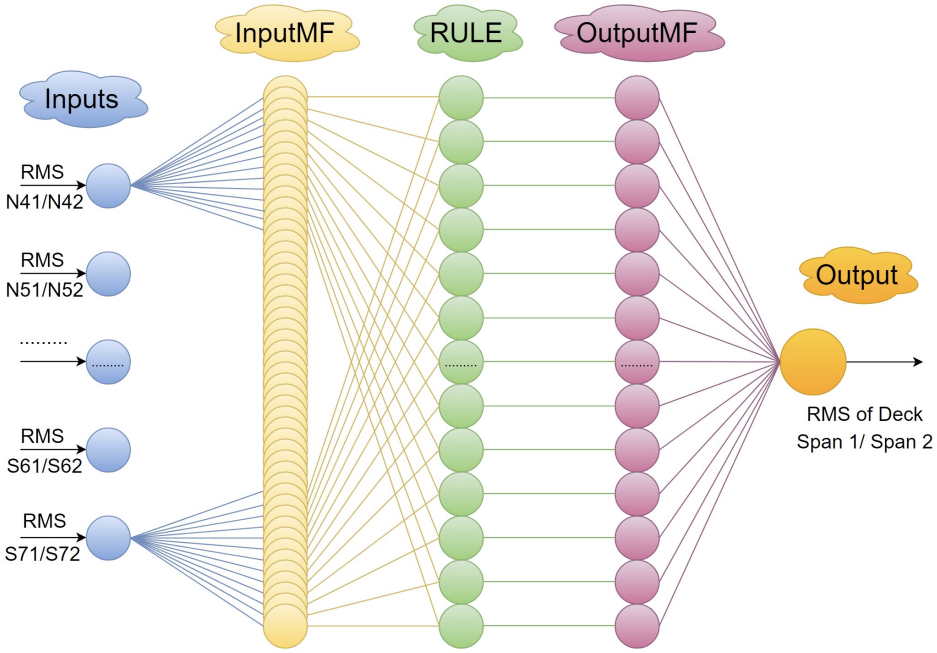

Figure 3.7: The architecture of ANFIS model [35].

3.3.2.3 Random forest method

Leo Breiman's and Adele Cutler's random forest method [113] developed for robust classification and regression of data problems and solutions could be used for training data sets in the field and subsets of data in computational simulation models based on the forest of multiple independent decision trees sampled from the input data [114], [115]. It could identify a large number of labeled features and important attributes of randomized input parameters that correspond to the output responses of various systems [116], [117], [118].

For the first case study, the independent input variables in the original data sets are sixteen RMS dynamic responses of eight hangers on bridge span 1. Moreover, the input variables are sixteen RMS responses of eight hangers on bridge span 2. For the second case study, the input variables are eight RMS magnitudes of the vector sum of two accelerations in the x-axis and y-axis directions for eight hangers on span 1; eight hangers on span 2. The RMS values of dynamic behavior on each bridge deck were collected from a long-term SHM system, which were designed as the output variable in the RF analysis.

The schematic diagram of the RF algorithm based on decision trees, in which each training tree is performed by random training data sets of input variables and output data, as shown in Figure 3.8. The main idea of the RF approach is to make estimates for the dynamic responses of hangers to dynamic behavior of the deck during passage of a train, as well as pre-processing tasks of large data sets. As a result, it can be used for recommendations of important input variables for training purposes in the ANN and ANFIS models to provide more accurate predictions and improve better decision making.

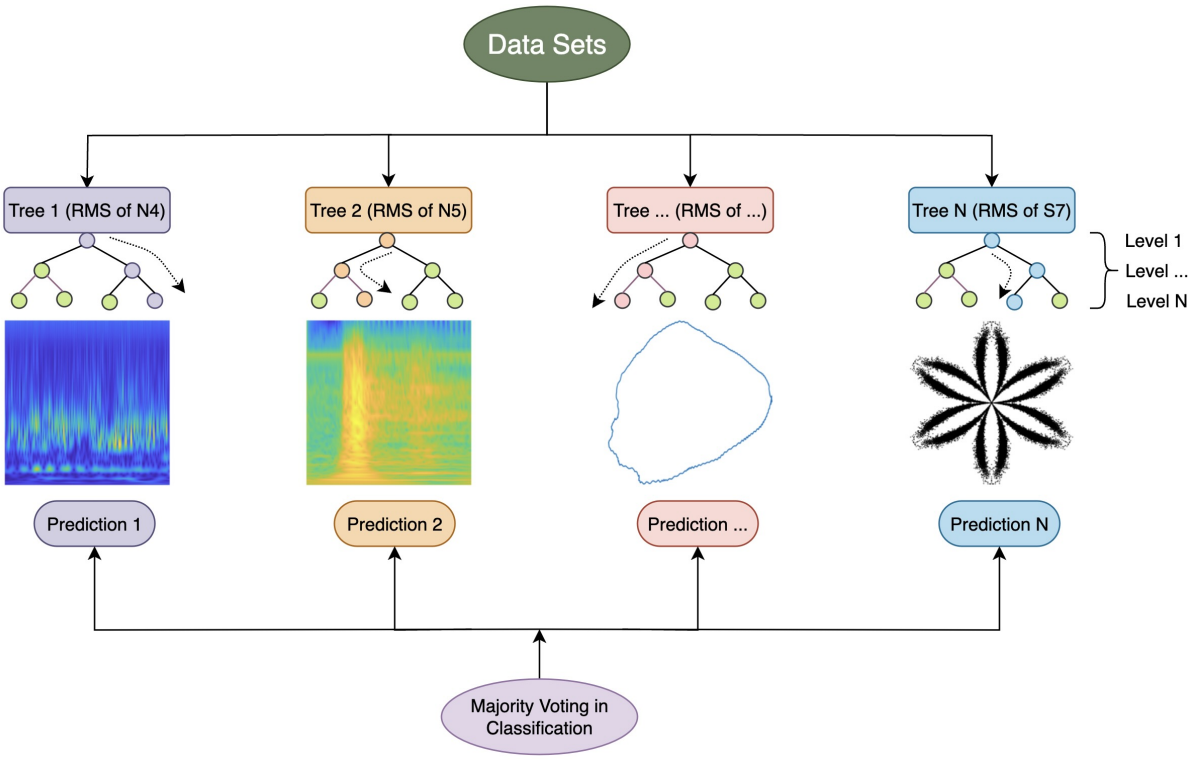

Figure 3.8: Random forest with data sets of RMS dynamic responses of structure [35].

3.3.2.4 Convolutional neural networks

CNNs are a key technology in applications such as medical imaging, audio processing, object detection, computational finance, natural language processing, and speech recognition, while CNN approaches are commonly used for classification and regression tasks on image data, time series data [119], [120], [121], [122]. The benefits of using CNNs for vibration-based SHM of civil structures are useful for signal regression and image classification tasks in processing large amounts of data, as well as extracting important features to produce highly accurate predictions [123], [124], [125].

The CNN consists of three main types of layers: convolutional layer; pooling layer; fully-connected (FC) layer. Some of CNN architectures for image classification models include AlexNet, GoogLeNet, SqueezeNet, ResNet, EfficientNet, DarkNet, ShuffleNet, Xception, MobileNet, DenseNet, VGG [126], [127], [128], [129]. This study used the GoogLeNet CNN architecture, which is a convolutional neural network with 22 layers deep [130]. The first layer was selected to edit the maximum image size, with GoogleNet requiring an image size of 224×224×3 for the input images. The final layer was edited to suit the number of classes. The utilized methods and codes have been implemented using the MATLAB software. The data sets were divided into two subsets: 70% of training and 30% validation [131], [132]. The model was trained using Adam optimizers, with a mini-batch size of 128 and a limitation of 30 epochs [133], [134], [135]. The cross-entropy was used as the loss function and the training rate was 0.001 [136], [137]. The results of wavelet analysis and CNN models were conducted using the following implementation configuration, including the MATLAB software R2023b; Processor AMD Ryzen 5 (1600) Six-Core Processor, 3200 MHz, 6 Cores, 12 Logical Processors; Installed Physical Memory (RAM) 128 GB; NVIDIA GeForce RTX 3060, VRAM 12 GB; and 64-bit Operating System.

3.3.2.5 Evaluation metrics for classification models

The performance of CNN-based classification models was evaluated using three common metrics: Accuracy, Precision, and Recall. These metrics are based on a number of True Positive (TP), True Negative (TN), False Positive (FP), and False Negative (FN) samples [138], [139]. As an example, the confusion matrix of two classes is a 2×2 table, as shown in Table 3.2 [140], [141]. The accuracy, F1-score, macro F1-score and weighted F1-score metrics of CNN models have the following definition [142], [143]:

$$\text{Accuracy} = \frac{\text{TP} + \text{TN}}{\text{TP} + \text{TN} + \text{FP} + \text{FN}} \times 100\%, \tag{3.6}$$

$$\mathrm{F1-score} = \frac{2 * \mathrm{Precision} * \mathrm{Recall}}{\mathrm{Precision} + \mathrm{Recall}}, \tag{3.7}$$

$$\mathrm{Macro\,F1-score} = \frac{\sum_{i=1}^{N} (\mathrm{F1-score})_i}{N}, \tag{3.8}$$

$$\mathrm{Weighted\,F1-score} = \sum_{i=1}^{N} w_i * (\mathrm{F1-score})_i, \tag{3.9}$$

where:

- TN: The response is actually negative and is predicted by the algorithm to be negative.
- FP: The response actually negative, the algorithm predicts it to be positive, this is known as false positive.
- TP: The response is actually positive; the algorithm predicts it to be positive.
- FN: The response is actually positive, and the algorithm predicts it to be negative. This is known as a false negative.
- Accuracy: The number of correct classifications made.
- Sensitivity: The proportion of positive responses is correctly identified as positive by the classifier [144].
- Specificity: The proportion of negative responses is correctly identified as negative by the classifier [144].
- PPV: The probability of an observation being classified as positive is truly positive.
- NPV: The probability of an observation classified as negative is truly negative.
- N is the number of labels (or classes); the weight (w_i) of each class is the ratio of the number of samples in class (or label) i^{th} divided by total number of samples in data set; the sum of all sampled weights $\sum_{i=1}^{N} w_i = 1$. The weighted F1-score is used to address imbalanced datasets.

Table 3.2: Confusion matrix and evaluation metrics for predicted and true class.

		Predicted Class		
		Positive	Negative	
True Class	Positive	True Positive (TP)	False Negative (FN)	Sensitivity, Recall or True Positive Rate (TPR) $\frac{TP}{TP+FN} \times 100\%$
	Negative	False Positive (FP)	True Negative (TN)	Specificity or True Negative Rate (TNR) $\frac{TN}{TN+FP} \times 100\%$
		Precision or Positive Predictive Value (PPV) $\frac{TP}{TP+FP} \times 100\%$	Negative Predictive Value (NPV) $\frac{TN}{TN+FN} \times 100\%$	

3.3.2.6 Evaluation metrics of regression models

The assessment measures of prediction regression model accuracy have been utilized for the evaluation of optimized ANN structures and ANFIS models such as: coefficient of determination (R^2, or R-Squared), root mean squared error (RMSE), mean absolute error (MAE), mean absolute percentage error (MAPE), Nash-Sutcliffe efficiency (NSE). Regression accuracy measurements such as: R-Squared, RMSE, MAE, MAPE and NSE are the most popular metrics used to evaluate statistical errors between predicted and actual values [145], [146], [147], [148], [149], [150], [151], [152].

The R^2 (or R-Squared) is Pearson correlation [153]. The R^2 ranges from 0 to 1, the assessment criteria of the R^2 values as shown Table 3.3 [154], [155], which can be given by the equation:

$$R^2 = \left(\frac{\sum_{i=1}^{N} \left(O_i - \overline{O}\right)\left(S_i - \overline{S}\right)}{\sqrt{\sum_{i=1}^{N} \left(O_i - \overline{O}\right)^2} \sqrt{\sum_{i=1}^{N} \left(S_i - \overline{S}\right)^2}} \right)^2, \tag{3.10}$$

where O_i are the true observed values in the field testing; S_i are the predicted values of the ANN and ANFIS models; $\overline{O}$ is the mean of the actual observed values; $\overline{S}$ is the mean of predicted values; N is the number of samples.

Table 3.3: Evaluation metrics of R^2 index.

R^2	Interpretation
$R^2 \geq 0.75$	Substantial
$0.50 \leq R^2 < 0.75$	Moderate
$0.25 \leq R^2 < 0.50$	Weak
$R^2 < 0.25$	Very weak

The RMSE is the square root of the average square difference between the observed and predicted values, which can be calculated as follows [156]:

$$\text{RMSE} = \sqrt{\frac{1}{N}\sum_{i=1}^{N}(O_i - S_i)^2}, \tag{3.11}$$

The MAE is the average of the difference between the observed and predicted values, which can be calculated as the following equation [156]:

$$\text{MAE} = \frac{1}{N}\sum_{i=1}^{N}|O_i - S_i|\,, \tag{3.12}$$

The MAPE computes the average absolute percentage difference between the observed and predicted values that Table 3.4 [157], [158] shows a description of the implementation of the evaluation MAPE metric for the accuracy of forecast models. It can be used to forecast errors calculated as the following equation [156]:

$$\text{MAPE} = \frac{100\%}{N}\sum_{i=1}^{N}\left|\frac{O_i - S_i}{O_i}\right|, \tag{3.13}$$

Table 3.4: Evaluation measures of MAPE index.

MAPE	Interpretation
MAPE < 10%	High Accurate
10% ≤ MAPE ≤ 20%	Good
20% ≤ MAPE ≤ 50%	Reasonable
MAPE > 50%	Inaccurate

The NSE [159], whose magnitude ranges from range from -∞ to 1.0, that determines the relative magnitude of the predicted variances in the ANN and ANFIS models compared to the observed data variances in field measurements. The NSE values are closer to 1.0 indicate variables that can be considered a perfect match of the predicted ANN and ANFIS models to the observed data. If the magnitude of the NSE is greater than 0.5, it indicates that the predictions of the optimized ANN models and the ANFIS models can be judged satisfactory [160], [161]. The NSE interpretation metric is used to assess the accurate predictions of the models, as shown in Table 3.5 [162], [163]. The following equation can be used to calculate the NSE:

$$\mathrm{NSE} = 1 - \frac{\sum_{i=1}^{N} (S_i - O_i)^2}{\sum_{i=1}^{N} \left(O_i - \overline{O}\right)^2}. \tag{3.14}$$

Table 3.5: Evaluation criteria for NSE index.

NSE	Interpretation
0.75 < NSE ≤ 1.0	Very Good
0.65 < NSE ≤ 0.75	Good
0.50 < NSE ≤ 0.65	Satisfactory
NSE ≤ 0.50	Unsatisfactory

3.4 Concluding remarks

This chapter presented data acquisition instruments for field bridge load testing and advanced signal processing approaches. The intelligent data processing approaches were applied to the data-driven bridge health monitoring system of the existing railway bridge. The primary applications of the proposed research methods are summarized as follows:

- Optimized ANN and ANFIS algorithms were introduced for the data-driven SHM system of the railway steel arch bridge.
- Wavelet transforms were proposed to convert 1D vibration signals from the bridge span into scalogram images used for CNN classification models. GoogLeNet CNN classification models were proposed to classify the hanger tension force and orbit-shaped pattern recognition of hanger vibration signals under healthy and unhealthy structural states.

In the current studies, the evaluation metrics consisting of R^2, RMSE, MAE, MAPE, and NSE were utilized for the regression ANN and ANFIS models, while the F1-score, macro F1-score and weighted F1-score metrics were used for the CNN classification models with the imbalanced data sets.

Chapter 4

Railway bridge health monitoring using machine learning

4.1 Introduction

This chapter presents vibration-based SHM of railway steel arch bridge with optimized ANN and ANFIS regression models [35] that summarized as follows:

- Developing the ANN and ANFIS-assisted models for predicting the future RMS values of the behavior of the bridge deck based on the historical data sets of the RMS values of the hanger vibration responses;
- Implementing the GA-based optimization approaches for adjusting the parameters including the number of hidden neurons in each hidden layer of ANN architectures for various proposed prediction strategies;
- Comparing the optimized GA-integrated ANN regression models with ANFIS models using the various performance metrics to assess the ML-based prediction models reliably and effectively;
- Using correlation coefficient analysis and random forest-based importance scores aiming to understand the overall relationship between the individual input features and output variables in the prediction regression models to provide valuable insights and help reduce the number of the input variables;
- Discussing the advantages and limitations of machine learning assisted approaches (ANN and ANFIS) for the vibration-based SHM of the complex railway steel arch bridge structure in Poland.

4.2 Bridge being the object of research: Dębica railway steel arch bridge

In the design of the heavy steel arch bridge hangers, they are crucial structural components in providing static and dynamic load distribution, structural stability, durability and safety service, and long-spanning capabilities, as well as costly replacements and maintenance. Existing hanger damage in the arches of the bridge structure can occur due to various reasons and incidents such as: overload, fatigue stress, buckling effects, corrosion, and impacts of environmental factors. Therefore, hanger health monitoring is necessary to identify these potential problems for arch bridge maintenance and safety management, helping to extend the age of the structure and ensure the safety of the steel bridge. For example, steel hanger design for some arch bridge structures in Poland, as shown in Figure 4.1.

In the context of steel arch bridges, the hanger being the weakest link is indeed a critical structural component responsible for transmitting and bearing tension forces, particularly the vertical train or vehicle loads applied to the bridge [164], [165]. For example, the impacts of the inclined and vertical hanger element replacements on the time-history seismic structural behavior were developed for health monitoring of long-span cable-stayed bridge under multi-support earthquake excitation [166]. As part of this related case, estimating the tension forces of suspension bridge hanger cables was proposed using vision-based systems and the image-based back analysis method [133]. Therefore, hanger vibration-based health monitoring is a proactive and essential practice for the safe operation and longevity of steel arch bridge, where the tension force of the hanger is considered one of the most important tasks enhancing through intelligent data processing and management of the railway SHM system.

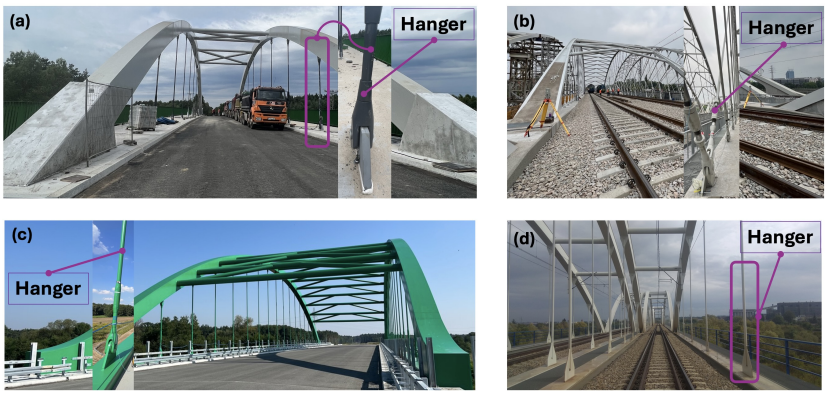

Figure 4.1: Design of hangers for some steel arch bridges in Poland: a) Viaduct bridge in Hucisko (DW 792 km 10+785); b) Vistula railway arch bridge in Krakow; c) Steel arch bridge on the Kędzierzyn-Koźle (DK40); d) Dębica railway steel arch bridge structure.

The Dębica bridge is two single-track railway arch bridge structures as shown in Figure 4.2. The steel bridge structure consists of three main bridge spans of 72.8 m length and one prestressed concrete span of 17 m. It spans the Wisłoka River at km 108.404 of line no. 91 Kraków-Medyka in Poland. The width of the steel structure is 5.4 m and the structural width of the railway arch bridge is 4.4 m. The height of the railway bridge structure in the middle of the span is 13.96 m. The steel structure is made of steel grade S355J2+N (18G2A). Table 4.1 and Figure 4.3 show the dimensions of the structural components of the steel arch bridge spans.

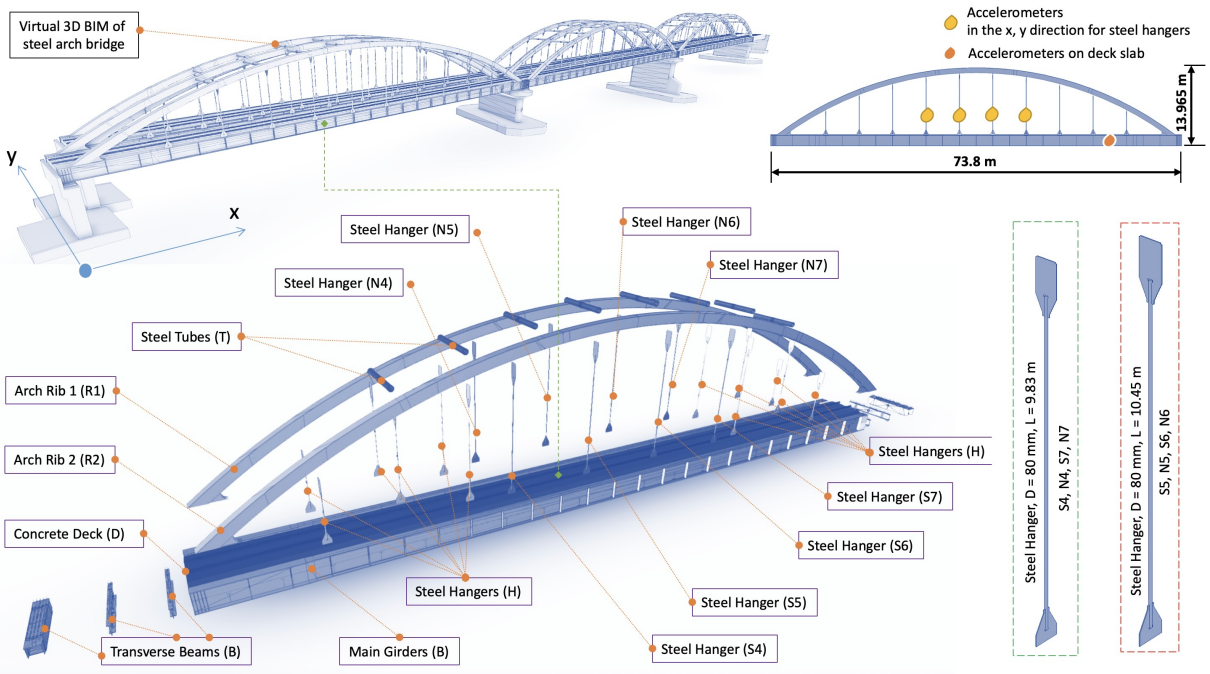

Figure 4.2: The bridge information management of Dębica railway steel arch bridge in Poland.

The two main steel girders are I-shaped beams with the largest cross-sectional dimensions, for example: section height of 1910 mm; flange width of 750 mm; web thickness of 16 mm; flange thickness of 40 mm. The radius of the two steel arch ribs is approximately 58.98 m with hollow rectangular cross sections whose height is 880 mm and width is 670 mm with several different cross-sectional dimensions at different locations in the profile; the largest thickness is 40 mm and the smallest thickness is 20 mm. There are 23 floor steel I-shaped beams that have the highest height and width of 920 mm and 400 mm, respectively. The two steel box-shaped beams at the end of two main girders have a height of 905 mm and a width of 920 mm with thicknesses of 40 mm and 20 mm. The eight steel circular tube beams are weld to connect two arch ribs that have outer and inner diameters of 508 and 486 mm, respectively. With 20 steel circular solid hangers have diameters of 80 mm and 100 mm. The reinforced concrete deck slab has a thickness of 300 mm.

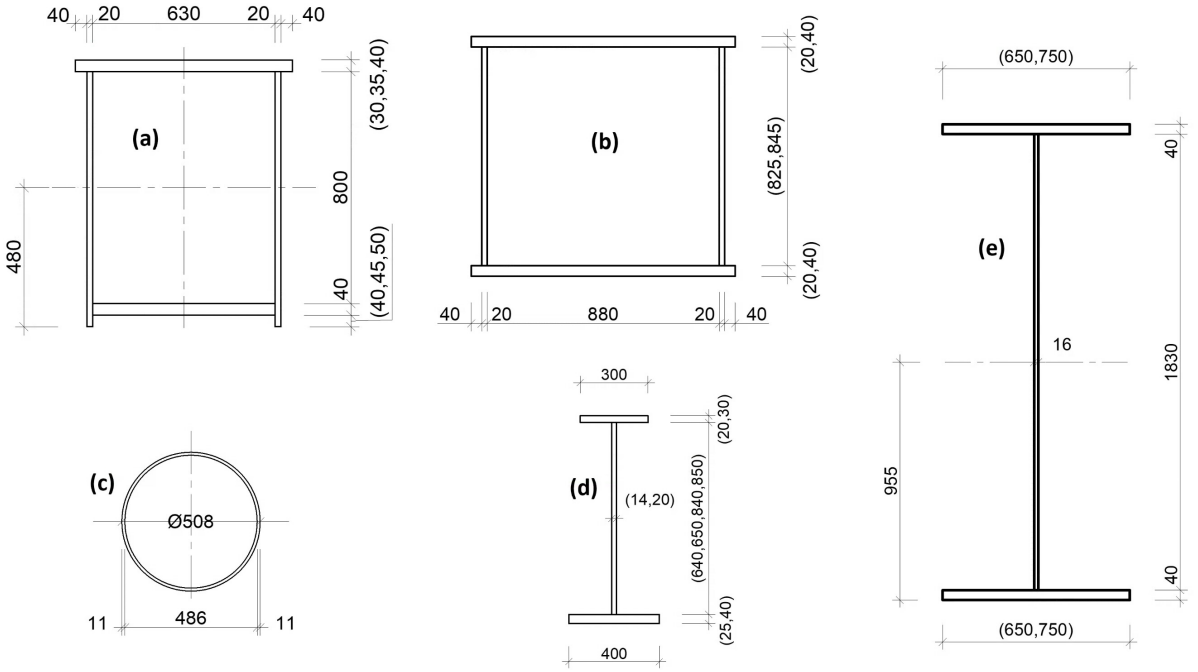

Figure 4.3: Design cross-sectional dimensions of structural members of steel arch bridge span: a) arch ribs; a) transverse beams; c) arch transverse beams; d) deck transverse beams; e) main girders.

Table 4.1: Statistical dimensions of main structural members.

Structural components	Cross-sections	Geometric properties	Dimensions (mm)
Arch ribs	Hollow rectangle or box	Outer width of the box Outer height of the box Wall thickness	670 860 ÷ 880 20 ÷ 40
Arch transversal beams	Circular tube	Inner radius of the tube Outer radius of the tube	486 508
Main girders	I-shaped section	Width of the top or bottom flanges Overall depth Flange thicknesses Web thicknesses	650, 750 1910 40 16
Tie transversal beams	I-shaped section	Width of the top flanges Width of the bottom flanges Overall depth Flange thicknesses Web thicknesses	300 400 695 ÷ 920 14 ÷ 20 20 ÷ 40
Transversal beams at the abutments or piers	Hollow rectangle or box	Outer width of the box Outer height of the box Wall thickness	920 885; 905 20; 40
Hangers	Circular solid	Radius	80; 100
Deck	Rectangle	Width Height	5384 300 ÷ 348

4.3 SHM system used for Dębica railway bridge

The vibration-based SHM system was installed in spans 1 and 2, with a more detailed description as shown in Figure 4.4, including 16 double axis-x and -y sensors for 8 per span 16 total, 1 IEPE (piezoelectric) per each span. The sampling frequency of the SHM system was 1024 resampled to 128 for storage. Data was recorded in nine-month period between December 2019 and September 2020. The hangers in span 1, namely: N41, N51, N61, N71, S41, S51, S61, and S71 were equipped with one biaxial accelerometer each to record the dynamic responses of the structure in the x- and y-directions. The other hangers in span 2, namely: N42, N52, N62, N72, S42, S52, S62, and S72 were equipped with one biaxial accelerometer each to collect the dynamic behavior history of the structural components under train events.

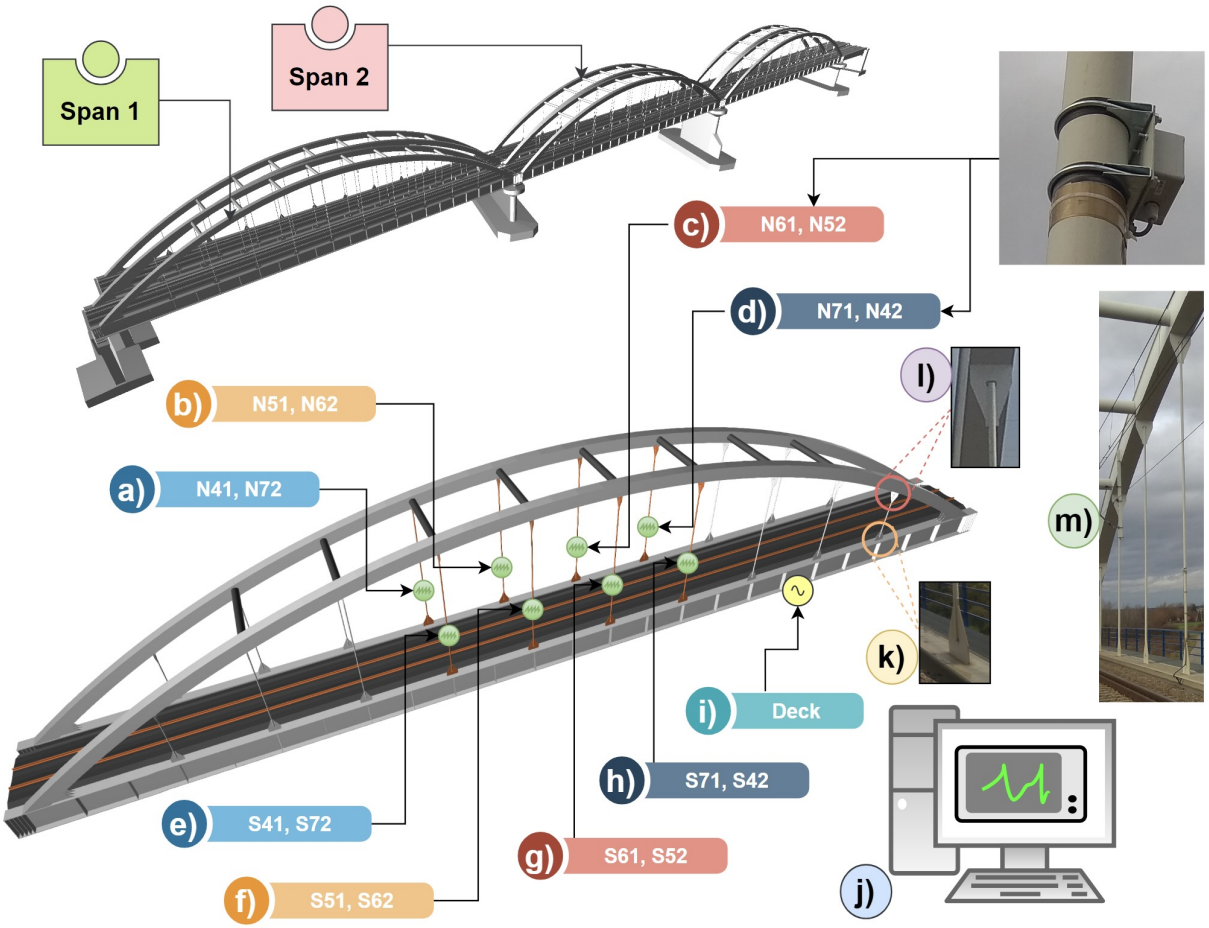

Figure 4.4: Vibration-based SHM system of Dębica railway steel arch bridge: a), b), c), d), e), f), g), h) accelerometers for hangers; i) piezoelectric accelerometer for the deck; j) data acquisition system; k) welded connection of hanger with I-shaped beam; l) welding connection of hanger with arch rib; m) hangers [35].

4.4 Vibration-based SHM of Dębica railway steel bridge with optimized ANN and ANFIS

4.4.1 Correlation coefficient and random forest analysis of SHM data sets

4.4.1.1 Case study 1

The correlation matrix of data sets is a descriptive multivariate statistic for the correlation analysis between various variables using the R software [167]. Pairing correlation coefficients could be estimated any values in the range from -1 to $+1$, which are free units of measurement. The values of the correlation coefficient closer to -1 indicate that the degree of correlation is a perfect non-linear (negative) relationship. The correlation coefficients closer to $+1$ mean that the level of correlation is a positive linear relationship. For example, correlation coefficients between 0.7 and 0.89 indicate that variables could be considered as a strong correlation; moderate correlation between 0.4 and 0.69; weak correlation between 0.1 and 0.39 as discussed in the literature [168], [169].

Figure 4.5 shows the visualization of the correlation coefficient matrix between the RMS of the deck bridge span 1 and the RMS of the dynamic behavior of the hangers. The deck was strongly correlated with N41x(0.758), N41y(0.756), S51y(0.734), S61y(0.720); and had a weak correlation with N51x(0.399) and S41x(0.167). Correlation coefficients between 0.3 and 0.5 indicated that the variables had a moderate correlation with the RMS of the deck, such as: N71y(0.694), S51x(0.594), N61y(0.571), N71x(0.536), S71y(0.531), S41y(0.486), N61x(0.464), S71x(0.451), N51y(0.439), S61x(0.430).

Figure 4.6 shows the correlation coefficients between the RMS values of the deck bridge span 2 and the RMS values of the dynamic responses of the hangers. RMS magnitude of the deck had a strong correlation with the parameters: S42y(0.843), S42x(0.782), N42y(0.779), S52y(0.765), S52x(0.762), S72y(0.737), N42x(0.722). RMS value of the deck was weekly correlated with S62y(0.277) and S62x(0.273). RMS value of the deck was moderately correlated with other parameters such as: N52y(0.624), N52x(0.600), N72y(0.600), N62x(0.565), N72x(0.561), N62y(0.539), and S72x(0.494).

Figure 4.5: Correlation coefficient of 16 RMS dynamic responses (A_x and A_y) for 8 hangers and RMS of the deck in bridge span 1 [35].

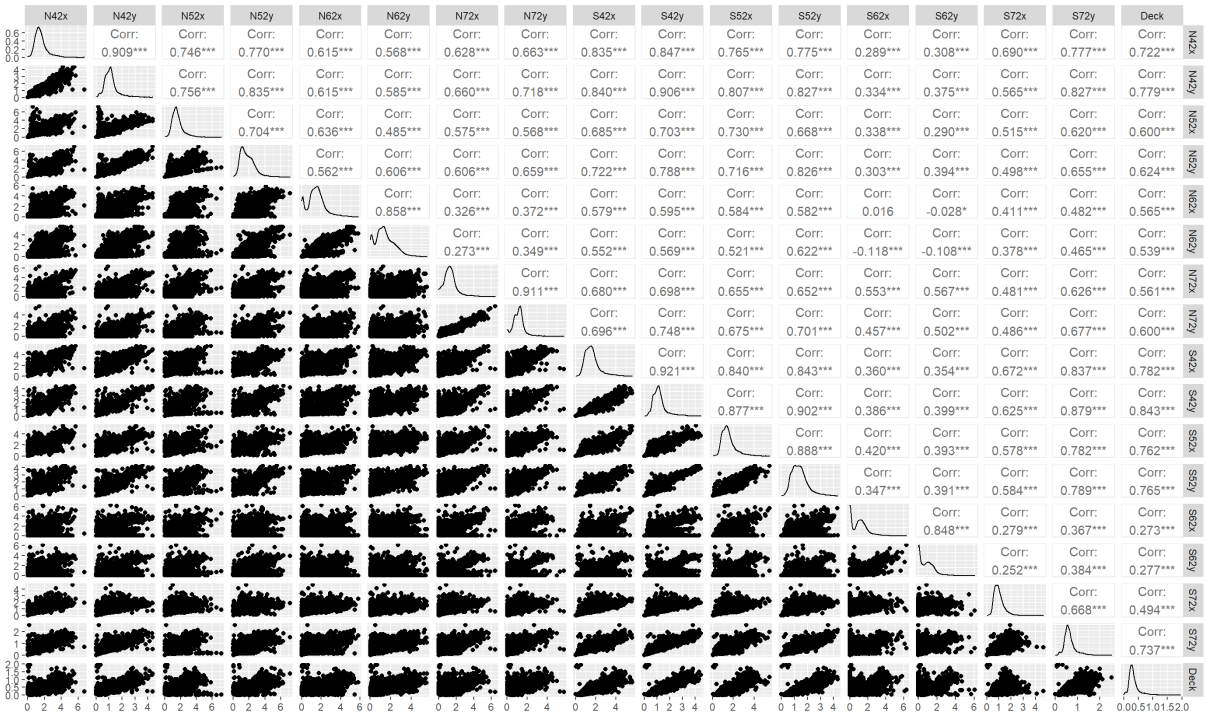

Figure 4.6: Correlation coefficient of 16 RMS dynamic responses (A_x and A_y) for 8 hangers and RMS of the deck on bridge span 2 [35].

Figure 4.7 shows the results of the variable importance measures of the RMS dynamic responses of the hangers with the RMS dynamic behavior of the the deck in spans 1 and 2 using the random forest algorithm in the R software. From the left plot of span 1 in Figure 4.7, it indicates that the importance measure in the simulation was highest for the variable N41(x~21.89, y~20.61). The weak influences on the dynamic behavior of span 1 were in variables N51(x~1.52, y~1.59); S41(x~1.67, y~1.81); S71(x~1.58, y~2.56); N61(x~2.02, y~3.78). Furthermore, the variables for S51(y~15.42) and S61(y~13.02) had higher importance scores in the RF analysis than other variables for N71(x~5.22, y~8.97); S51(x~3.51) and S61(x~2.69). Based on the RF ranking that could divide into two groups, for example: (N41x, N41y, S51y, S61y) for the most important variables and (N51x, N51y, N61x, N61y, N71x, N71y, S41x, S41y, S51x, S61x, S71x, S71y) for subsets with lower ranking values. The right graph in Figure 4.7 shows the results of the RF analysis for bridge span 2, in which two groups could be described for the variables (S42y~71.54, N42y~41.60, S52x~30.20, S42x~26.77, S52y~23.10, N42x~14.26, S72y~10.18) with the highest values of the characteristic measures; and other variables (N52x~5.20, N52y~4.94, N62x~5.76, N62y~6.4, N72y~3.91, N72x~3.30, S62x~3.00, S62y~2.98, S72x~5.74) with less effect on the RF scores.

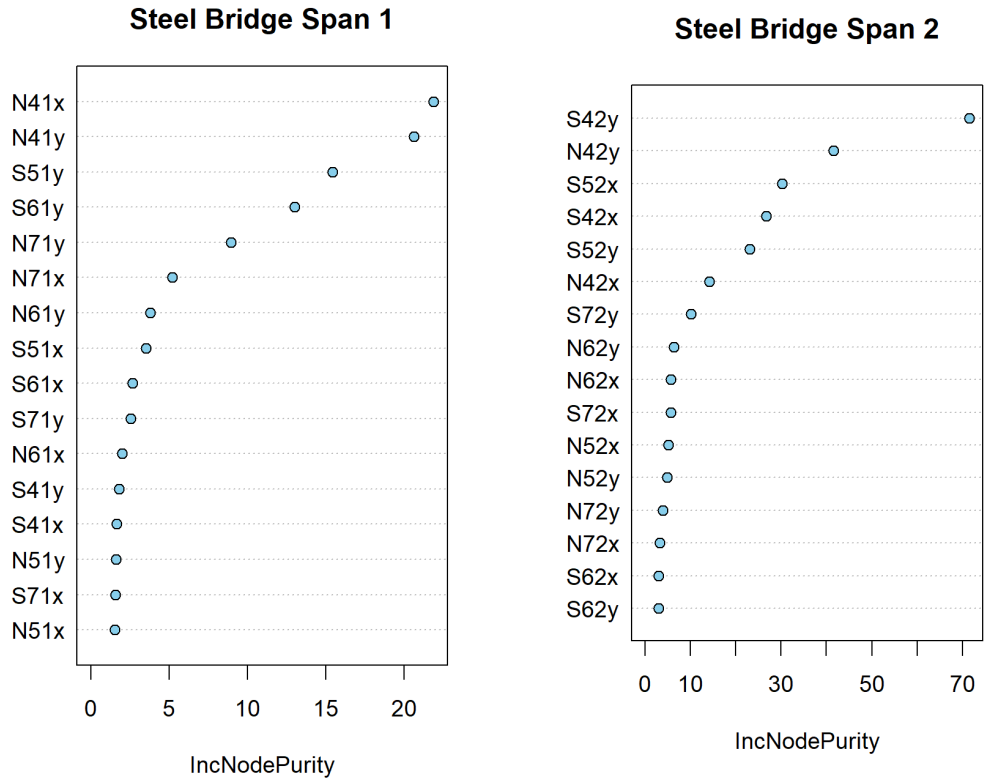

Figure 4.7: The results of random forest analysis for 16 input RMS accelerometers on the bridge spans 1 and 2 [35].

4.4.1.2 Case study 2

Figure 4.8 reports a visualization of the correlation matrix between the RMS of the deck bridge span 1 and the RMS of the dynamic responses of the hangers. The RMS of the deck had a strong correlation with N41(0.778); weak correlation with S41(0.263); moderate correlation with variables: S51(0.673), N71(0.663), S61(0.561), N61(0.529), S71(0.501), N51(0.427). The correlation coefficients of the RMS values between the hangers ranged from 0.309 (S41-N51) to 0.828 (N71-N41). Two groups were introduced: (N41, N51, N61, N71) and (S41, S51, S61, S71) the correlation coefficients of each group having values greater than 0.4 as moderate. The correlation coefficient values were evaluated between these two groups ranged from more than 0.309 regarded as weak to 0.792 considered as strong.

Figure 4.9 visualizes the correlation matrix between the RMS of the deck bridge span 2 and the RMS of the dynamic responses of the hangers. The RMS of the deck had a strong correlation with S42(0.818), S52(0.782), N42(0.754); weak correlation with S62(0.285); moderate correlation with variables: N52(0.646), S72(0.604), N72(0.588), N62(0.564). The relationships between the hangers showed that the correlation coefficient of the paired S42-N42 was 0.879 of the highest value, indicating that two paired variables had a strong correlation, the paired S62-N62 whose magnitude was -0.053 which could be uncorrelated when close to 0. Other paired variables of hangers had correlation coefficients of more than 0.331 (S62-N42).

For the classification task, the RF approach was used to measure the variable importance of individual characteristics, indicating that there were eight model parameters in each bridge span that served as RF input features shown in Figure 4.10. According to the IncNodePurity (Increase in Node Purity in RF algorithm) index of the left plot for span 1, the hanger N41 was very important with a value of 30.68, while the contribution of hanger S41 was the smallest with a value of 4.44. The contribution of hangers N71 and S51 was higher than other input variables with values equal to 18.67 and 18.5, respectively. The ranking of the contribution from bands 6.83 to 12.27 corresponding to hangers S61, S71, N61, and N51 was less important than hangers N41, N71, and S51. Compared to the results of the correlation analysis in Figure 4.10, which could divide one group with correlation values greater than 0.6 and the other group with fewer values than 0.6.

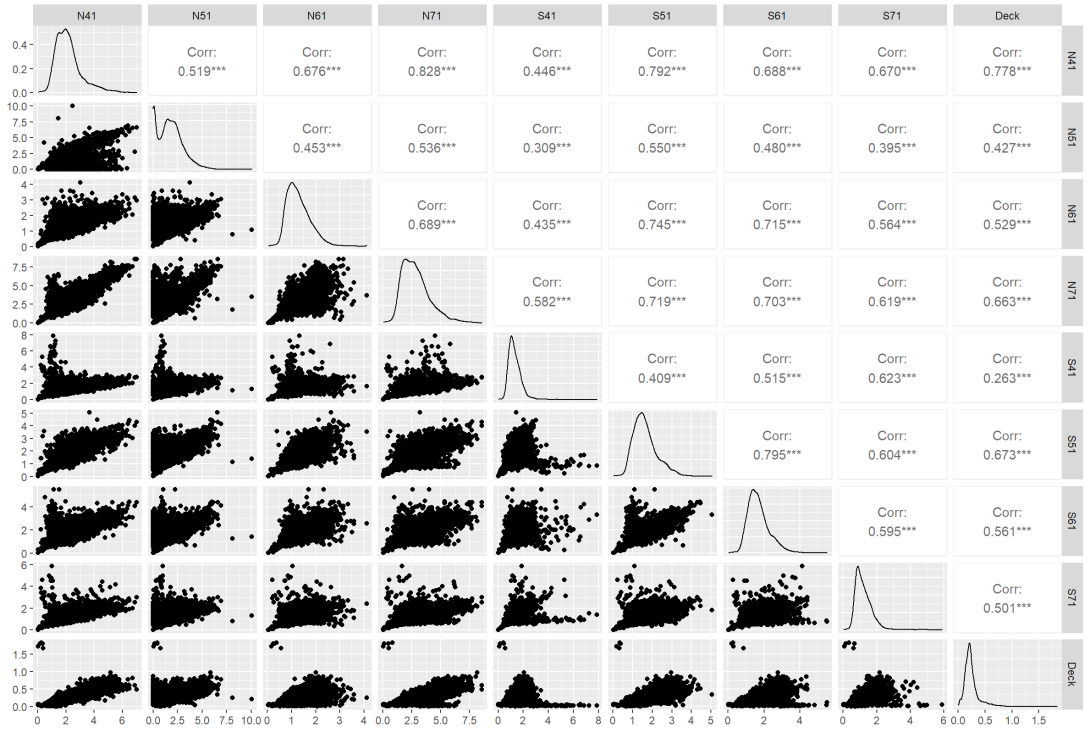

Figure 4.8: Correlation coefficient of 8 RMS dynamic responses ($A = \sqrt{A_x^2 + A_y^2}$) for 8 hangers and RMS of the deck on bridge span 1 [35].

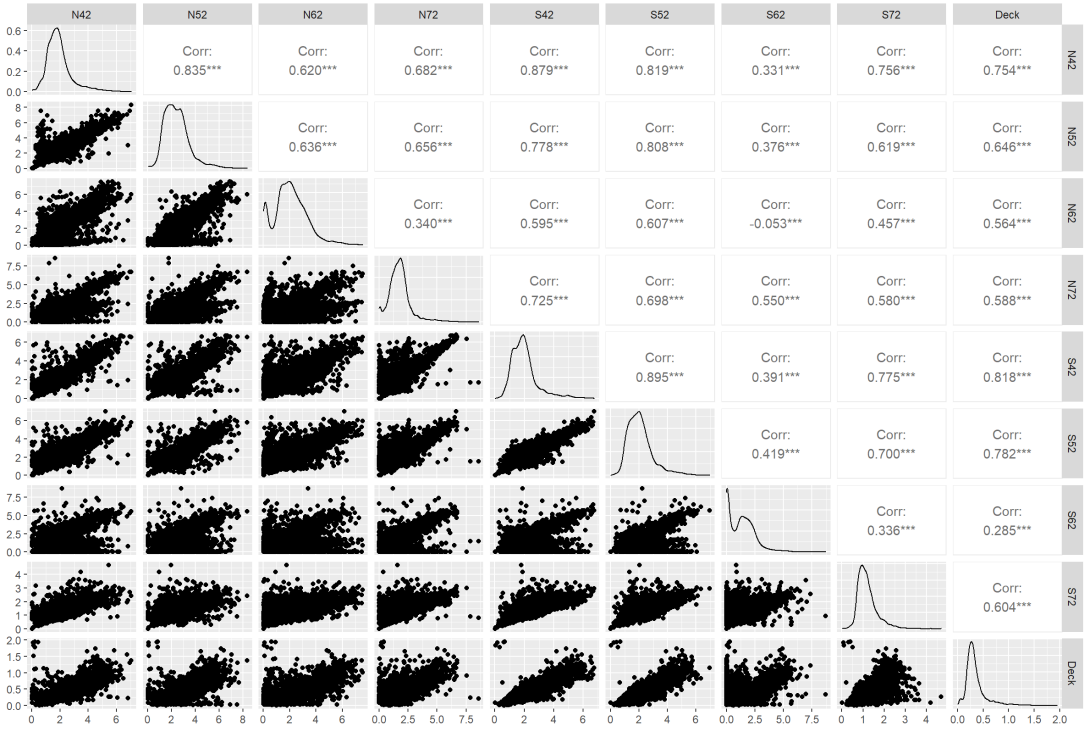

Figure 4.9: Correlation coefficient of 8 RMS dynamic responses ($A = \sqrt{A_x^2 + A_y^2}$) for 8 hangers and RMS of the deck on bridge span 2 [35].

As presented in the right plot of Figure 4.10 for bridge span 2, the hangers S42, S52, and N42 had the strongest influence on the IncNodePurity values with strength values of 64.71, 55.57, and 45.63, respectively, while the hanger S62 had the lowest impact with a value of 8.82. The hangers N52, N62, N72, and S72 also had a significant effect with IncNodePurity values of 26.54, 21.73, 18.23, and 17.14, respectively. In addition, these hangers had a moderate correlation considering the correlation coefficient analysis. Therefore, based on these findings, the input variables could be divided into two groups such that one group had a strong correlation (N42, S42, S52), and the other group had a moderate and weak correlation (N52, N62, N72, S62, S72).

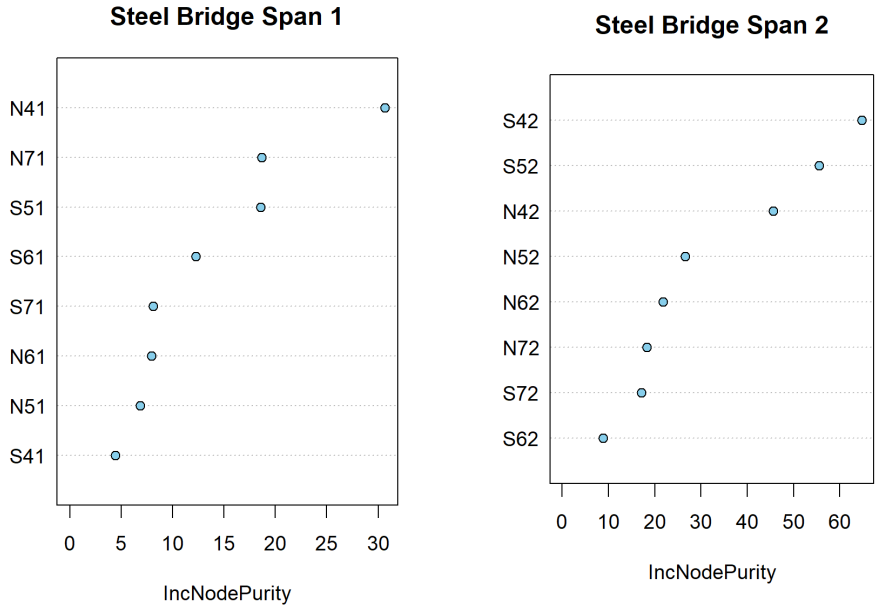

Figure 4.10: The results of random forest analysis for 8 input RMS variables on bridge spans 1 and 2 [35].

4.4.2 ANN and ANFIS regression models for SHM of span 1

The predicted results of the optimized ANN models are summarized in Table 4.2 for the RMS of dynamic behavior in the deck span 1 that were produced from the RMS values of dynamic responses on eight hangers using the GA optimization approach of the ANN architecture corresponding to six case studies. Based on the investigation of optimized ANN architectures, the influence of the number of hidden units in various layers for the cases 1, 2, 3, 4, 5 and 6 as shown in Figures 4.11, 4.13, 4.15, 4.17, 4.19 and 4.21, respectively. The accuracy of the optimized ANN structures could be determined corresponding to the lowest RMSE values of the optimal zone in the range with the number of hidden units, such as: {1,..., 30} neurons in the first layer, the second layer and the third layer.

Table 4.2: The results of optimized ANN models for bridge span 1 [35].

Strategies	Hidden Layers	Optimized Neurons	Data Sets	R^2	RMSE	MAE	MAPE	NSE
Case 1 (16 inputs): N41x, N41y, N51x, N51y, N61x, N61y, N71x, N71y, S41x, S41y, S51x, S51y, S61x, S61y, S71x, S71y	1	{9}	Training	0.83	0.0543	0.0379	15.27	0.83
			Testing	0.71	0.0656	0.0391	16.22	0.70
	2	{15, 12}	Training	0.84	0.0518	0.0366	14.53	0.84
			Testing	0.78	0.0555	0.0386	16.10	0.78
	3	{17, 11, 7}	Training	0.85	0.0501	0.0357	14.28	0.85
			Testing	0.77	0.0570	0.0375	15.82	0.77
Case 2 (4 inputs): N41x, N41y S51y, S61y	1	{27}	Training	0.73	0.0681	0.0415	18.40	0.73
			Testing	0.70	0.0662	0.0426	17.77	0.69
	2	{10, 9}	Training	0.80	0.0583	0.0401	16.81	0.80
			Testing	0.73	0.0626	0.0419	17.54	0.72
	3	{26, 16, 2}	Training	0.83	0.0541	0.0384	15.34	0.83
			Testing	0.74	0.0615	0.0417	18.00	0.73
Case 3 (12 inputs): N51x, N51y, N61x, N61y, N71x, N71y, S41x, S41y, S51x, S61x, S71x, S71y	1	{23}	Training	0.76	0.0646	0.0403	17.08	0.76
			Testing	0.69	0.0673	0.0439	18.59	0.68
	2	{26, 16}	Training	0.82	0.0551	0.0388	15.40	0.82
			Testing	0.72	0.0631	0.0427	17.95	0.72
	3	{19, 15, 10}	Training	0.83	0.0532	0.0378	14.94	0.83
			Testing	0.72	0.0630	0.0433	18.61	0.72
Case 4 (8 inputs): N41, N51, N61, N71, S41, S51, S61, S71	1	{24}	Training	0.67	0.0752	0.0429	19.62	0.67
			Testing	0.76	0.0587	0.0418	17.18	0.76
	2	{17, 30}	Training	0.79	0.0591	0.0388	15.74	0.79
			Testing	0.74	0.0611	0.0419	17.65	0.74
	3	{24, 10, 9}	Training	0.79	0.0601	0.0400	15.79	0.79
			Testing	0.73	0.0617	0.0416	17.32	0.73
Case 5 (3 inputs): N41, N71, S51	1	{10}	Training	0.65	0.0778	0.0437	20.51	0.65
			Testing	0.75	0.0592	0.0429	17.75	0.75
	2	{13, 17}	Training	0.75	0.0655	0.0421	17.84	0.75
			Testing	0.74	0.0607	0.0432	18.10	0.74
	3	{20, 16, 13}	Training	0.77	0.0632	0.0413	17.34	0.77
			Testing	0.74	0.0613	0.0426	18.12	0.73
Case 6 (5 inputs): N51, N61, S41, S61, S71	1	{29}	Training	0.59	0.0845	0.0515	22.92	0.58
			Testing	0.63	0.0730	0.0516	21.17	0.63
	2	{19, 10}	Training	0.72	0.0690	0.0474	19.11	0.72
			Testing	0.63	0.0736	0.0512	20.92	0.62
	3	{14, 23, 10}	Training	0.72	0.0695	0.0470	19.40	0.72
			Testing	0.64	0.0716	0.0496	20.83	0.64

For the case 1 with 16 inputs, the result of the testing data sets in which the use of one layer (R^2~0.71 moderate, NSE~0.70 good) could not be sufficient to provide high predictive precision compared to the use of two layers (R^2~0.78 substantial, NSE~0.78 very good) and three layers (R^2~0.77 substantial, NSE~0.77 very good). Based on the R^2, MAE and NSE values of the case 2 with 4 inputs, it can be observed that the testing data sets using two layers (R^2~0.73 moderate, MAE~0.0419, NSE~0.72 good) and three layers (R^2~0.74 moderate, MAE~0.0417, NSE~0.73 good) in the optimal ANN architecture were better than using one layer (R^2~0.70 moderate, MAE~0.0426, NSE~0.69 good). For the case 3 with 12 inputs, the best performances were obtained with optimal ANN models, which provided accurate testing data sets for using one layer (R^2~0.69 moderate, MAPE~18.59 good, NSE~0.68 good), two layers (R^2~0.72 moderate, MAPE~17.95 good, NSE~0.72 good) and three layers (R^2~0.72 moderate, MAPE~18.61 good, NSE~0.72 good).

For the case 4 with 8 inputs, the result of testing data sets in optimized ANN models using one layer (R^2~0.76 substantial, MAPE~17.18 good, NSE~0.76 very good) was better than using two layers (R^2~0.74 moderate, MAPE~17.65 good, NSE~0.74 good) and three layers (R^2~0.73 moderate, MAPE~17.32 good, NSE~0.73 good). The results of the case 5 with 3 inputs showed that testing data sets in optimized ANN models performed the best using one layer (R^2~0.75 moderate, MAPE~17.75 good, NSE~0.75 good); two layers (R^2~0.74 moderate, MAPE~18.10 good, NSE~0.74 good), and three layers (R^2~0.74 moderate, MAPE~18.12 good, NSE~0.73 good). From the case 6 with 5 inputs, there was a significant decrease in the metrics of using one layer (R^2~0.63 moderate, MAPE~21.17 reasonable, NSE~0.63 satisfactory); two layers (R^2~0.63 moderate, MAPE~20.92 reasonable, NSE~0.62 satisfactory); and three layers (R^2~0.64 moderate, MAPE~20.83 reasonable, NSE~0.64 satisfactory). However, the training data sets of two and three layers had a higher R^2, MAPE, and NSE-value than using one layer for the cases 4, 5 and 6.

The results of the regression graphs between the predicted and actual data sets of the optimized ANN models for training, testing, and all data sets in cases 1, 2, 3, 4, 5 and 6 as shown in Figures 4.12, 4.14, 4.16, 4.18, 4.20, and 4.22, respectively. Overall, the optimized ANN models performed very well with all R score values greater than 0.75 for predicting all data sets. The performance of the case 6 achieved the lowest R value and slope of (0.75, 0.58) one layer, (0.79, 0.67) two layers, and (0.75, 0.58) three layers, while the ANN models of the case 3 had the best performance with the R value and slope of (0.83, 0.71), (0.84, 0.80), and (0.86, 0.76) for one, two, and three layers, respectively. In addition, the results of the cases 1, 2, and 3 indicated that the ANN model of the case 1 had the best performance of two layers with R values (0.86 training, 0.87 testing) and slopes (0.75 training, 0.82 testing), followed by the case 2 with R values (0.84 training, 0.84 testing) and slopes (0.73 training, 0.79 testing) under three layers of ANN model; the case 3 with R values (0.87 training, 0.84 testing) and slopes (0.76 training, 0.77 testing) under three layers of optimized ANN model. With comparison of ANN models in all cases 4, 5, and 6, it can be observed that the case 5 had the best accuracy of updated two layers with the R scores (0.79 training, 0.84 testing) and slopes (0.74 training, 0.84 testing), followed by the case 4 with the R values (0.81 training, 0.86 testing) and slopes (0.67 training, 0.76 testing) under two layers.

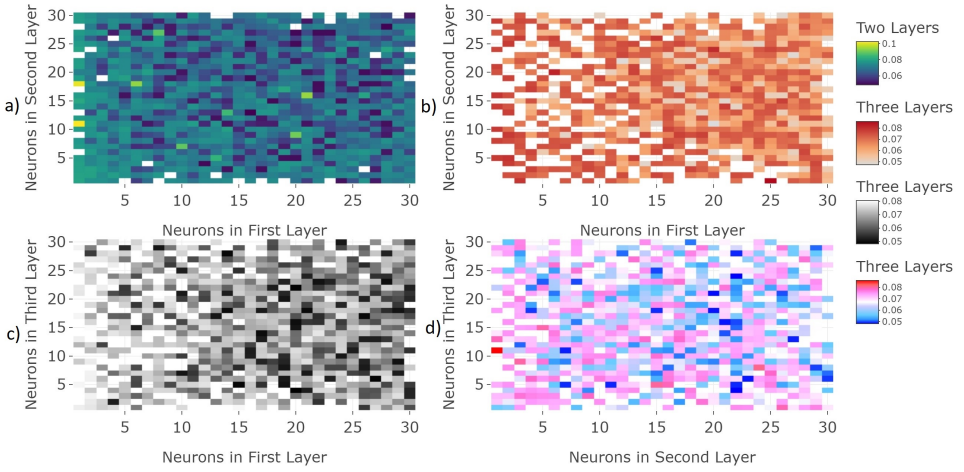

Figure 4.11: The influence of the number of neurons in hidden layers on RMSE index of training data in optimized ANN models for the case 1: a) neurons in first layer versus second layer in two hidden layers; b) first layer versus second layer; c) first layer versus third layer; d) second layer versus third layer in three hidden layers [35].

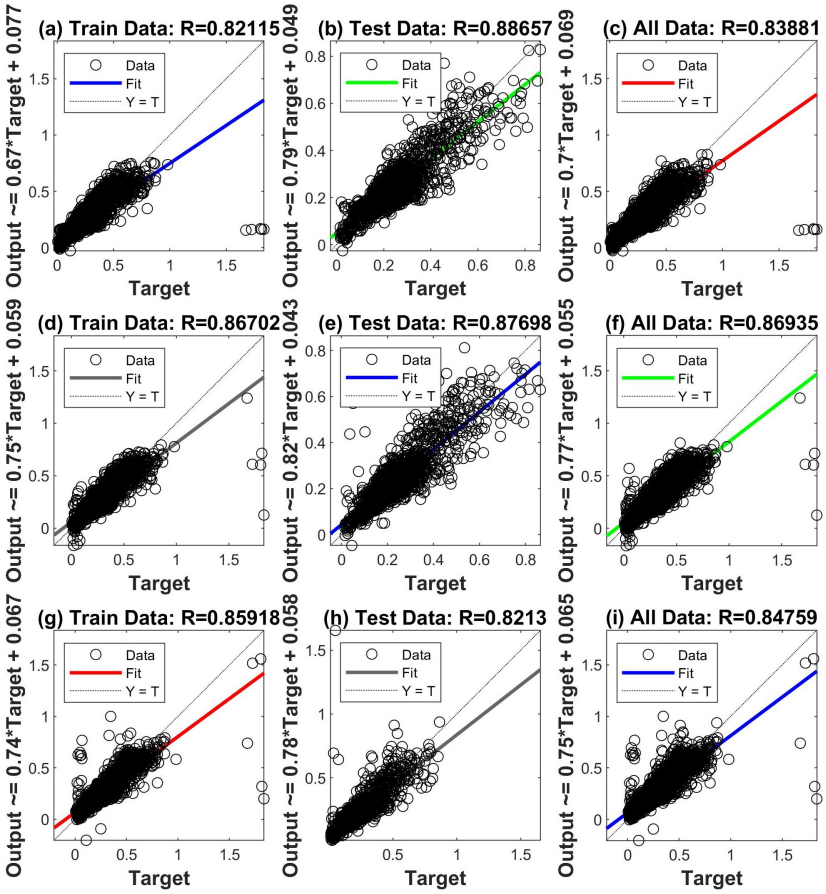

Figure 4.12: Relationship between predicted and actual values in optimized ANN models for the case 1: (a), (b), (c) for 1 hidden layer; (d), (e), (f) for 2 hidden layers; (g), (h), (i) for 3 hidden layers; (units: m/s^2) [35].

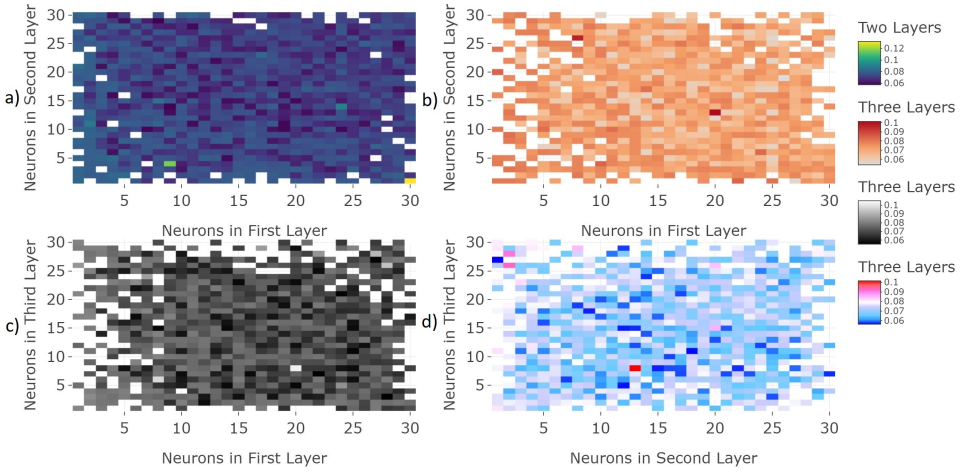

Figure 4.13: The influence of the number of neurons in hidden layers on RMSE index of training data in optimized ANN models for the case 2: a) neurons in first layer versus second layer in two hidden layers; b) first layer versus second layer; c) first layer versus third layer; d) second layer versus third layer in three hidden layers [35].

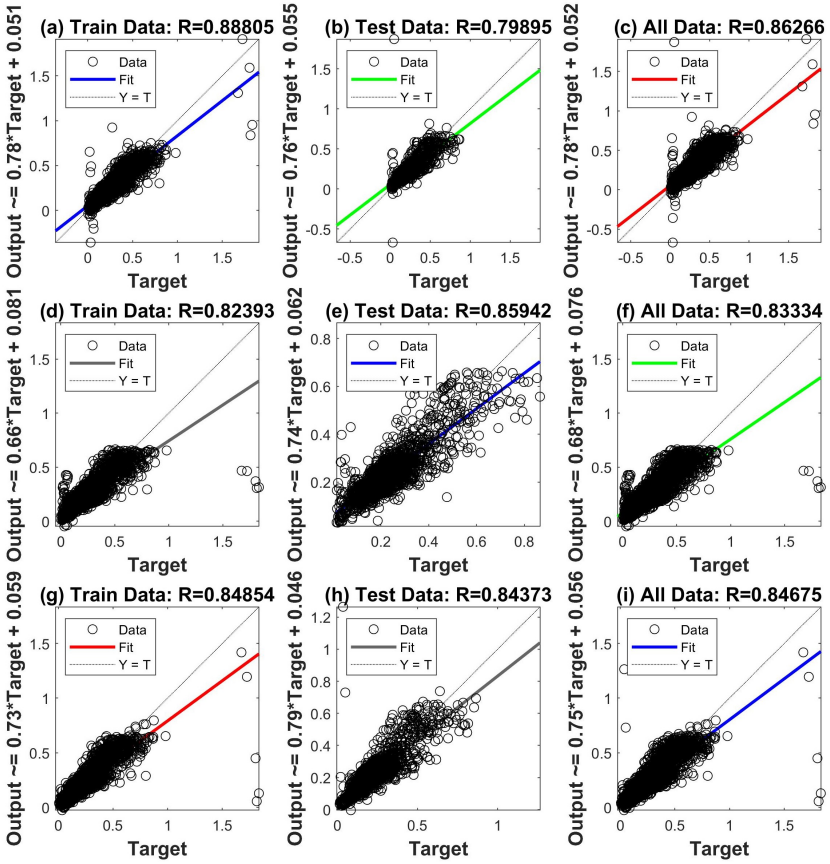

Figure 4.14: Relationship between predicted and actual values in optimized ANN models for the case 2: (a), (b), (c) for 1 hidden layer; (d), (e), (f) for 2 hidden layers; (g), (h), (i) for 3 hidden layers; (units: m/s^2) [35].

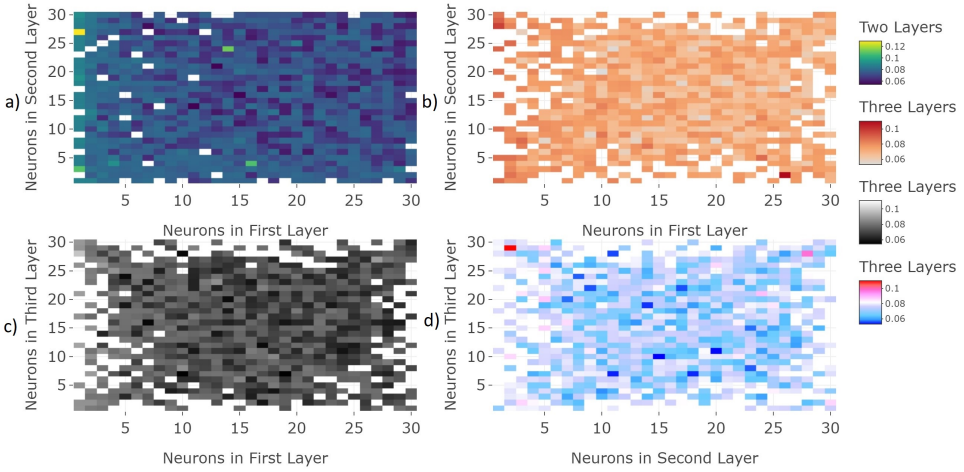

Figure 4.15: The influence of the number of neurons in hidden layers on RMSE index of training data in optimized ANN models for the case 3: a) neurons in first layer versus second layer in two hidden layers; b) first layer versus second layer; c) first layer versus third layer; d) second layer versus third layer in three hidden layers [35].

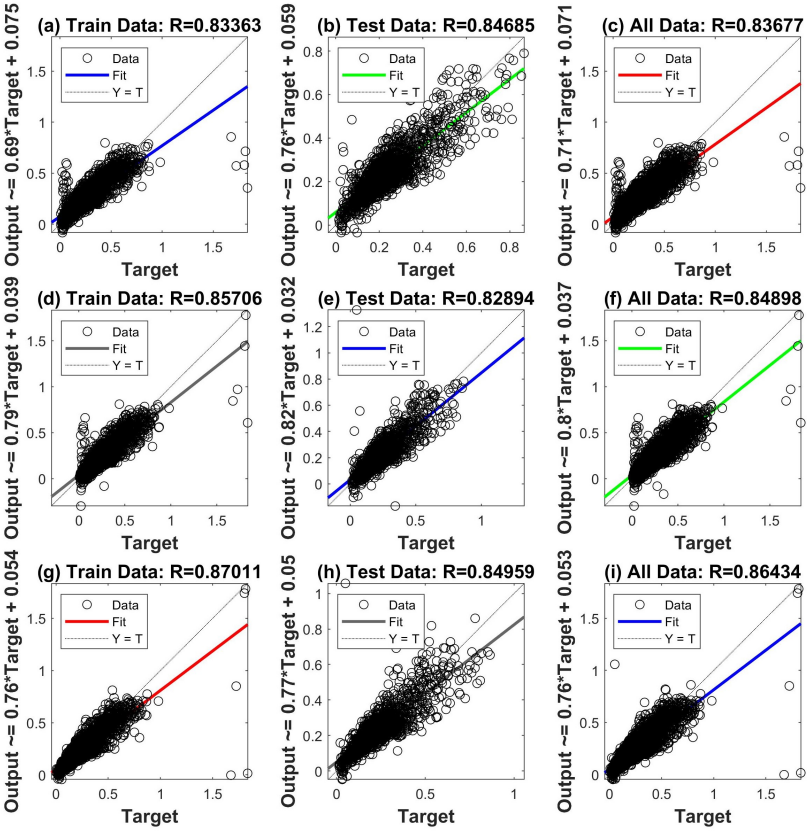

Figure 4.16: Relationship between predicted and actual values in optimized ANN models for the case 3: (a), (b), (c) for 1 hidden layer; (d), (e), (f) for 2 hidden layers; (g), (h), (i) for 3 hidden layers; (units: m/s^2) [35].

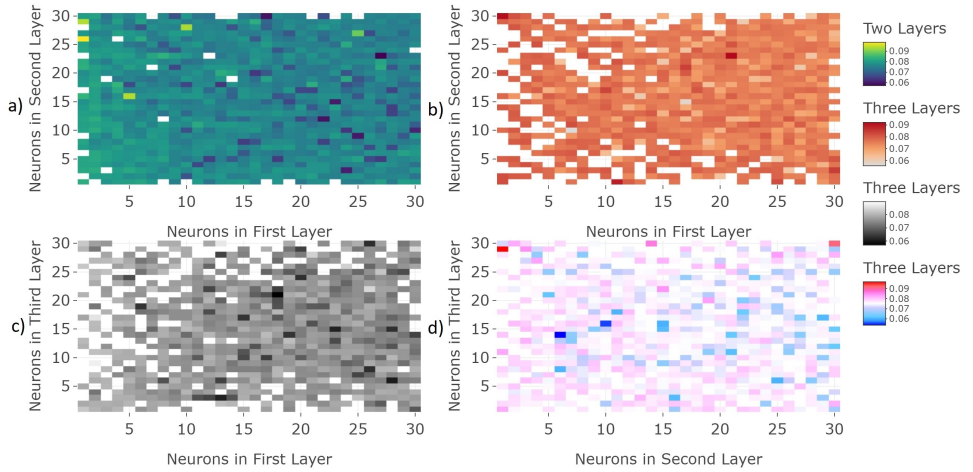

Figure 4.17: The influence of the number of neurons in hidden layers on RMSE index of training data in optimized ANN models for the case 4: a) neurons in first layer versus second layer in two hidden layers; b) first layer versus second layer; c) first layer versus third layer; d) second layer versus third layer in three hidden layers [35].

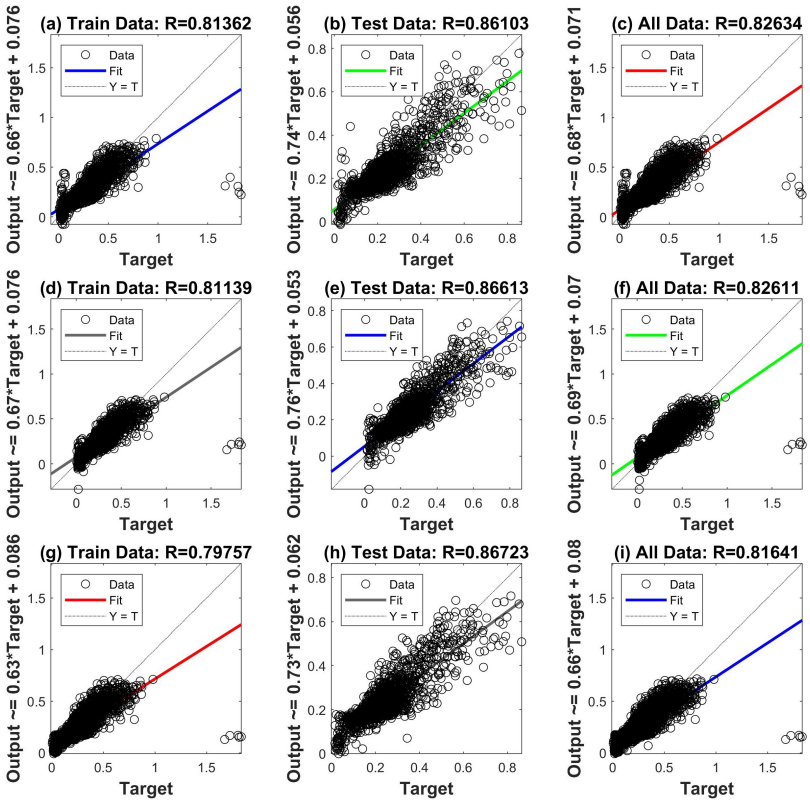

Figure 4.18: Relationship between predicted and actual values in optimized ANN models for the case 4: (a), (b), (c) for 1 hidden layer; (d), (e), (f) for 2 hidden layers; (g), (h), (i) for 3 hidden layers; (units: m/s^2) [35].

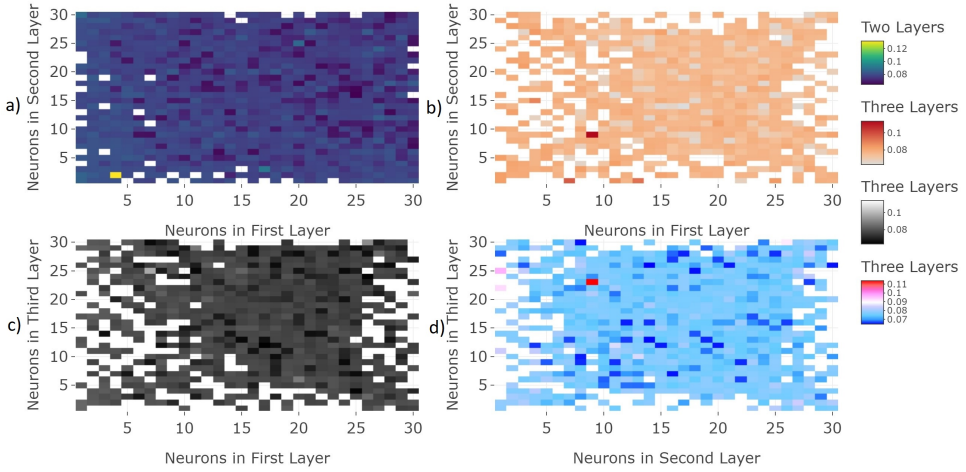

Figure 4.19: The influence of the number of neurons in hidden layers on RMSE index of training data in optimized ANN models for the case 5: a) neurons in first layer versus second layer in two hidden layers; b) first layer versus second layer; c) first layer versus third layer; d) second layer versus third layer in three hidden layers [35].

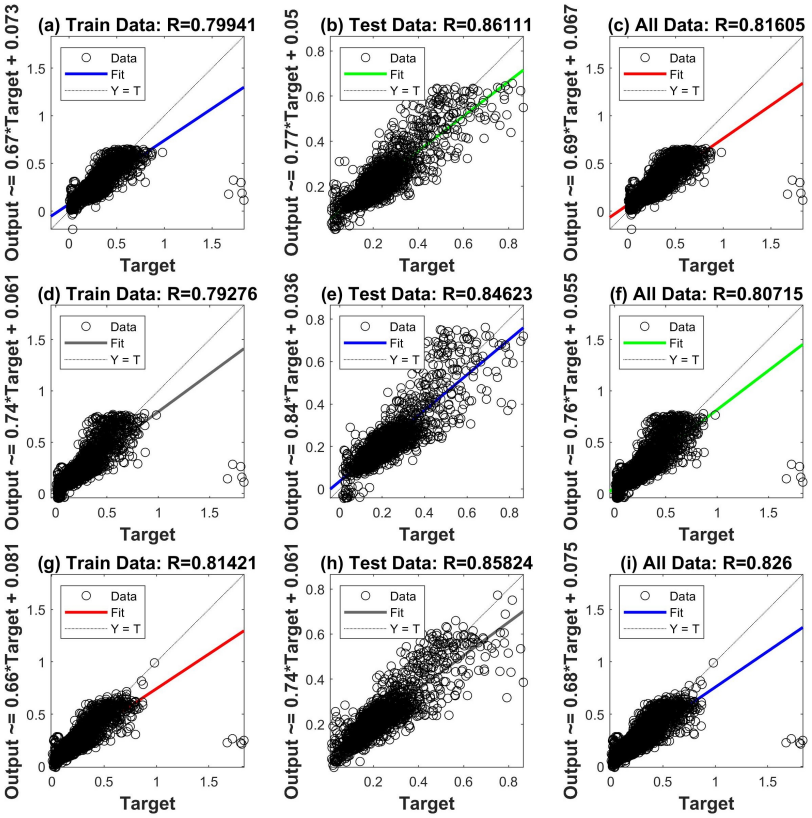

Figure 4.20: Relationship between predicted and actual values in optimized ANN models for the case 5: (a), (b), (c) for 1 hidden layer; (d), (e), (f) for 2 hidden layers; (g), (h), (i) for 3 hidden layers; (units: m/s^2) [35].

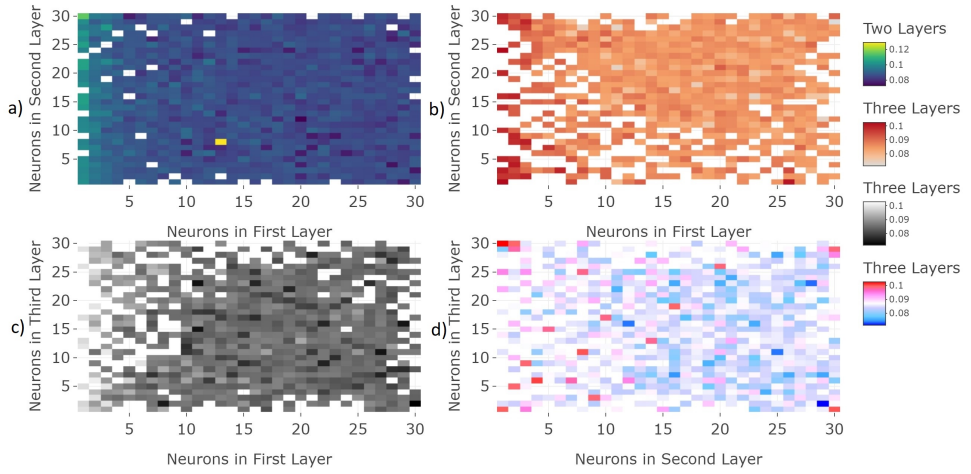

Figure 4.21: The influence of the number of neurons in hidden layers on RMSE index of training data in optimized ANN models for the case 6: a) neurons in first layer versus second layer in two hidden layers; b) first layer versus second layer; c) first layer versus third layer; d) second layer versus third layer in three hidden layers [35].

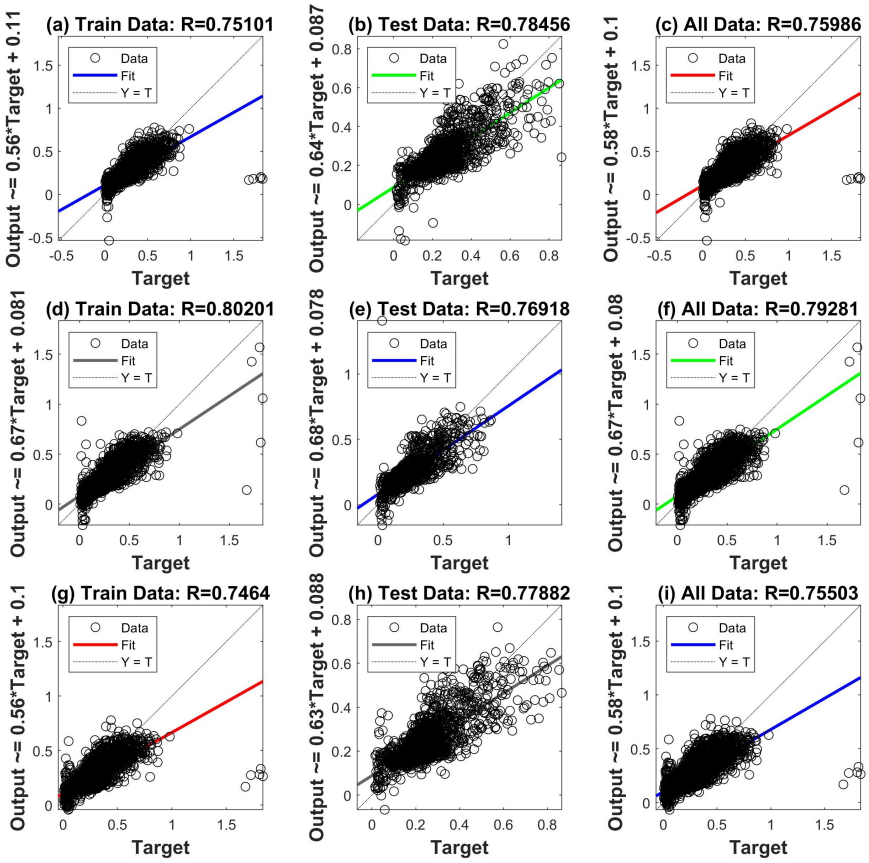

Figure 4.22: Relationship between the predicted and actual values in optimized ANN models for the case 6: (a), (b), (c) for 1 hidden layer; (d), (e), (f) for 2 hidden layers; (g), (h), (i) for 3 hidden layers; (units: m/s^2) [35].

Table 4.3 shows the results of the ANFIS models to predict the RMS value of the dynamic behavior on the deck span 1 produced from the RMS values of the dynamic responses of the hangers. It could be seen that the ANFIS model of the case 2 with 4 input variables had the best prediction accuracy in testing data (R^2~0.75 substantial, MAPE~22.63 reasonable, NSE~0.74 good). The ANFIS model in the case 6 had the lowest accurate prediction focused on the testing part that the magnitudes of R^2, MAPE, and NSE reach values of 0.56 moderate, 30.53 reasonable, and 0.56 satisfactory, respectively.

Based on R^2 and MAPE criteria, it can be seen that all optimized ANN models showed better results than the ANFIS models developed. For example, the R^2 values of training and testing data sets obtained from the ANFIS model for the case 1 are 0.69 and 0.72 which were lower than the updated ANN models with three layers, are 0.85 and 0.77, respectively. In the case 2, R^2 and MAPE results of (0.71, 23.22%) and (0.75, 22.63%) were obtained for training and testing data of the ANFIS model, respectively, where these values were (0.83, 15.34%), (0.74, 18.00%) for the optimized ANN model with three layers, which indicated better prediction. As a result of the case 3, R^2 and MAPE of the ANFIS model were 0.67 and 25.57% for testing data, while the values of the ANN model with three layers were 0.72 and 18.61% more accurate compared to this ANFIS model. With the case 4, ANFIS model provided the lower value of R^2, which was 0.70, while the R^2 value of the GA-based ANN model with three layers was 0.73 for testing data. The ANN model with three layers for the testing data of the case 5 produced the highest R^2 value of 0.74, while the value R^2 of ANFIS model was 0.71. The lowest value of R^2 obtained from the ANFIS model whose magnitude was 0.56 for the testing data of the case 6, while the R^2 value of ANN model with three layers was 0.64.

Table 4.3: The results of ANFIS models for bridge span 1 [35].

Strategies	Data Sets	R^2	RMSE	MAE	MAPE	NSE
Case 1 (16 inputs): N41x, N41y, N51x, N51y, N61x, N61y, N71x, N71y, S41x, S41y, S51x, S51y, S61x, S61y, S71x, S71y	Training	0.69	0.0717	0.0421	20.95	0.69
	Testing	0.72	0.0659	0.0424	23.52	0.72
Case 2 (4 inputs): N41x, N41y S51y, S61y	Training	0.71	0.0718	0.0426	23.22	0.71
	Testing	0.75	0.0578	0.0413	22.63	0.74
Case 3 (12 inputs): N51x, N51y, N61x, N61y, N71x, N71y, S41x, S41y, S51x, S61x, S71x, S71y	Training	0.64	0.0777	0.0466	24.09	0.64
	Testing	0.67	0.0724	0.0479	25.57	0.67
Case 4 (8 inputs): N41, N51, N61, N71, S41, S51, S61, S71	Training	0.67	0.0749	0.0460	24.15	0.67
	Testing	0.70	0.0657	0.0471	27.14	0.70
Case 5 (3 inputs): N41, N71, S51	Training	0.66	0.0760	0.0433	23.31	0.66
	Testing	0.71	0.0647	0.0438	24.08	0.71
Case 6 (5 inputs): N51, N61, S41, S61, S71	Training	0.59	0.0845	0.0527	28.42	0.59
	Testing	0.56	0.0795	0.0546	30.53	0.56

Figures 4.23 and 4.24 show that the R score values for the ANFIS models were carried out from the case 1 to 6 with all regression plots of testing, training, and all data sets. The R score measures the strength of the relationship between the actual and predicted samples of ANFIS models in the range from 0 to 1. The higher R value closer to 1 indicates better prediction regression model accuracy. Regarding the R score for all data sets, the ANFIS models performed very well from the lowest R value of 0.76 (case 6) to the highest value of 0.84 (case 2). In terms of the cases 1, 2, and 3, it can be observed that the result of the case 2 (R~0.86 testing, R~0.84 training) had the highest prediction accuracy, the lowest performance was found for the case 3 (R~0.81 testing, R~0.80 training). The comparison of all cases 4, 5, and 6 indicated that the prediction accuracy of the case 5 (R~0.84 testing, R~0.81 training) was higher than in the case 4 (R~0.83 testing, R~0.82 training) and the case 6 (R~0.75 testing, R~0.76 training).

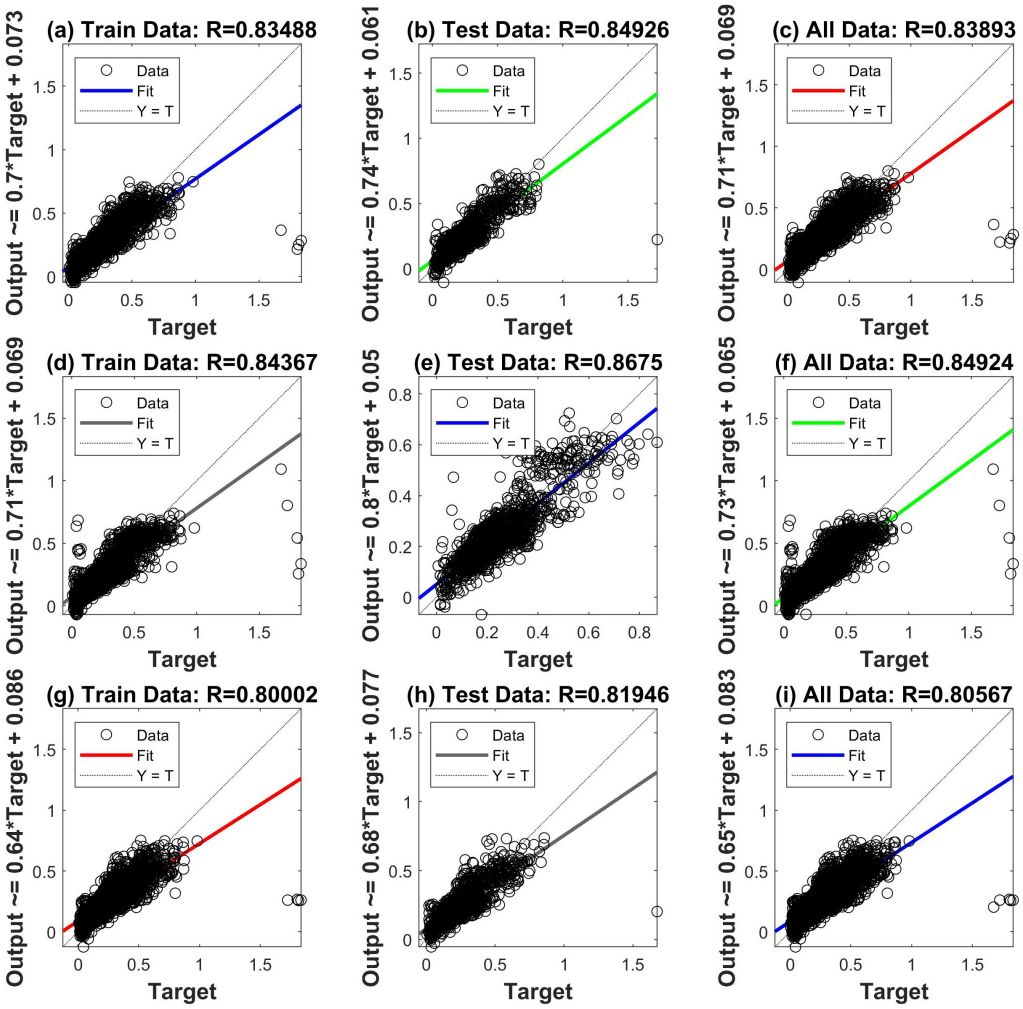

Figure 4.23: Relationship between predicted and actual values in ANFIS models: (a), (b), (c) for the case 1; (d), (e), (f) for the case 2; (g), (h), (i) for the case 3; (units: m/s^2) [35].

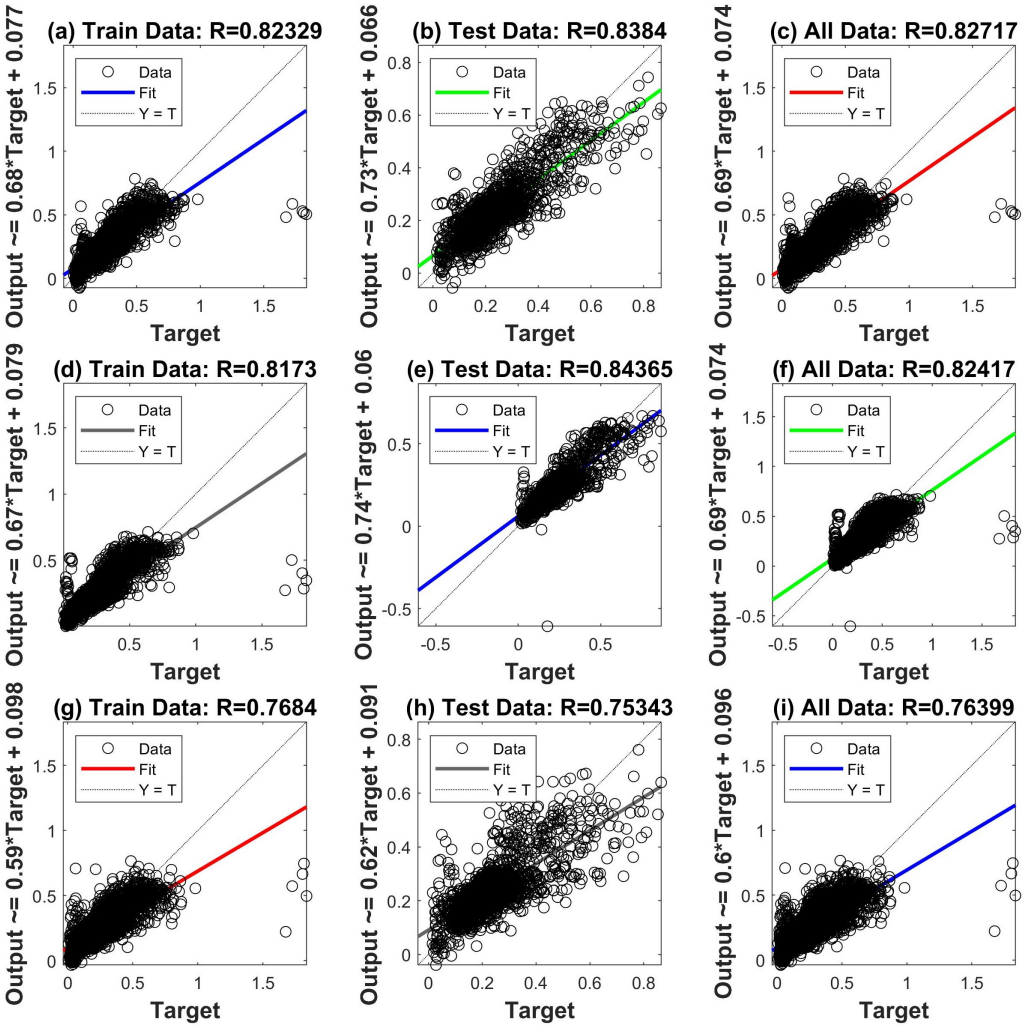

Figure 4.24: Relationship between predicted and actual values in ANFIS models: (a), (b), (c) for the case 4; (d), (e), (f) for the case 5; (g), (h), (i) for the case 6; (units: m/s^2) [35].

4.4.3 ANN and ANFIS regression models for SHM of span 2

The predicted results and the summary of the updated ANN models are shown in Tables 4.4 for the prediction of the RMS values of the dynamic behavior in the deck span 2 based on the RMS values of the dynamic responses of the hangers. Figures 4.25, 4.27, 4.29, 4.31, 4.33, 4.35 illustrated the influence of the number of hidden neurons in various hidden layers of ANN models for the cases 7, 8, 9, 10, 11 and 12, respectively. The lowest RMSE values have been carried out to determine the best ANN architecture.

Table 4.4: The results of optimized ANN models for bridge span 2 [35].

Strategies	Hidden Layers	Optimized Neurons	Data Sets	R^2	RMSE	MAE	MAPE	NSE
Case 7 (16 inputs): N42x, N42y, N52x, N52y, N62x, N62y, N72x, N72y, S42x, S42y, S52x, S52y, S62x, S62y, S72x, S72	1	{15}	Training	0.76	0.0948	0.0612	17.90	0.76
			Testing	0.78	0.0918	0.0637	18.46	0.78
	2	{14, 21}	Training	0.83	0.0791	0.0581	16.01	0.83
			Testing	0.75	0.0979	0.0628	17.98	0.75
	3	{17, 13, 11}	Training	0.84	0.0770	0.0568	15.38	0.84
			Testing	0.76	0.0977	0.0623	17.71	0.75
Case 8 (7 inputs): N42x, N42y, S42x, S42y, S52x, S52y, S72y	1	{10}	Training	0.76	0.0950	0.0635	18.48	0.76
			Testing	0.76	0.0964	0.0655	18.47	0.76
	2	{23, 8}	Training	0.78	0.0899	0.0622	17.85	0.78
			Testing	0.77	0.0936	0.0643	18.62	0.77
	3	{25, 19, 11}	Training	0.77	0.0915	0.0617	18.07	0.77
			Testing	0.79	0.0904	0.0628	18.39	0.79
Case 9 (9 inputs): N52x, N52y, N62x, N62y, N72y, N72x, S62x, S62y, S72x	1	{20}	Training	0.69	0.1071	0.0679	20.39	0.69
			Testing	0.72	0.1053	0.0712	20.42	0.71
	2	{25, 14}	Training	0.78	0.0909	0.0646	18.07	0.78
			Testing	0.69	0.1124	0.0722	21.27	0.67
	3	{25, 23, 13}	Training	0.77	0.0929	0.0635	18.01	0.77
			Testing	0.70	0.1084	0.0722	21.11	0.70
Case 10 (8 inputs): N42, N52, N62, N72, S42, S52, S62, S72	1	{18}	Training	0.75	0.0985	0.0646	18.66	0.75
			Testing	0.77	0.0902	0.0650	18.31	0.77
	2	{24, 14}	Training	0.74	0.0977	0.0629	18.68	0.74
			Testing	0.78	0.0929	0.0653	18.45	0.78
	3	{25, 18, 9}	Training	0.79	0.0890	0.0605	17.08	0.79
			Testing	0.74	0.1022	0.0671	19.26	0.73
Case 11 (3 inputs): N42, S42, S52	1	{13}	Training	0.73	0.0995	0.0645	19.28	0.73
			Testing	0.76	0.0959	0.0663	19.29	0.76
	2	{21, 2}	Training	0.76	0.0950	0.0641	18.78	0.76
			Testing	0.76	0.0960	0.0663	19.09	0.76
	3	{21, 7, 16}	Training	0.75	0.0959	0.0633	18.69	0.75
			Testing	0.77	0.0935	0.0647	18.99	0.77
Case 12 (5 inputs): N52, N62, N72, S62, S72	1	{14}	Training	0.68	0.1088	0.0714	20.66	0.68
			Testing	0.68	0.1111	0.0774	21.58	0.68
	2	{23, 19}	Training	0.69	0.1077	0.0704	20.40	0.69
			Testing	0.70	0.1081	0.0753	20.93	0.70
	3	{20, 18, 11}	Training	0.69	0.1077	0.0708	20.68	0.69
			Testing	0.70	0.1074	0.0749	20.73	0.70

For the case 7, the optimized ANN models showed the prediction accuracy of testing data sets for one layer (R^2~0.78 substantial, MAPE~18.46 good, NSE~0.78 very good); two layers (R^2~0.75 substantial, MAPE~17.98, NSE~0.75 good) and three layers (R^2~0.76 substantial, MAPE~17.71 good, NSE~0.75 good). For the case 8, the prediction accuracies of optimized ANN models were obtained for testing data sets using one layer (R^2~0.76 substantial, MAPE~18.47 good, NSE~0.76 very good); two layers (R^2~0.77 substantial, MAPE~18.62 good, NSE~0.77 very good) and three layers (R^2~0.79 substantial, MAPE~18.39 good, NSE~0.79 very good). For the case 9, the prediction accuracy values of testing data sets in updated ANN models were achieved for one layer (R^2~0.72 moderate, MAPE~20.42 reasonable, NSE~0.71 good); two layers (R^2~0.69 moderate, MAPE~21.27 reasonable, NSE~0.67 good) and three layers (R^2~0.70 moderate, MAPE~21.11 reasonable, NSE~0.70 good).

Furthermore, the case 10 showed that the forecast accuracy values of the ANN models for testing data sets with one layer (R^2~0.77 substantial, MAPE~18.31 good, NSE~0.77 very good); two layers (R^2~0.78 substantial, MAPE~18.45 good, NSE~0.78 very good) and three layers (R^2~0.74 moderate, MAPE~19.26 good, NSE~0.73 good). For the case 11, the ANN models showed the best prediction accuracy of testing data sets for one layer (R^2~0.76 substantial, MAPE~19.29 good, NSE~0.76 very good); two layers (R^2~0.76 substantial, MAPE~19.09 good, NSE~0.76 very good) and three layers (R^2~0.77 substantial, MAPE~18.99 good, NSE~0.77 very good). For the case 12, the forecast accuracy values of ANN models were collected for testing data sets using one layer (R^2~0.68 moderate, MAPE~21.58 reasonable, NSE~0.68 good); two layers (R^2~0.70 moderate, MAPE~20.93 reasonable, NSE~0.70 good) and three layers (R^2~0.70 moderate, MAPE~20.73 reasonable, NSE~0.70 good).

A visualization of the linear regression plots between predicted and observed samples in the optimized ANN models are shown in Figures 4.26, 4.28, 4.30, 4.32, 4.34, 4.36 for the cases 7, 8, 9, 10, 11, and 12 respectively. All optimized ANN models had the best performance and prediction accuracy of R values greater than 0.8 for all data sets under various hidden layers. The ANN model of the case 7 provided the most accurate prediction of R value (0.89) and slope (0.82) with three layers, while the result of the case 12 provided the lowest R value (0.80) and slope (0.66) in the ANN model with one layer to predict all data sets. Based on the results of the comparison in all cases 7, 8 and 9 indicating that the case 7 with three layers had the highest R values (0.90 training, 0.88 testing) and slopes (0.82 training, 0.83 testing), followed by the case 8 with R values (0.86 training, 0.88 testing) and slopes (0.75 training, 0.80 testing) under three layers; and then the case 9 with R values (0.83 training, 0.83 testing) and slopes (0.71 training, 0.75 testing) under three layers. In addition, the ANN model with three layers in the case 10 had the best performance with R values (0.89 training, 0.83 testing) and slopes (0.80 training, 0.79 testing), while the case 11 (three layers) had high values of R scores (0.85 training, 0.87 testing) and slopes (0.73 training, 0.80 testing) and the case 12 (three layers) with R values (0.82 training, 0.81 testing) and slopes (0.68 training, 0.72 testing).

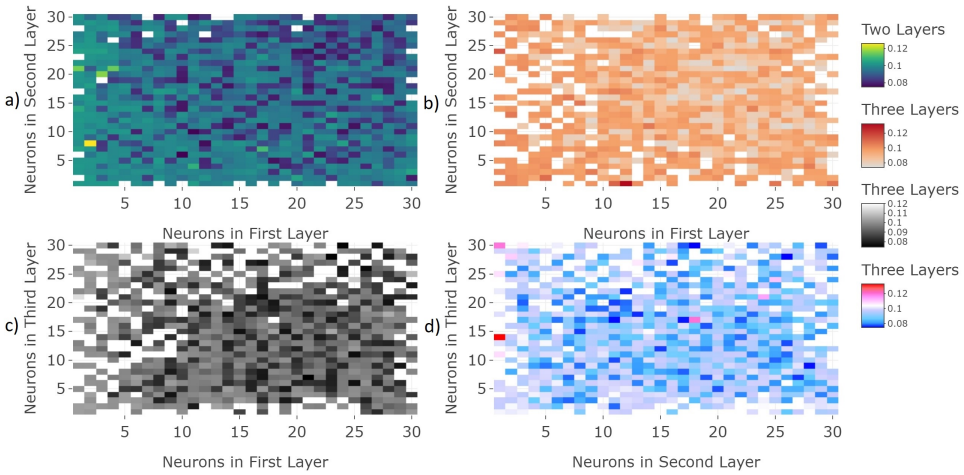

Figure 4.25: The influence of the number of neurons in hidden layers on RMSE index of training data in optimized ANN models for the case 7: a) neurons in first layer versus second layer in two hidden layers; b) first layer versus second layer; c) first layer versus third layer; d) second layer versus third layer in three hidden layers [35].

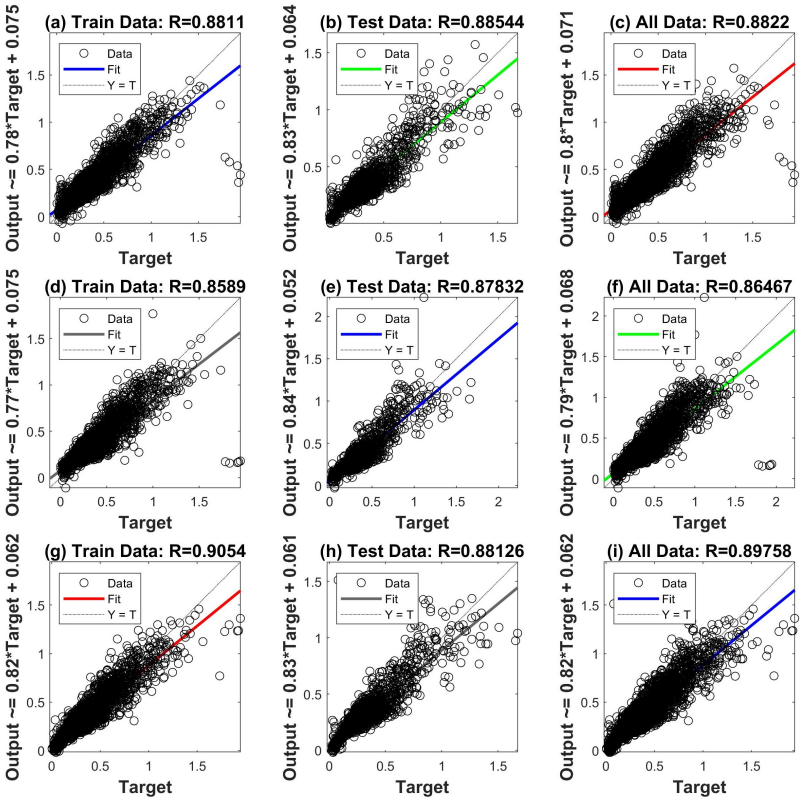

Figure 4.26: Relationship between predicted and actual values in optimized ANN models for the case 7: (a), (b), (c) for 1 hidden layer; (d), (e), (f) for 2 hidden layers; (g), (h), (i) for 3 hidden layers; (units: m/s^2) [35].

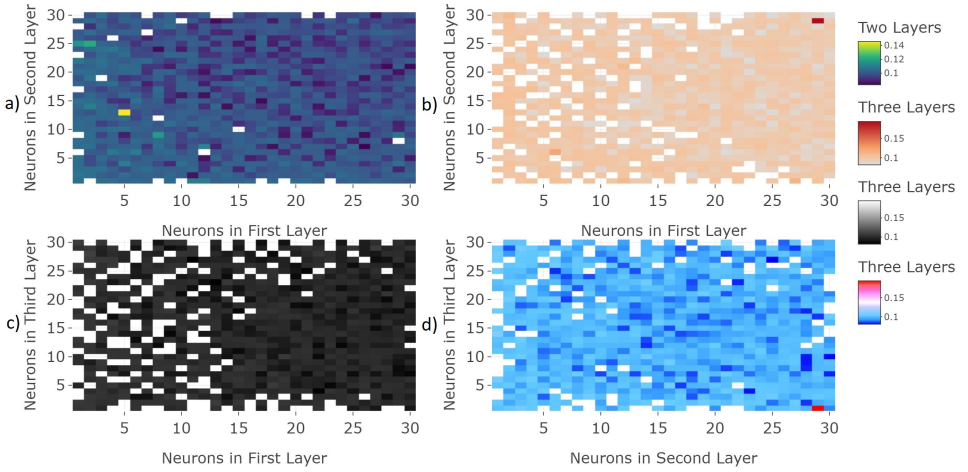

Figure 4.27: The influence of the number of neurons in hidden layers on RMSE index of training data in optimized ANN models for the case 8: a) neurons in first layer versus second layer in two hidden layers; b) first layer versus second layer; c) first layer versus third layer; d) second layer versus third layer in three hidden layers [35].

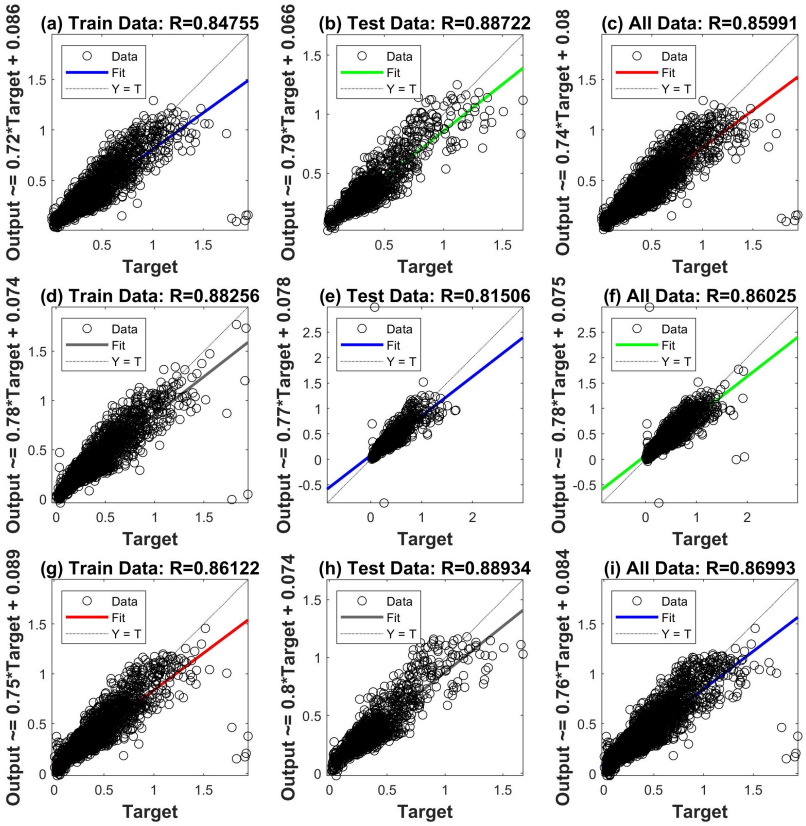

Figure 4.28: Relationship between predicted and actual values in optimized ANN models for the case 8: (a), (b), (c) for 1 hidden layer; (d), (e), (f) for 2 hidden layers; (g), (h), (i) for 3 hidden layers; (units: m/s^2) [35].

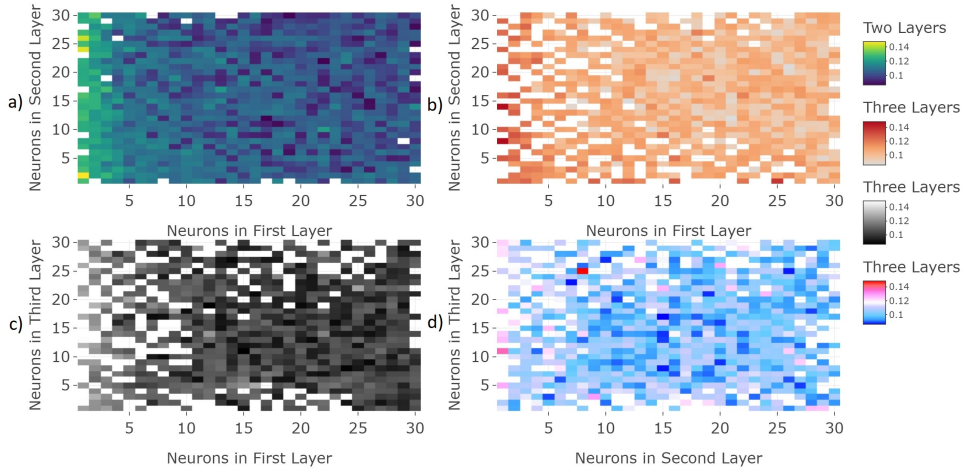

Figure 4.29: The influence of the number of neurons in hidden layers on RMSE index of training data in optimized ANN models for the case 9: a) neurons in first layer versus second layer in two hidden layers; b) first layer versus second layer; c) first layer versus third layer; d) second layer versus third layer in three hidden layers [35].

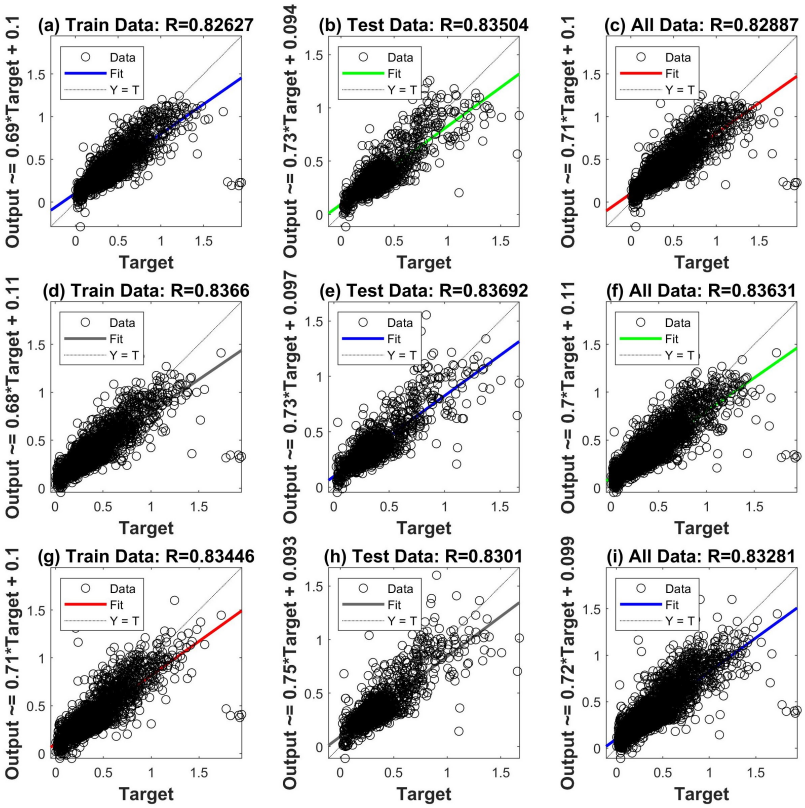

Figure 4.30: Relationship between predicted and actual values in optimized ANN models for the case 9: (a), (b), (c) for 1 hidden layer; (d), (e), (f) for 2 hidden layers; (g), (h), (i) for 3 hidden layers; (units: m/s^2) [35].

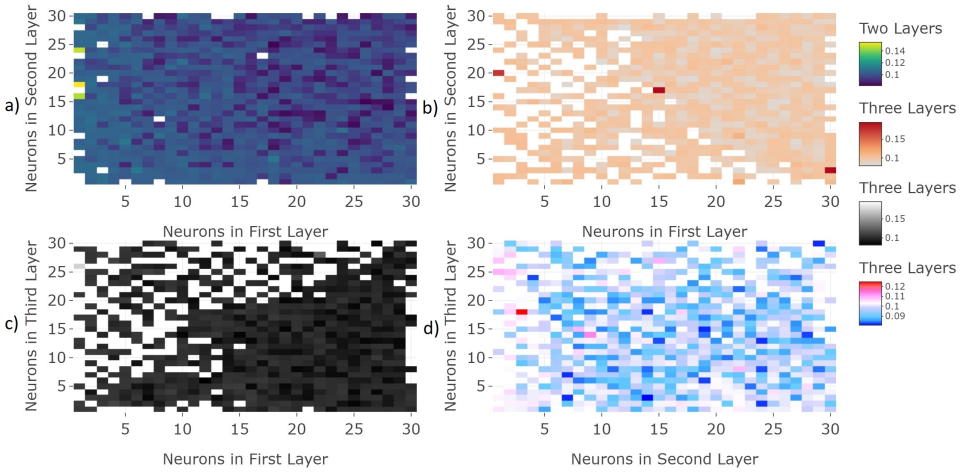

Figure 4.31: The influence of the number of neurons in hidden layers on RMSE index of training data in optimized ANN models for the case 10: a) neurons in first layer versus second layer in two hidden layers; b) first layer versus second layer; c) first layer versus third layer; d) second layer versus third layer in three hidden layers [35].

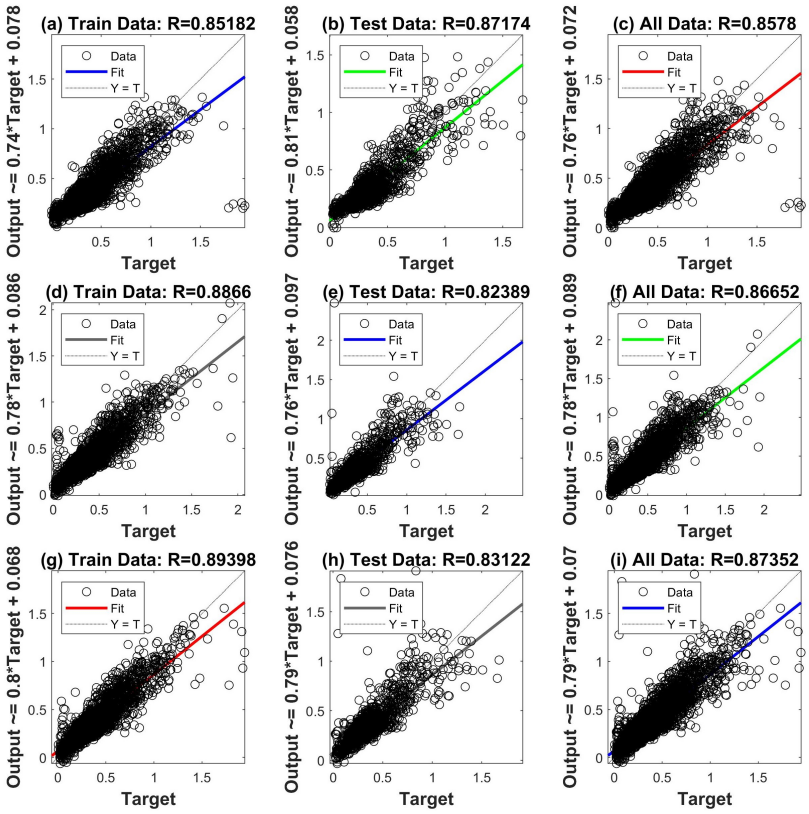

Figure 4.32: Relationship between predicted and actual values in optimized ANN models for the case 10: (a), (b), (c) for 1 hidden layer; (d), (e), (f) for 2 hidden layers; (g), (h), (i) for 3 hidden layers; (units: m/s^2) [35].

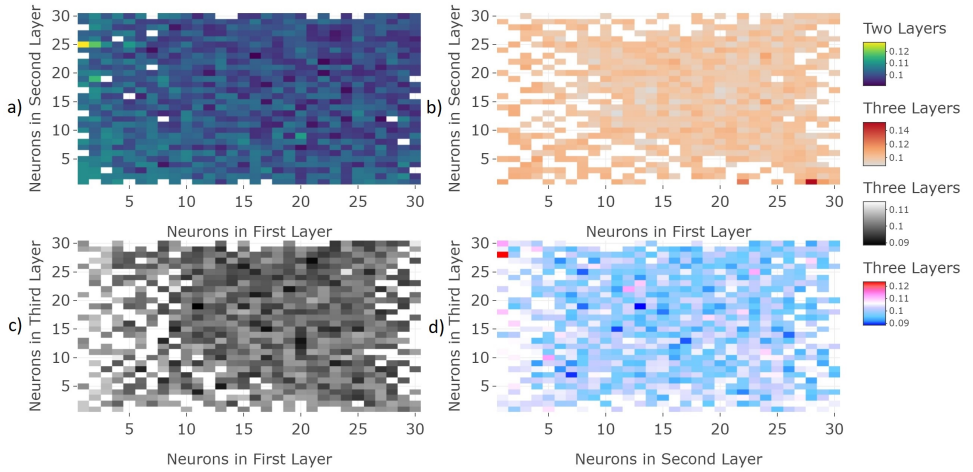

Figure 4.33: The influence of the number of neurons in hidden layers on RMSE index of training data in optimized ANN models for the case 11: a) neurons in first layer versus second layer in two hidden layers; b) first layer versus second layer; c) first layer versus third layer; d) second layer versus third layer in three hidden layers [35].

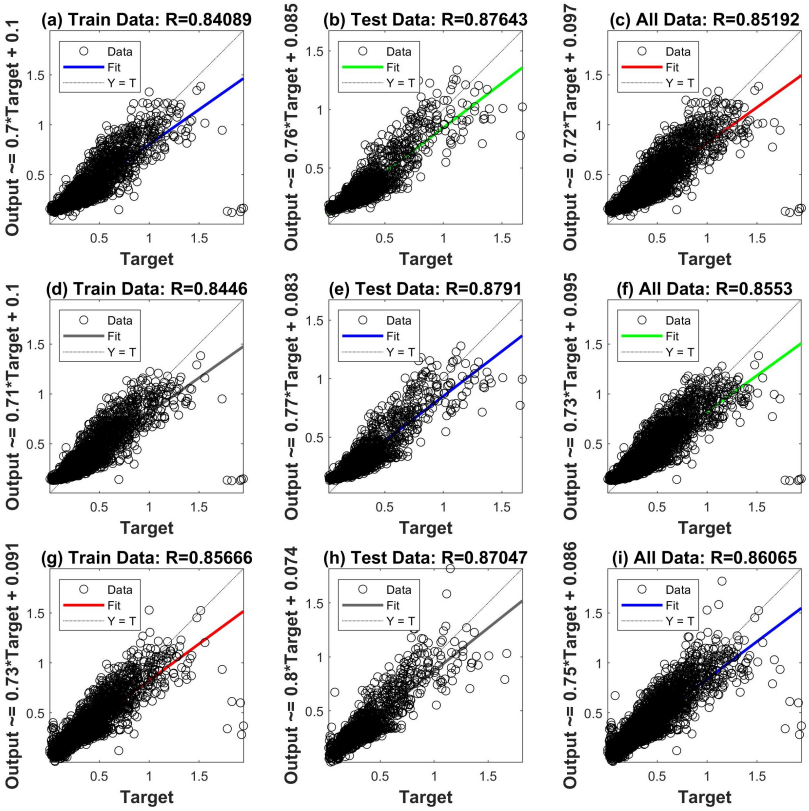

Figure 4.34: Relationship between predicted and actual values in optimized ANN models for the case 11: (a), (b), (c) for 1 hidden layer; (d), (e), (f) for 2 hidden layers; (g), (h), (i) for 3 hidden layers; (units: m/s^2) [35].

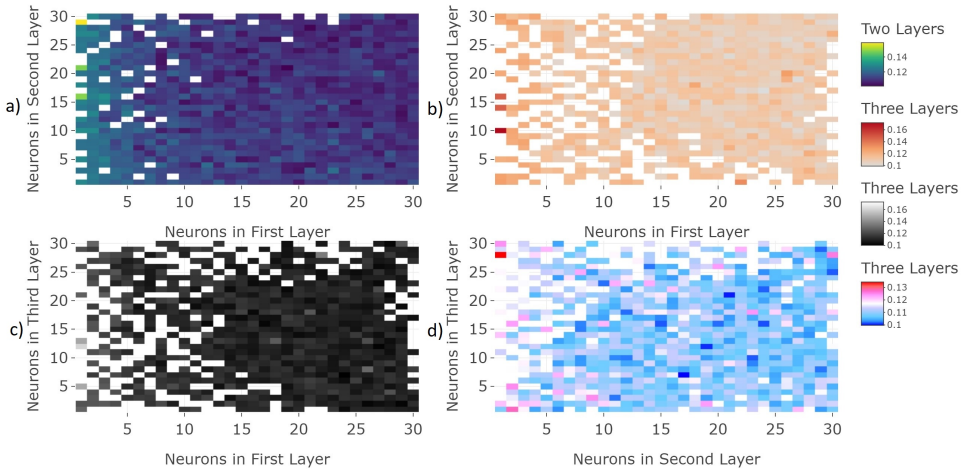

Figure 4.35: The influence of the number of neurons in hidden layers on RMSE index of training data in optimized ANN models for the case 12: a) neurons in first layer versus second layer in two hidden layers; b) first layer versus second layer; c) first layer versus third layer; d) second layer versus third layer in three hidden layers [35].

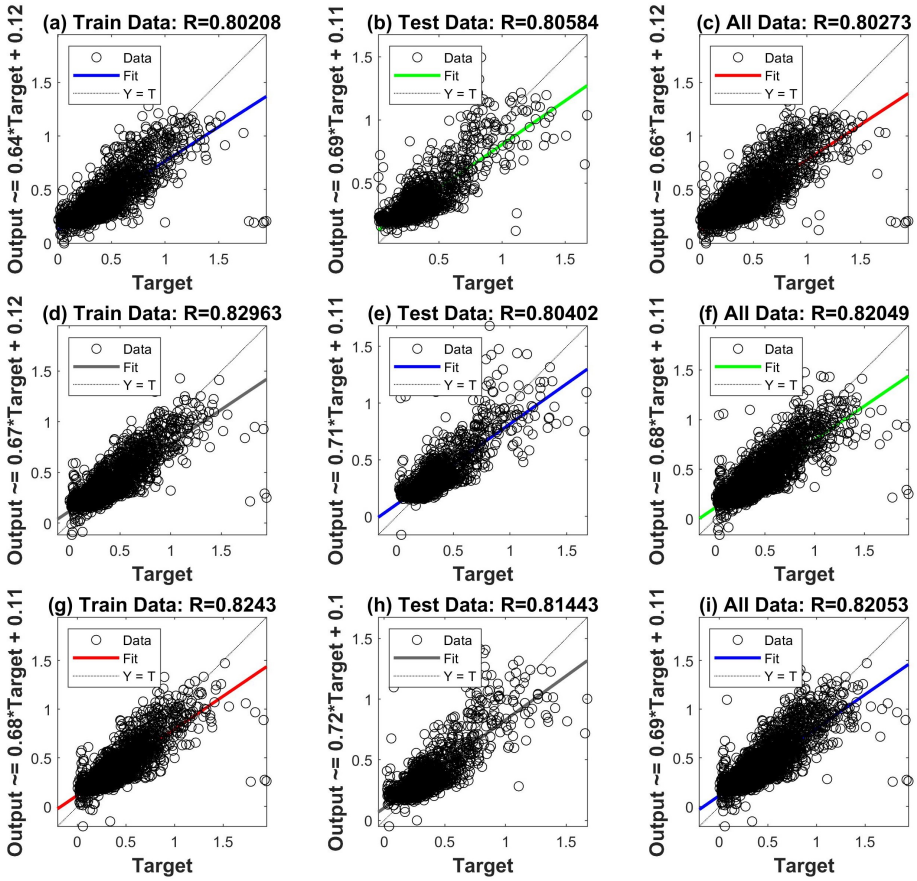

Figure 4.36: Relationship between predicted and actual values in optimized ANN models for the case 12: (a), (b), (c) for 1 hidden layer; (d), (e), (f) for 2 hidden layers; (g), (h), (i) for 3 hidden layers; (units: m/s^2) [35].

Table 4.5 shows the results of the ANFIS models for predicting the RMS values of the vibration signals on the deck span 2 from the RMS values of the vibration signals of the hangers. From the results of R^2, RMSE, MAE, MAPE and NSE metrics, it can be concluded that ANFIS models offered a less reliable and accurate prediction in optimized ANN models. The best ANFIS model was in the case 8 with MAPE and NSE values of (22.10% reasonable, 0.82 very good) and (25.20% reasonable, 0.73 good) for training and testing data sets, respectively. The lowest values of MAPE (29.62% reasonable) and NSE (0.68 good) were for the testing part in the case 12, while these values of the training part were 29.76% reasonable for MAPE and 0.67 good for NSE.

From testing data sets for the case 7, the optimized ANN model (three layers) with MAPE (17.71% good) and NSE (0.75 good) performed better than the ANFIS model with MAPE (21.92% reasonable) and NSE (0.74 good). In the case 8 during the testing phase, the values of MAPE and NSE were the testing samples of the ANFIS model (25.20% reasonable, 0.73 good) lower performance prediction accuracy than the calibrated ANN model (three layers) with MAPE and NSE values of 18.39% good and 0.79 very good, respectively. Followed by the ANFIS model of the case 9 with values of (MAPE~26.76% reasonable, NSE~0.64 satisfactory) had lower predictive ability than the ANN model (MAPE~21.11% reasonable, NSE~0.70 good) for optimized three layers of testing phase.

Table 4.5: The results of ANFIS models for bridge span 2 [35].

Strategies	Data Sets	R^2	RMSE	MAE	MAPE	NSE
Case 7 (16 inputs): N42x, N42y, N52x, N52y, N62x, N62y, N72x, N72y, S42x, S42y, S52x, S52y, S62x, S62y, S72x, S72	Training	0.78	0.0925	0.0597	19.82	0.78
	Testing	0.75	0.0944	0.0642	21.92	0.74
Case 8 (7 inputs): N42x, N42y, S42x, S42y, S52x, S52y, S72y	Training	0.82	0.0844	0.0595	22.10	0.82
	Testing	0.73	0.0966	0.0654	25.20	0.73
Case 9 (9 inputs): N52x, N52y, N62x, N62y, N72y, N72x, S62x, S62y, S72x	Training	0.69	0.1101	0.0704	24.81	0.69
	Testing	0.65	0.1108	0.0730	26.76	0.64
Case 10 (8 inputs): N42, N52, N62, N72, S42, S52, S62, S72	Training	0.73	0.1018	0.0661	23.74	0.73
	Testing	0.77	0.0893	0.0652	23.13	0.77
Case 11 (3 inputs): N42, S42, S52	Training	0.73	0.1023	0.0659	24.18	0.73
	Testing	0.77	0.0894	0.0638	23.03	0.77
Case 12 (5 inputs): N52, N62, N72, S62, S72	Training	0.67	0.1138	0.0738	29.76	0.67
	Testing	0.68	0.1063	0.0738	29.62	0.68

Generally, in terms of all cases 10, 11 and 12 revealed that the optimized ANN models had better performance and prediction accuracy of testing samples than ANFIS models. For example, the result of the case 10 that indicated the prediction accuracy of (MAPE~23.13% reasonable, NSE~0.77 very good) for the ANFIS model was less efficient than the ANN model (MAPE~18.45% good, NSE~0.78 very good) with updated two layers of the testing database. Furthermore, the performance of the optimized ANN model (three layers) for the case 11 of the testing set had the MAPE and NSE values of 18.99% (good) and 0.77 (very good), respectively, better prediction accuracy than the ANFIS model with statistical index values of

MAPE (23.03% reasonable) and NSE (0.77 very good). The result of the case 12 showed that the scores of (MAPE~29.62% reasonable, NSE~0.68 good) and (MAPE~20.73% reasonable, NSE~0.70 good) were the lowest performance in the ANFIS and ANN models (three layers), respectively, for the testing part.

The visualized results of the linear regression plots between the observed and predicted data sets illustrate for all cases 7, 8, 9, 10, 11 and 12 regarding the ANFIS models as shown in Figures 4.37 and 4.38. The ANFIS model of the case 8 was the best predictive model of all data sets with the R value of 0.89, while the lowest predictive models were in the case 9 (R~0.82) and the case 12 (R~0.82). The testing performance of ANFIS models for the case 7 (R~0.86) and the case 8 (R~0.85) were better prediction accuracy than the model of the case 9 (R~0.80). Moreover, the R value of the case 12 (R~0.82 testing, R~0.81 training) was slightly less than in the case 10 (R~0.88 testing, R~0.85 training) and the case 11 (R~0.88 testing, R~0.85 training). Therefore, the conclusion was drawn that the ANFIS models achieved the best performance predictions with the R score greater than 0.8 in all cases verified with testing, training and all part.

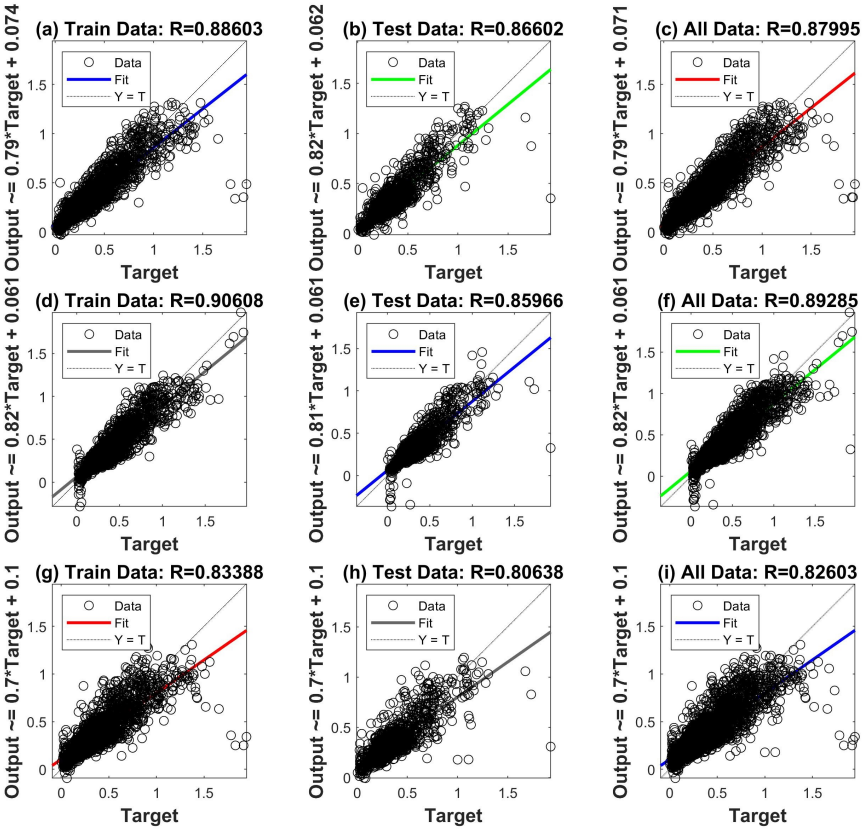

Figure 4.37: Relationship between predicted and actual values in ANFIS models: (a), (b), (c) for the case 7; (d), (e), (f) for the case 8; (g), (h), (i) for the case 9; (units: m/s^2) [35].

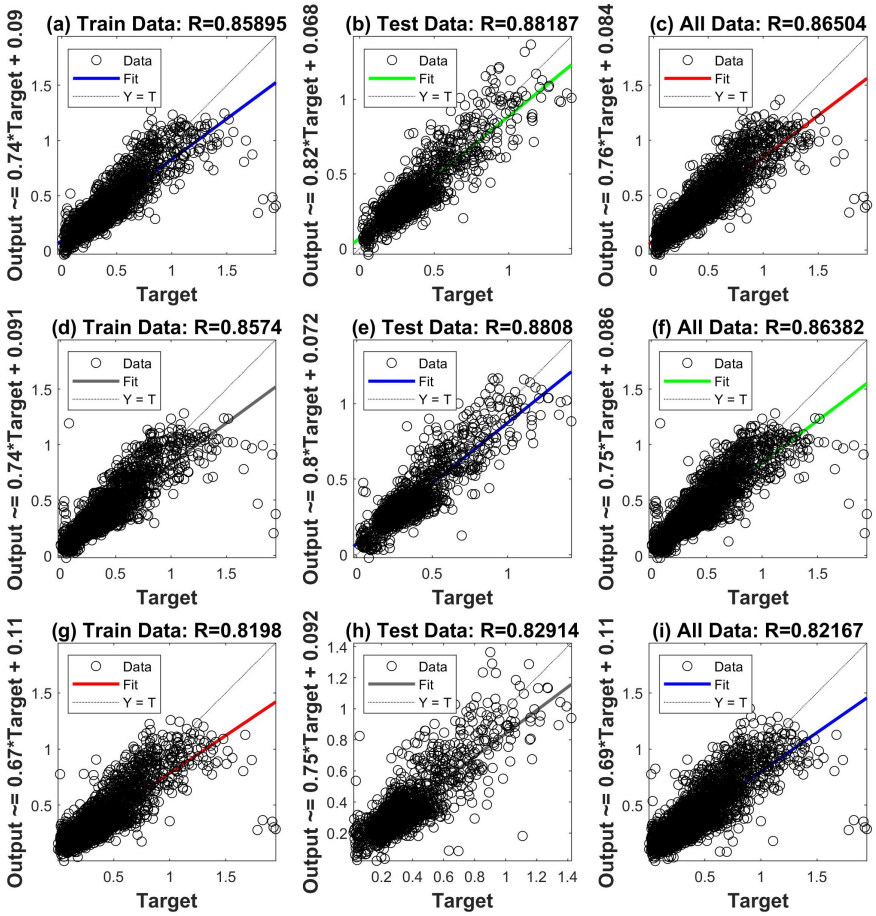

Figure 4.38: Relationship between predicted and actual values in ANFIS models: (a), (b), (c) for the case 10; (d), (e), (f) for the case 11; (g), (h), (i) for the case 12; (units: m/s^2) [35].

4.5 Concluding remarks

This chapter has presented innovative techniques of the optimized GA-based ANN architecture and the ANFIS approach to predict the RMS values of the dynamic behavior of railway steel arch bridge based on the RMS values of dynamic responses of the hangers collected from the long-term VSHM system. To improve the prediction accuracy of ANN model, the GA method was utilized to determine the number of neurons in each hidden layers of ANN structure. Data sets were collected from sixteen vibration sensors of eight hangers and sensor of the deck on each span in which the RMS amplitudes of vibration signals were analyzed by RF algorithm to judge various features of past data. Therefore, the main conclusions and findings can be drawn as follows:

- RMS values of the vibration signals of hangers and the deck were used for training and testing data sets based on robust ANN techniques using the Levenberg–Marquardt algorithm with the GA approach, as well as ANFIS models have been developed and validated to predict the dynamic behavior of the structure for bridge span 1 and span 2 with six various strategic inputs during the passage of the train.

- Implementing the proposed ML-assisted regression models for predicting future RMS values of bridge deck from the past RMS values of vibration signals of hangers if the trained and tested models meet the evaluation metrics and performance criteria. Simulated scenarios where the new RMS values of the dynamic behavior of hangers are increased or decreased, and input these variations into trained models to visualize the corresponding RMS values of the bridge span under various health potential problems in each hanger. Indeed, it's possible to use data from different positions (inputs) for predicting a localized or specific position (target or output) through the accurate and reliable representations of trained regression models.

- The accuracy of proposed prediction models is shown by the performance results, still limited to 85% for training and reached a maximum of 79% for testing. The effectiveness of these proposed strategies can depend on the specific characteristics and features of these data sets. To enhance the high accuracy, the future exploration of principal component analysis engaged machine learning approaches could be considered.

Chapter 5

Railway bridge health diagnosis using wavelet analysis and deep learning

5.1 Introduction

In this chapter, deep learning approaches for data-driven SHM for Dębica railway arch bridge are proposed. In Figure 5.1, GoogLeNet CNN classification models are employed to classify hanger health conditions under train load events and weather changes over a nine-month period.

First, wavelet-based scalograms of vibration signals recorded on the deck are used as the image input of CNN models, whereas the output is the hanger states based on the tension force extracted from the experimental natural frequencies of hangers. The FE model calibration of the railway steel arch bridge is developed to reproduce the tension force values of the hangers using the bridge design standards.

Second, orbit-shaped CNN models are developed for the dynamic behavior of each hanger recorded in the longitudinal and transverse directions. FFT techniques of hanger vibration signals in the discrete frequency domain are performed to convert two-axis accelerometers of each hanger into displacement-based orbit-shaped images.

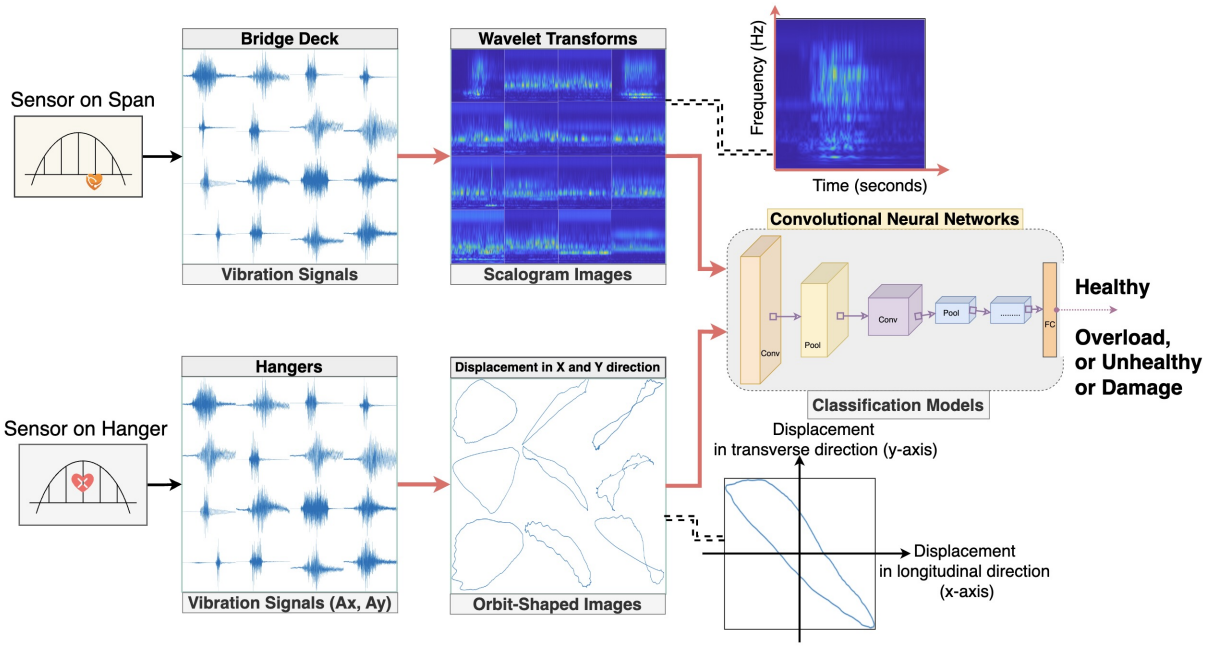

Figure 5.1: Wavelet-based CNN-assisted SHM and vibration orbit-based image diagnostic.

5.2 Railway bridge health monitoring using orbit-shaped and wavelet-integrated CNN

5.2.1 Data collection from vibration-based SHM system used for Dębica bridge

The vibration-based SHM system was used to monitor two bridge spans, as shown in Figure 5.2. In the span 1 of the Dębica bridge, these hangers are as follows: W4S, W5S, W6S, W7S, W4N, W5N, W6N, W7N, which were equipped with one biaxial accelerometer each as in Figure 5.2c, d and e. The bridge span 1 was instrumented with an IEPE sensor to measure vertical vibration, labeled as "ST". The weather monitoring station was equipped on the arch rib of the span 1 with various weather-related factors such as: wind speed, wind direction, temperature, pressure, and humidity, as shown in Figure 5.2b.

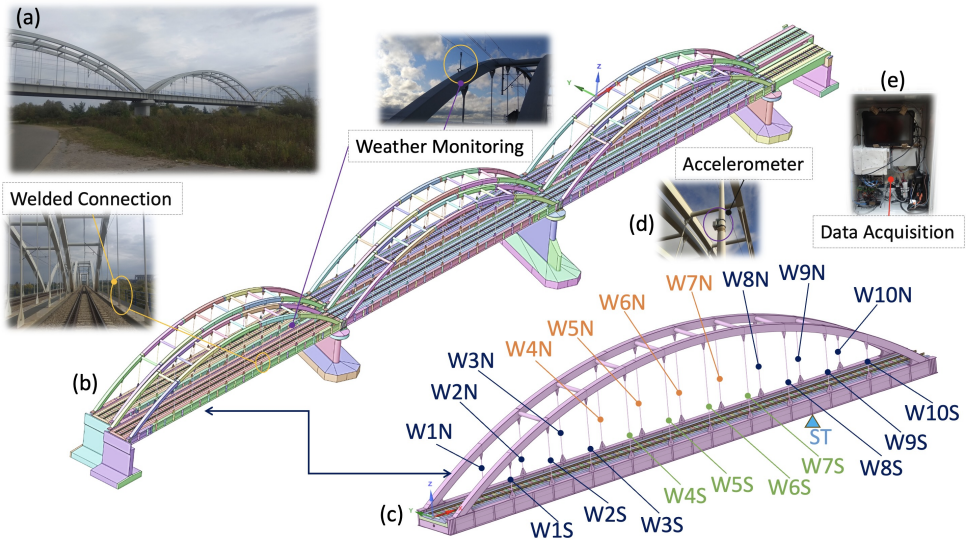

Figure 5.2: Vibration-based SHM system for railway steel arch bridge: a) Overview of Dębica railway bridge; b) Dębica bridge information modeling ; c) Bridge span 1 with hangers; d) Biaxial accelerometer on each hanger; e) Data acquisition system.

5.2.2 Estimation of hanger tension force using the measured natural frequency

The tension force values are in fact key parameters of the steel arch bridge that must be carefully assessed during the building design, construction, and operation phases. Hanger health monitoring is an essential approach to ensure safe and reliable operation of the bridge. The vibration-based SHM of the hanger utilizes accelerometers to continuously measure the dynamic behavior of the hanger under various loads such as wind speed, wind direction, temperature, pressure, and train. The analysis of the vibration signal of the hangers is to determine their natural frequencies and then to predict the tension force (T) as following equation, [56]:

$$T = \rho A \left(\frac{2 L f_n}{n} \right)^2, \tag{5.1}$$

where ρ is the density of steel, kg/m^3; A is the section area, m^2; L is the hanger effective length, m; f_n is the n^{th} natural frequency, Hz; $n = 1, 2, 3, \ldots$

The purpose of predicting the tension force is to gain informative insight into the historical structural behavior of hangers. The SHM system for a railway bridge span 1, monitoring eight hangers consisting of W4S, W5S, W6S, W7S, W4N, W5N, W6N, and W7N, for which the vibration signals are extracted to achieve the natural frequencies for the estimation of the tension force for each hanger. The maximum tension force among all hangers was determined to label the representative classes of hanger health conditions.

5.2.3 FE modeling of steel bridge structure due to lack of hanger

One of the most common limitations of using the CNN model for CWT image classification is to assign a class label or category to an input image. To improve this problem, FE model updating of the steel arch bridge structure is developed in the SOFISTIK software to calibrate OMA-based parameters, as shown in Figure 5.3. The main goal of the FE model is to determine the tension force of the hangers under the design load models of the railway loading in both damage or overload and undamaged or healthy scenarios for healthy classification tasks.

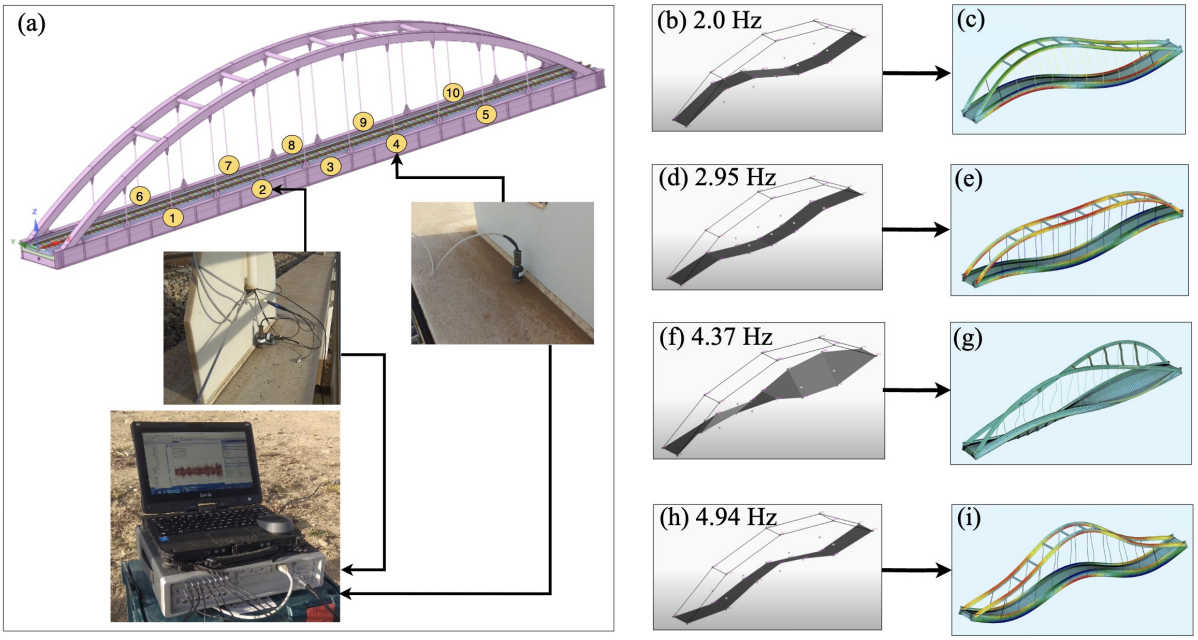

Figure 5.3: Vibration-based diagnostic testing for bridge span 1: a) field vibration measurement using single-axis accelerometers (PCB Piezotronics) installed at 10 positions along the two main girders; b), d), f), h) operational modal analysis using Siemens LMS TestLab software; c), e), g), i) FE model updating.

The 3D FE models of Dębica railway steel arch bridge were developed based on the following assumptions and structural parameters:

- The steel arches, main girders, and other structural members are modeled as 3D beam elements defined by two nodes each. The full bridge model has a total of 2204 beam elements and 5760 shell elements. The vertical hangers are fixed at the main arches and girders. The boundary conditions are pinned to the supports at the ends of the tie girders.

- The FE model updating was performed by minimizing the objective function:

$$\text{Error} = \frac{1}{N}\sum_{i=1}^{N}\left|\frac{f_m^i - f_c^i}{f_m^i}\right| < 10\%, \tag{5.2}$$

where f_c and f_m are the numerical and experimental natural frequencies of the i^{th} vibration mode; N denotes the number of natural frequencies and mode shapes identified by the OMA technique during the FE model updating procedure. The optimization approach employed the genetic algorithm in the MATLAB software to optimize vibration-based FE model automatically. Table 5.1 reports the relative differences between the experimental and numerical frequencies of the initial and updated FE model.

- Table 5.2 summarizes the material properties of the FE model updating with the global upper and lower material bounds. Two different types of stiffness parameters were chosen to calibrate FE model, consisting of density and Young's modulus, regarding the material properties of the structural components of the steel bridge [8], [14], [56].

- Four types of the load cases include the dead load, the load model 71, the load model SW/0, the load model SW/2 according to EN 1991-2:2003 [170], [171], as shown in Figures 5.4 and 5.5.

Several groups of load models for railway loading scenarios are given in Figure 5.5, according to European standards, specifically EN1991-2, which provides engineering guidelines for the assessment of railway traffic actions specifically for railway bridge structures. The load model 71 and the load model SW/0 for continuous span bridges are used to represent normal traffic on mainline railways, while the load model SW/2 is designed to represent heavy train load on the bridges. The characteristic values of vertical loads shall be modified by a factor α, when analyzing railway lines with traffic loads that are either heavier or lighter than the standard railway traffic action. This factor α shall be chosen from one of the following values: 0.75 – 0.83 – 0.91 – 1.00 – 1.10 – 1.21 – 1.33 – 1.46, [170], [171]. Based on this standard, $\alpha \approx 1.21$ was used for the Dębica railway bridge.

Table 5.1: Measured and computational natural frequencies.

Natural Frequency	Experimental Measurement, Hz	Description of Mode	Initial FE Model, Hz	Final Updated Frequencies, Hz
f_1	2.00	1^{st} Vertical Bending	2.25 (12.50%)	1.87 (6.5%)
f_2	2.95	2^{nd} Vertical Bending	3.81 (29.15%)	3.17 (7.45%)
f_3	4.37	1^{st} Torsional	5.66 (29.51%)	4.69 (7.32%)
f_4	4.94	3^{rd} Vertical Bending	5.89 (19.23%)	4.91 (0.60%)

Table 5.2: Stiffness parameters of steel bridge structure.

Material Properties	Initial variables		Young's modulus (E); Density (ρ) (Scaled)		Final variables	
	E, GPa	ρ, kg/m^3	Lower Bound	Upper Bound	E, GPa	ρ, kg/m^3
S355J2+N (18G2A)	210	7850	0.80	1.20	174.53	9413.1
C40/50(B50)	35	2500			28	2990.3

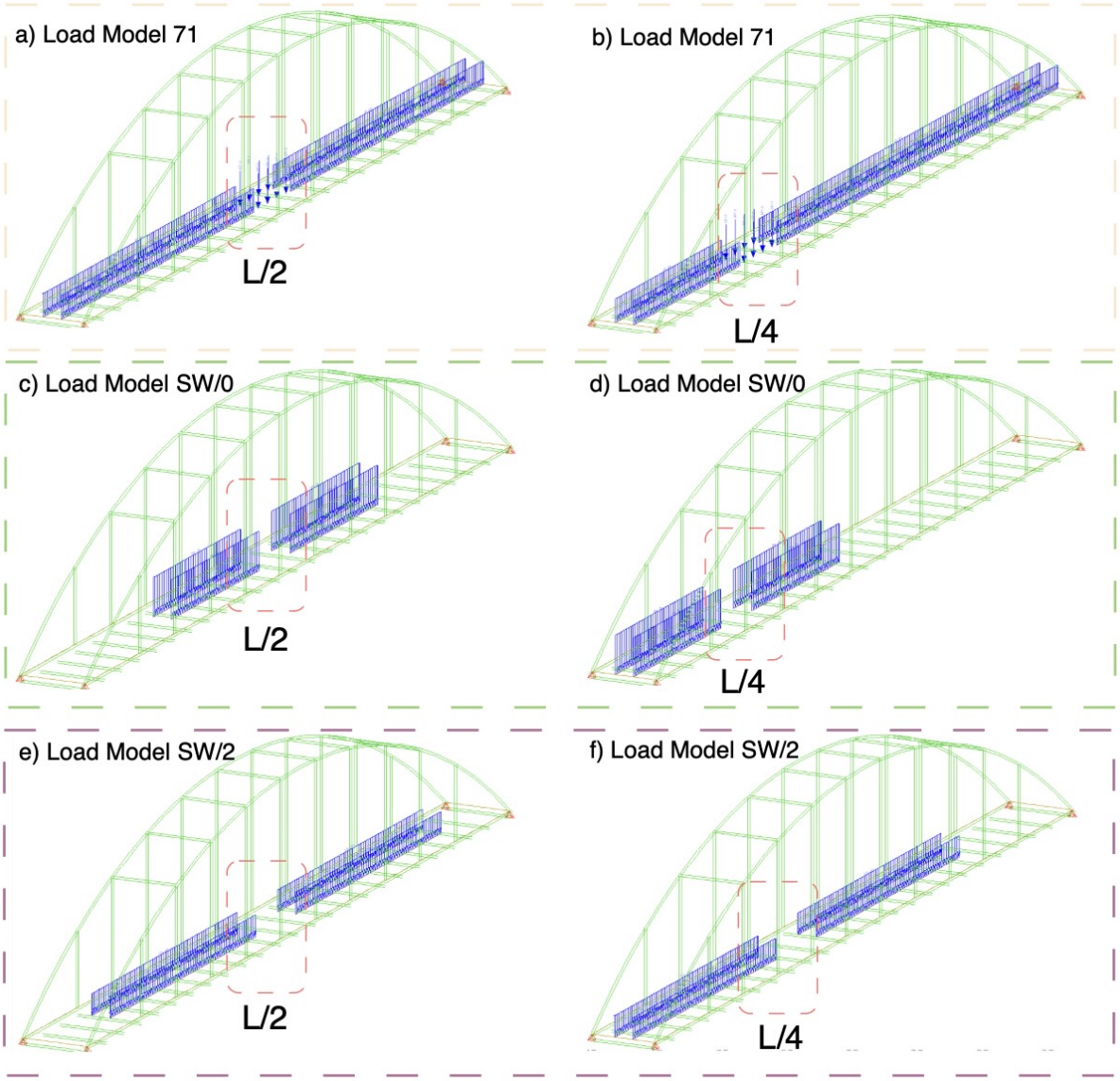

Figure 5.4: FE modeling of Dębica steel arch bridge span 1: a), b) for the load model 71; c), d) for the load model SW/0; e), f) for the load model SW/2.

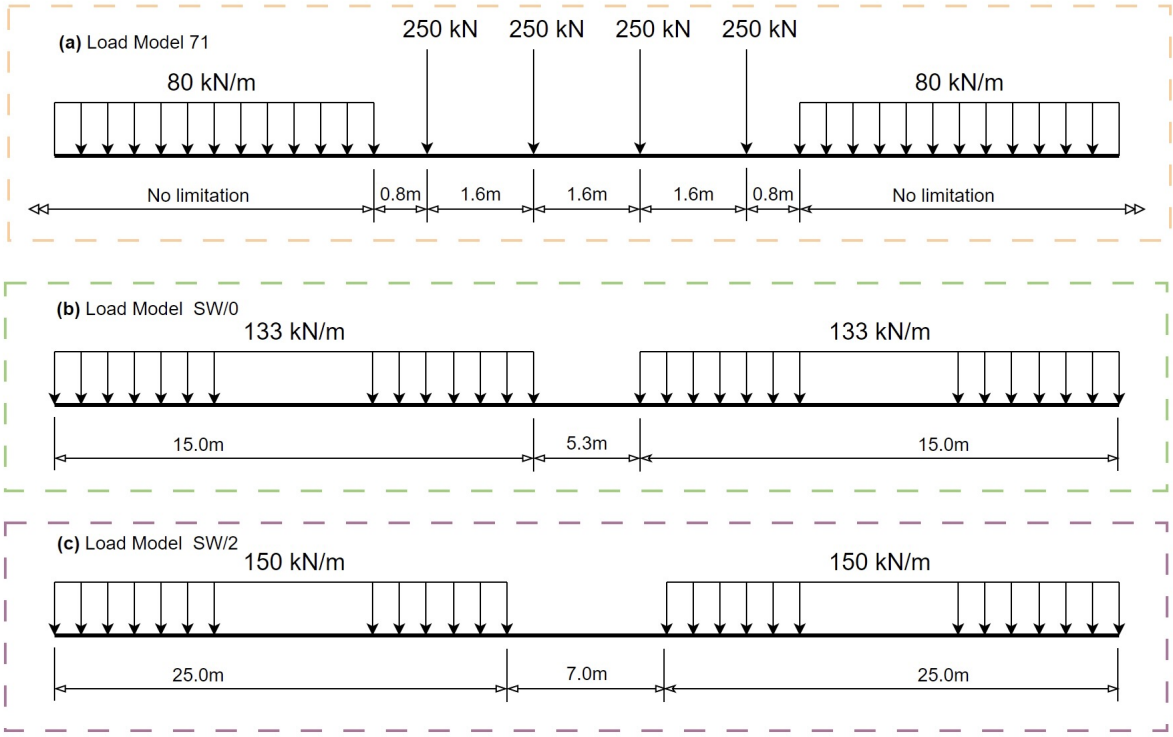

Figure 5.5: Load models 71, SW/0 and SW/2 according to EN1991-2.

The results of structural damage detection due to the lack of hanger in the bridge FE model, as shown in Figure 5.6. The objective of calculating the tension force of eight hangers subjected to various load cases (load models 71, SW/0 and SW/2) is to determine the maximum allowable tension force in each of (W4S, W5S, W6S, W7S, W4N, W5N, W6N, W7N) hanger group. There are 20 damage scenarios for the lack of a single hanger, labeled as W1S (Damage 1), W2S (Damage 2), ..., W10S, W1N, W2N, ..., W10N (Damage 20). With a removed hanger of the FE model is applied to 49 different load cases corresponding to each load model multiplied by a factor α, providing the tension force values as in Figure 5.6b. Furthermore, Figure 5.6a shows the tension force values on eight hangers when there is no structural damage (or healthy, intact). The loss of a specific hanger can have a significant impact on the load distribution within the bridge structure and identifying potential areas of localized stress concentration or increased tension force values for other neighboring hangers. When the load redistribution exceeds a significant threshold, more than 82.20 tons, it can significantly affect the safety and stability of the bridge structure. Note that the lack of a hanger is indeed used to describe situations where a hanger is no longer functioning as expected or is not in its designed position. It is a solution for categorizing labels such as overload or damage class (> 82.20 tons) and intact class (< 82.20 tons) or healthy.

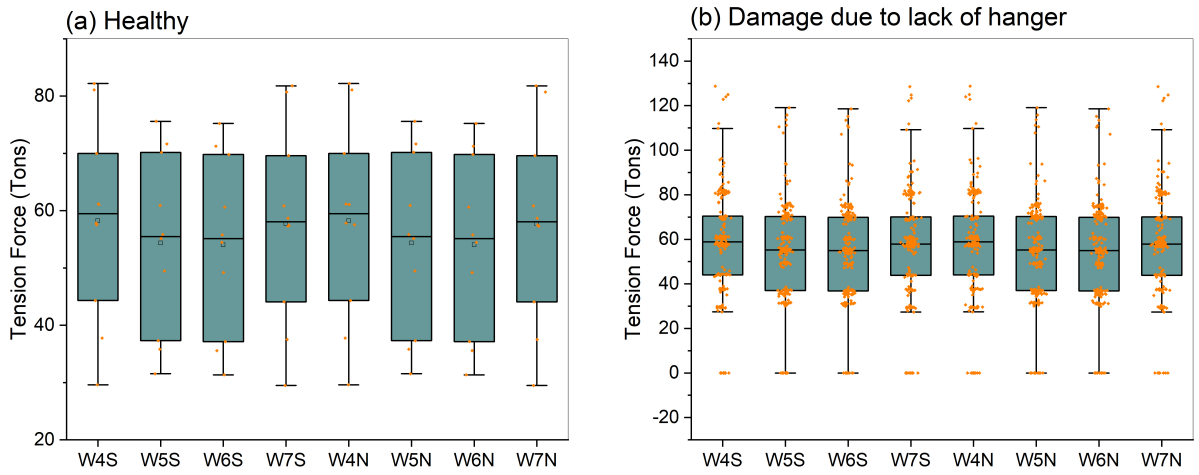

Figure 5.6: The numerical FE results of tension force values for hangers under load cases: a) intact or healthy; b) damage, unhealthy or overload.

5.2.4 Hanger health diagnostic using orbit-based image pattern recognition

The orbit-shaped or mapped pattern recognition scheme is proposed using machine learning, for example: convolutional neural networks, the characteristics of the input images being extracted from the vibration signals of the hanger in the x and y directions corresponding to the longitudinal and transverse axes of the bridge. The vibration behavior of the hanger is collected over time, and orbit-shaped plots are generated from displacement data obtained from accelerometers. Historical displacement data represent the oscillation or movement of a specific point on hanger shaft visualized over time, corresponding to specific hanger healthy states (i.e. damage or unhealthy, overload). The representations of the orbit-shaped image stages are summarized in Figure 5.7. The hanger orbit-shaped feature image extraction uses the following steps:

- Step 1: Collect vibration signals along the x and y directions for each hanger as shown in Figures 5.7a and 5.7b, with the x-axis representing longitudinal directions and the y-axis corresponding to the transverse direction, under different load conditions during a year.
- Step 2: Apply FFT algorithms to transform discrete acceleration data into displacement data.
- Step 3: Generate and visualize hanger orbit-based images, with the x-axis corresponding to the longitudinal displacement signal and the y-axis corresponding to the transverse displacement signal.

- Step 4: Categorize the geometric characteristics of these extracted orbit-shape images with three typical classes including: healthy (circle or normal), minor healthy (ellipse or unbalance) and unhealthy (eight, heart, banana, tornado, rubbing, line, or misalignment) [172], [173], [174], as illustrated in Figure 5.7c, d and e.

- Step 5: Provide orbit-shaped images as input to CNN classification model for training and testing image-based pattern recognition.

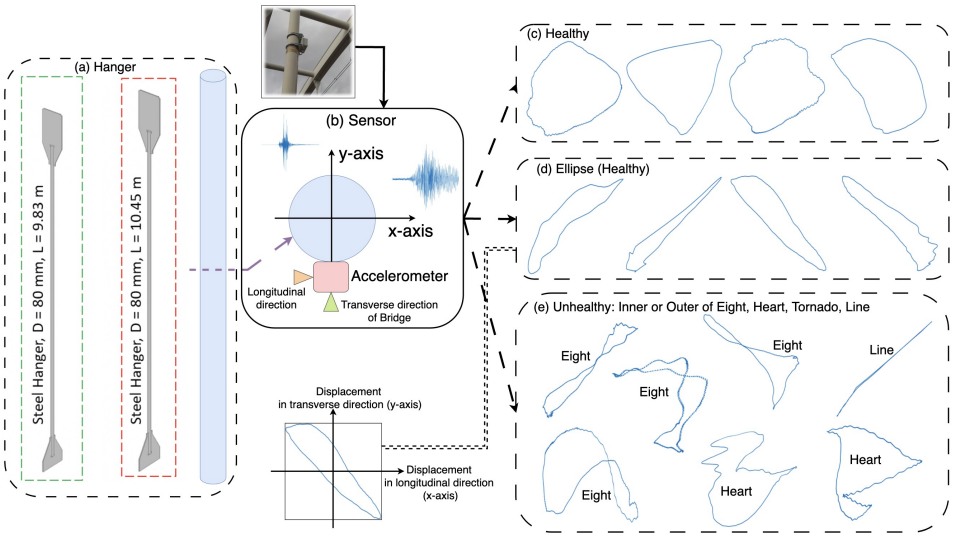

Figure 5.7: Some different orbit shapes of types of hanger healthy states: a) hangers; b) accelerometers or vibration sensors; c) and d) healthy; e) unhealthy.

The benefit of identifying orbit-shaped image patterns from vibration signals is to provide a visual representation of recorded complex vibration signal patterns and characteristics to understand the hanger structural behavior. The representation of orbit-shaped feature images corresponds to the potential structural identification problems such as: healthy or unhealthy.

5.2.5 Wavelet-based CNN classification models for bridge span

The first problem provides the results of CNN classification models integrated with different wavelet families, such as Bump, Morlet, and Morse, for vibration responses of the bridge span under dynamic train loads. Wavelet-based image data sets from vibration signals of the bridge deck contain a total of 31460 images (224×224 pixels) as input to the CNN model and are divided into two different categories consisting of healthy and overload classes as output determined from the historical vibration behavior of eight hangers. The purpose of the proposed wavelet-assisted CNN classification models is to identify hanger heath diagnostic using one vibration sensor.

Table 5.3 shows the performance results of CNN classification models for the testing and training data of hanger tension force thresholds with different wavelet transforms. CNN classification models utilizing Bump, Morlet, and Morse wavelet filters were observed to have training accuracy, which was greater than 92%, and validation accuracy, which was greater than 83%. The highest training loss was 16%, while the validation loss was 96%. The Bump wavelet-based CNN model classified in hanger healthy and overload states achieving training and validation accuracies of 92.96% and 83.67%, respectively. The classification accuracy of the Morlet wavelet-integrated CNN model had 96.87% for training and 83.11% for validation data. The Morse wavelet-engaged CNN classification model obtained the accuracies of 96.09% and 83.44% for training and validation, respectively. The CNN classification models took 4117 s, 4104 s and 3904 s for training and validation data sets of Bump, Morlet, and Morse wavelet-based scalograms, respectively. When addressing class imbalance issue, the performance metrics of CNN models consist of the F1-score, macro F1-score and weighted F1-score as shown in Table 5.4.

Table 5.3: The comparison results of wavelet-based CNN models for tension force classes.

Type of Wavelets	Training Accuracy (%)	Training Loss	Validation Accuracy (%)	Validation Loss	Elapsed Time
Bump	92.96	0.16	83.67	0.57	1hr 8min 37s
Morlet	96.87	0.12	83.11	0.96	1hr 8min 24s
Morse	96.09	0.10	83.44	0.75	1hr 5min 4s

Table 5.4: The results of CNN models with F1-score, macro F1-score and weighted F1-score.

CNN Models	Classes	F1-score (%)	Macro F1-score (%)	Weighted F1-score (%)
Bump		Training		
	Healthy Overload	95.63 94.79	95.21	95.23
		Validation		
	Healthy Overload	85.37 81.51	83.44	83.54
Morlet		Training		
	Healthy Overload	98.40 98.26	98.33	98.33
		Validation		
	Healthy Overload	83.81 82.33	83.07	83.11
Morse		Training		
	Healthy Overload	96.45 96.02	96.24	96.25
		Validation		
	Healthy Overload	84.72 81.94	83.33	83.40

Figure 5.8 presents the confusion matrix of three different CNN classification models using wavelet-based scalograms of vibration signals from the bridge span. For the Bump wavelet-based scalograms in the validation set consisting of 30% of the data sets in Figure 5.8b, the recall (precision) was 90.9% (80.5%) for healthy, and 75.7% (88.2%) for overload. In Figure 5.8d, the Morlet wavelet-based CNN model achieved a recall (precision) of 83.4% (84.3%) for healthy state, and 82.8% (81.9%) for overload problem in the validation data. In Figure 5.8f, the Morse wavelet-based CNN model in validation data sets, where the recall (precision) was 87.5% (82.2%) for healthy, and 79.0% (85.1%) for overload. These outcomes show that the healthy classes classified by the wavelet-assisted CNN approach are highly similar to the overload classes. Therefore, the proposed wavelet-based CNN classification models can efficiently classify bridge structural healthy cases.

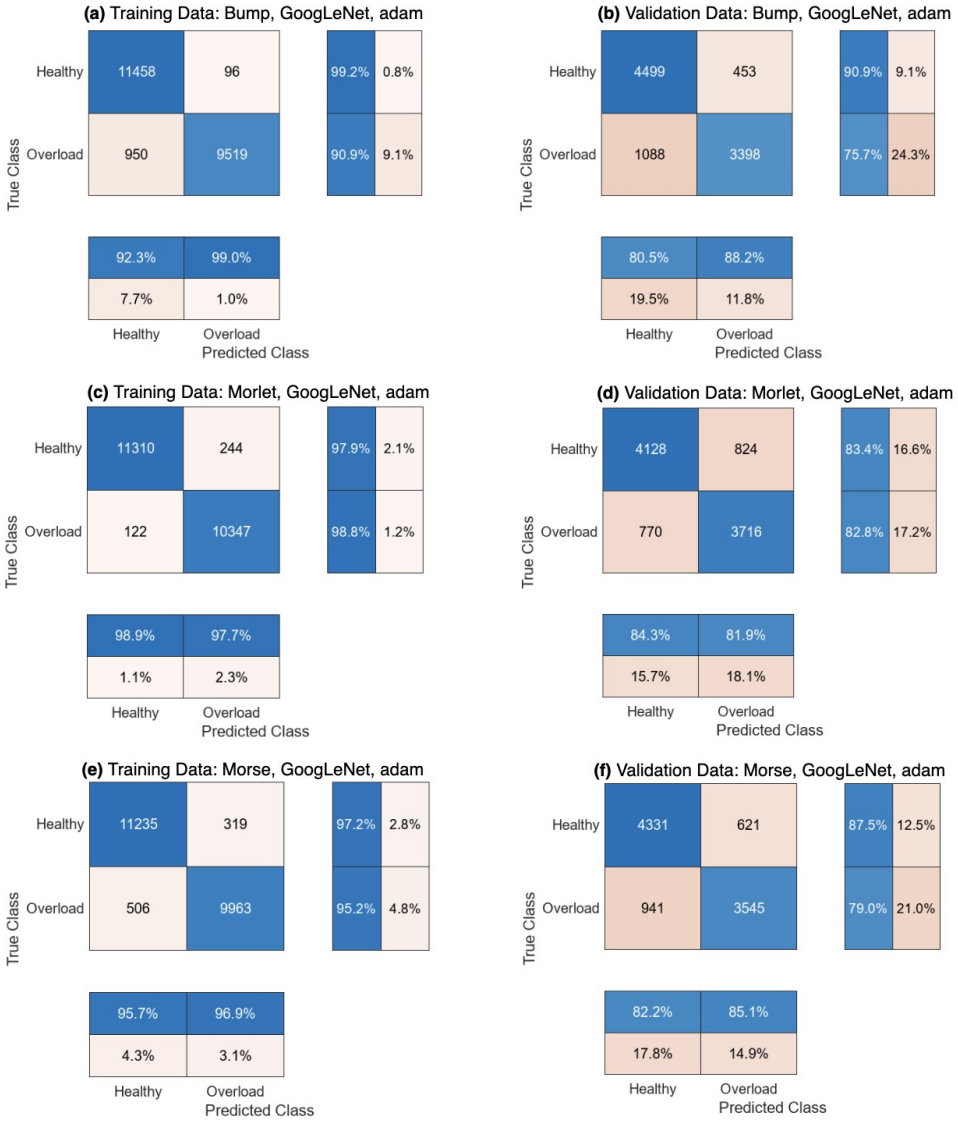

Figure 5.8: Wavelet-based CNN classification models using one IEPE sensor on the bridge deck.

5.2.6 Orbit-shaped CNN classification models for hanger dynamic behavior

The second problem aims to automatically classify hanger health states as: healthy, ellipse (minor healthy), and unhealth (eight, line, etc.) image-based patterns which were trained on the CNN classification models. The data sets of orbit-shaped images were analyzed from the dynamic behavior of the hangers recorded along the two x- and y- axis (or longitudinal and transverse directions). The data sets for CNN models include: 30993 images (W4N); 30884 images (W4S); 30799 mages (W5N); 30738 images (W5S); 30923 images (W6N); 30341 images (W6S); 30832 images (W7N) and 30857 images (W7S), all featuring orbit-shaped patterns. Resize images to a common size (224×224 pixels), is a common practical input size of CNN classification model. CNN-based approach has been used for the classification of hanger health conditions using two scenarios, 70% of training and 30% of test images. The overall accuracy for hanger health diagnostic cases of orbit-shaped CNN classification models is summarized in Table 5.5. The CNN classification models achieved training accuracies of 94.53%, 100%, 97.65%, 98.43%, 98.43%, 98.43%, 99.21%, 99.21% for W4N, W4S, W5N, W5S, W6N, W6S, W7N and W7S, respectively. The validation accuracies of the CNN models were 88.66% (W4N), 91.36% (W4S), 90.55% (W5N), 90.76% (W5S), 90.81% (W6N), 91.19% (W6S), 91.45% (W7N) and 90.89% (W7S). The elapsed time of the orbit-shaped CNN classification models required 3927 s (W4N), 3905 s (W4S), 3885 s (W5N), 3789 s (W5S), 3851 s (W6N), 3778 s (W6S), 3846 s (W7N) and 3873 s (W7S). The training loss of W4N had highest value at 23%, while the validation loss was 43%. The validation loss of W4S reached its maximum value at 48%.

Table 5.5: The comparison results of orbit-shaped CNN classification models for hangers.

Hangers	Training Accuracy (%)	Training Loss	Validation Accuracy (%)	Validation Loss	Elapsed Time
W4N	94.53	0.23	88.66	0.43	1hr 5min 27s
W4S	100	0.01	91.36	0.48	1hr 5min 5s
W5N	97.65	0.04	90.55	0.41	1hr 4min 45s
W5S	98.43	0.04	90.76	0.38	1hr 3min 9s
W6N	98.43	0.05	90.81	0.40	1hr 4min 11s
W6S	98.43	0.04	91.19	0.35	1hr 2min 58s
W7N	99.21	0.04	91.45	0.31	1hr 4min 6s
W7S	99.21	0.02	90.89	0.46	1hr 4min 33s

Figures 5.9 to 5.12 show the confusion matrix of CNN classification models using orbit-shaped images of bi-direction vibration signals for hangers (W4N, W4S, W5N, W5S, W6N, W6S, W7N, W7S). The orbit-shaped CNN classification models were trained with precision and recall scores of greater than 89%. For the hanger W4N of validation data in Figure 5.9b, the recall (precision) was 89.2% (72.4%) for ellipse, 81.5% (86.9%) for healthy, and 90.1% (95.0%) for unhealthy images. The W4S model in Figure 5.9d, it recorded the recall (precision) of 65.1% (80.2%) for ellipse, 72.6% (88.7%) for healthy, and 97.6% (92.8%) for unhealthy class.

In Figure 5.10b, the recall (precision) scores of the W5N classification model were 90.1% (87.3%), 93.2% (82.6%) and 90.3% (95.1%) for ellipse, healthy and unhealthy cases, respectively, for the validation data sets of orbit-shaped images. The W5S model's recall (precision) values were 81.9% (83.6%) for ellipse, 82.3% (87.9%) for healthy, and 95.2% (93.4%) for unhealthy labels in Figure 5.10d. Furthermore, the W6N model in Figure 5.11b demonstrated that the recall (precision) values of validation data for the ellipse, healthy, and unhealthy classes, were 75.8% (90.2%), 90.1% (85.0%), and 96.4% (92.5%), respectively. The W6S model for validation data in Figure 5.11d, achieved the recall (precision) of 86.4% (79.1%), 85.0% (85.8%), and 93.8% (96.1%) corresponding to ellipse, healthy and unhealthy classes, respectively. The recall (precision) values of the W7N model in Figure 5.12b, were 88.7% (80.3%) for ellipse, 86.0% (87.5%) for healthy, and 93.3% (96.4%) for unhealthy. The W7S model for the validation data in Figure 5.12d, the recall (precision) was 76.5% (83.4%) of ellipse, 86.6% (81.5%) of healthy and 95.3% (94.4%) of unhealthy. These results demonstrate that the proposed CNN classification models can be applied effectively to automatically extract particle features from orbit-shaped signal images of hanger health monitoring. For handling imbalanced classification data sets, the obtained results for comparing all CNN models based on F1-score, macro F1-score and weighted F1-score are illustrated in Table 5.6.

The field experimental data sets were utilized to verify the effectiveness and efficiency of the proposed algorithms. In Figure 5.13, the different types of orbit images used for CNN models, consisting of healthy (or circle, normal); minor healthy (or ellipse); and unhealthy (or eight, heart, line) shapes in hanger vibration status, were caused by wind excitation and live train loads. The representative circular and ellipse orbit shapes corresponded to bending vibration, while other eight or heart or line orbits represented the torsional (twist) behavior of the centerline of each hanger. The orbits were combined from the displacement data of a pair of sensors placed at 0^o and 90^o out of each hanger cross-section, so that it can be seen the presence or absence of torsional vibration, which can indicate structural steady state or instability. The simulation dynamic behavior of the hanger validated under experimental wind loads could also be considered to produce numerical orbit data to visualize the structural vibration state used for CNN classification models.

Furthermore, the kinetic and potential energies of Lagrangian dynamics [175], [65], [176], [177] could be employed to build the bending and torsional vibration of the fixed-fixed (or pinned-pinned) hanger, from which the analytical dynamic responses could be extracted from the motion system under simulated force excitation, used to identify various orbit shapes. The limitation of these orbit-shaped CNN models is to manually classify the field signal images before pretraining in CNN classifications, that preprocessing can be performed mathematically for the reconstructed orbit shapes [172], [174].

The vibration orbit trajectories using a pair of sensors in the time domain, were presented in different distribution terms representing displacement, velocity, and acceleration points in the 2D plane (x- and y-directions), as shown in Figure 5.14. Utilizing displacement orbits significantly improved the distinctiveness of the shapes compared to the representations based on acceleration and velocity responses.

Table 5.6: The results of F1-score, macro F1-score and weighted F1-score used for CNN models.

CNN Models	Classes	Training			Validation		
		F1-score (%)	Macro F1-score (%)	Weighted F1-score (%)	F1-score	Macro F1-score (%)	Weighted F1-score (%)
W4N	Ellipse	94.38	96.61	97.54	79.92	85.50	88.88
	Healthy	96.88			84.11		
	Unhealthy	98.58			92.48		
W4S	Ellipse	93.21	95.82	97.87	71.86	82.28	91.00
	Healthy	95.42			79.84		
	Unhealthy	98.83			95.13		
W5N	Ellipse	96.84	97.09	97.63	88.67	89.63	90.61
	Healthy	95.85			87.58		
	Unhealthy	98.58			92.63		
W5S	Ellipse	97.84	98.54	98.97	82.74	87.34	90.67
	Healthy	98.34			85.00		
	Unhealthy	99.44			94.29		
W6N	Ellipse	96.18	97.65	98.20	82.37	88.08	90.64
	Healthy	97.72			87.47		
	Unhealthy	99.04			94.40		
W6S	Ellipse	96.81	97.86	98.63	82.58	87.64	91.31
	Healthy	97.38			85.39		
	Unhealthy	99.39			94.93		
W7N	Ellipse	97.47	98.33	98.76	84.29	88.61	91.52
	Healthy	98.24			86.74		
	Unhealthy	99.29			94.82		
W7S	Ellipse	96.95	97.62	98.72	79.80	86.20	90.81
	Healthy	96.31			83.97		
	Unhealthy	99.59			94.84		

Figure 5.9: Orbit-shaped image CNN classification models of hanger dynamic behavior using one bi-directional vibration sensor: a) and b) for W4N; c) and d) for W4S.

Figure 5.10: Orbit-shaped image CNN classification models of hanger dynamic behavior using one bi-directional vibration sensor: a) and b) for W5N; c) and d) for W5S.

Figure 5.11: Orbit-shaped image CNN classification models of hanger dynamic behavior using one bi-directional vibration sensor: a) and b) for W6N; c) and d) for W6S.

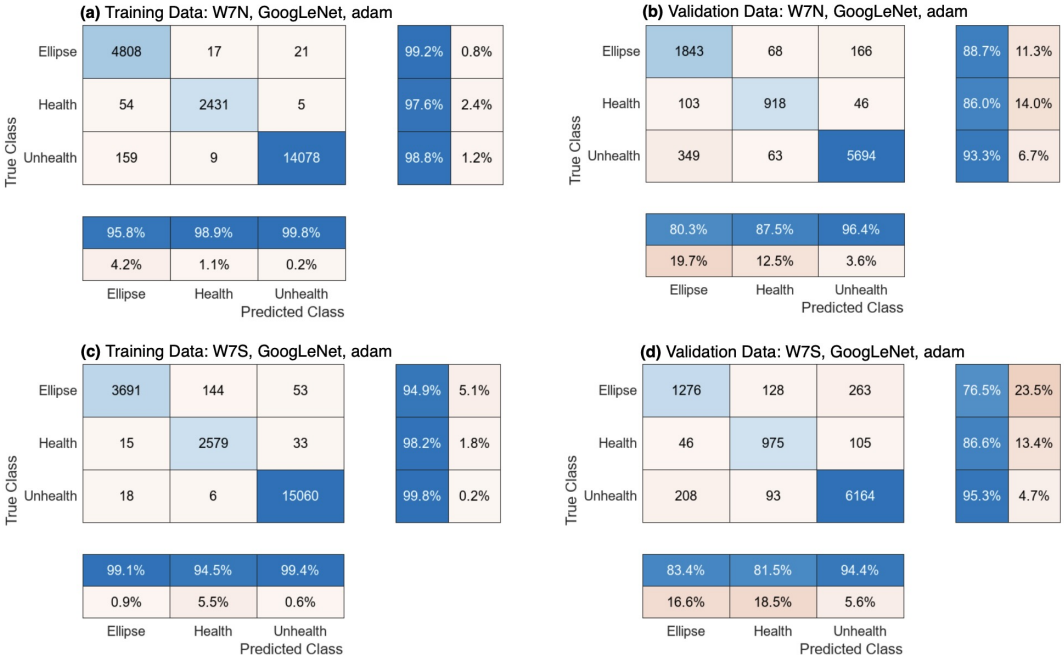

Figure 5.12: Orbit-shaped image CNN classification models of hanger dynamic behavior using one bi-directional vibration sensor: a) and b) for W7N; c) and d) for W7S.

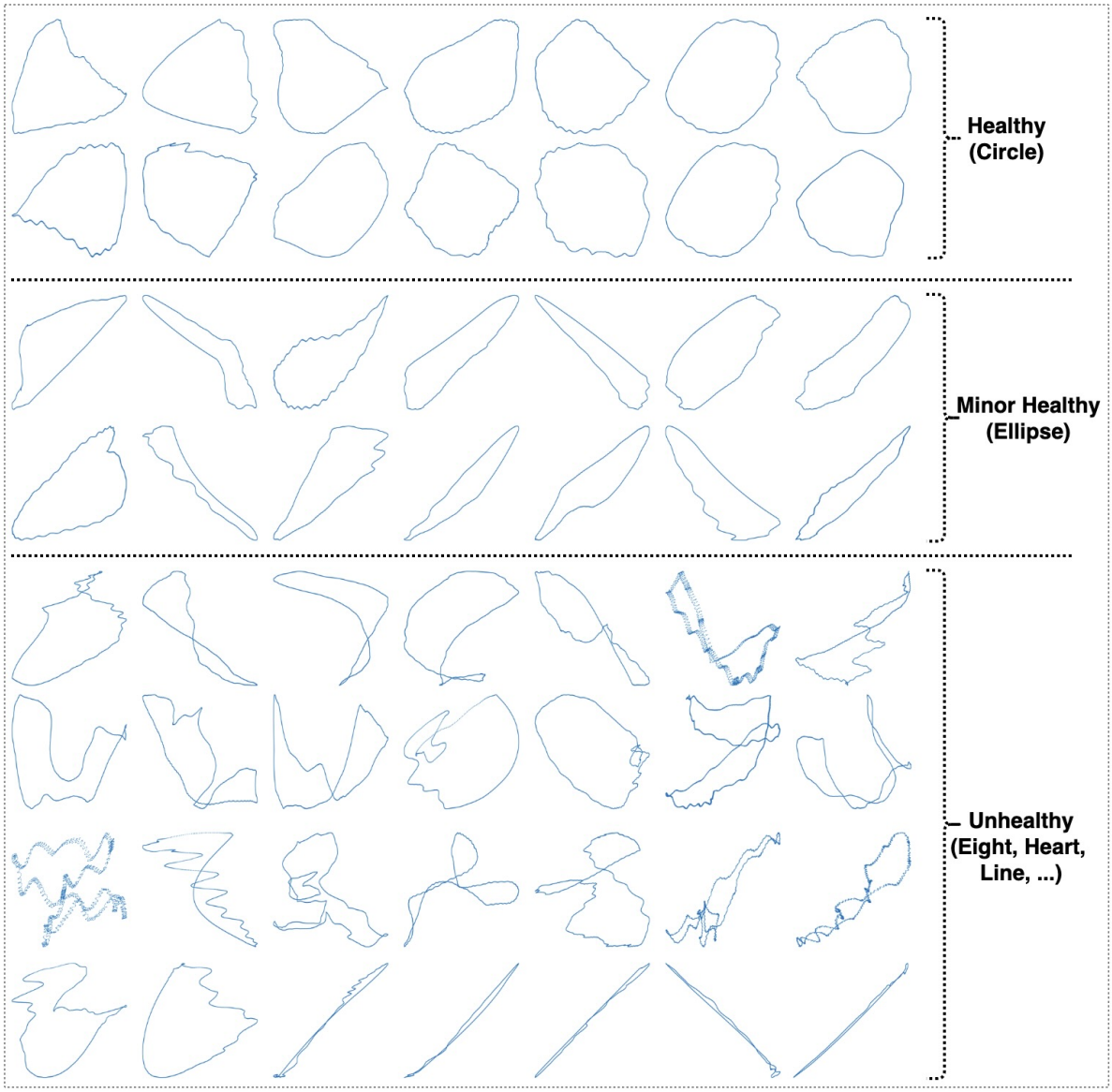

Figure 5.13: Typical orbits used for CNN classification models.

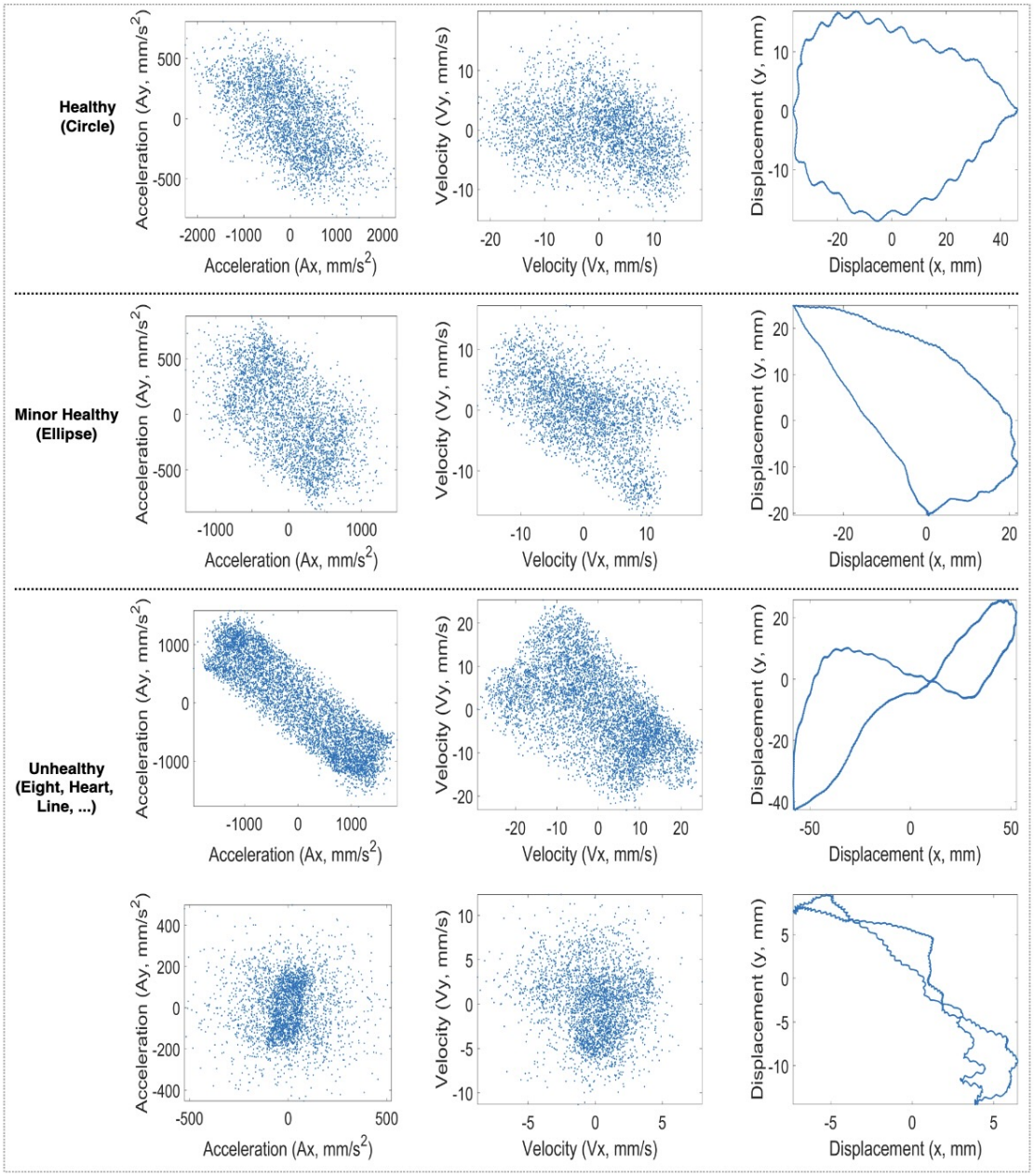

Figure 5.14: Orbits for acceleration Ax vs Ay; velocity Vx vs Vy; displacement x vs y.

5.3 Concluding remarks

This chapter proposed the wavelet-integrated and orbit-shaped image CNN classification approaches for automatically classifying hanger and structural health conditions. The following findings can be obtained:

- Wavelet-attention CNN classification models were developed to predict hanger healthy conditions. The input was wavelet-based scalograms of vibration signals of the bridge span, while the output was to classify hanger states with two classes, consisting of healthy and overload (or unhealthy) states based on the maximum tension force values of 8 hangers. The FE model updating of the steel bridge was developed to determine the tension force threshold due to the lack of a hanger to label the healthy and overload classes in these CNN models. The trained wavelet CNN models can be utilized to identify the healthy condition of hangers based on a signal accelerometer installed on the span. Furthermore, there may be a dispute regarding the categorization of the "healthy" and "overload" (or unhealthy, damage) classes, for which CNN regression models might be considered in future studies.

- Orbit-shaped CNN classification models were constructed to forecast the structural health of each hanger on the existing railway steel arch bridge under different train and weather events. These CNN models were trained using the input data of orbit-based displacement signal images extracted from vibration signals measured in both longitudinal and transverse directions of a bidirectional sensor on each hanger. The output of these CNN models was the potential healthy problems of each hanger, denoted by labels: healthy (circle or normal), ellipse (or minor healthy) and unhealthy (or eight, heart, line, etc.).

- Both wavelet-assisted and orbit-shaped CNN classification models achieved macro and weighted F1-score values greater than 82% for imbalanced validation data. These results have been demonstrated that wavelet-assisted and orbit-shaped CNN may be a useful and robust approach for data-driven hanger health diagnosis, as well as automated railway bridge health monitoring performed in an accurate, reliable, and efficient way.

- The limitation of the study is the presence of vibration signal noise that impacted or influenced the interpretation of CNN classification models. Therefore, the misclassification rates of up to 24.3% for the Bump wavelet-based CNN model and 34.9% for the W4S orbit-shaped CNN model in image classification tasks were observed. To reduce misclassification rates and enhance overall performance, advanced signal processing techniques should be implemented.

Chapter 6

Bridge diagnostic load ratings using automated FE model updating

6.1 Introduction

This chapter concerns updating the FE model using the PSO and GA optimization methods so that the final calibrated FE models can be used for the diagnostic load testing of existing bridge structures. The scripts and functions in MATLAB contain optimization algorithms that interface with the CADINP language script with the FE modeling of the bridge structure implemented in SOFISTIK TEDDY to automatically update the cross-sectional stiffness variables of structural members [8]. The full-scale FE model updating of the existing bridge through the field-measured natural frequencies are compared and modified with the numerical natural frequencies of the analytical FE model implemented in the MATLAB software to communicate with the ANSYS APDL software [14]. The main objective for producing calibrated full-scale models is to have one realistic model to compute load rating procedures and predict load limits using the design specifications of the American Association of State Highway and Transportation Officials design specifications [178], which can be performed for any load configuration. The final field calibrated models can be used to evaluate the capacities of structural members according to design standards.

6.2 Automated bridge FE model updating approach

The proposed methodology for updating bridge models is based on the interaction between the ANSYS APDL software (or SOFISTIK software) and the MATLAB functions used for optimization of the parameters of the FE model following the flowchart presented in Figure 6.1. The process includes performing parameter analysis using field experimental responses in the MATLAB software, structural FE modeling and analysis in the ANSYS software (or SOFISTIK), data comparison in the objective function in the MATLAB software, and calibration of the FE model after every step in the FE softwares. The final calibrated FE model is used to apply load cases according to bridge design standards.

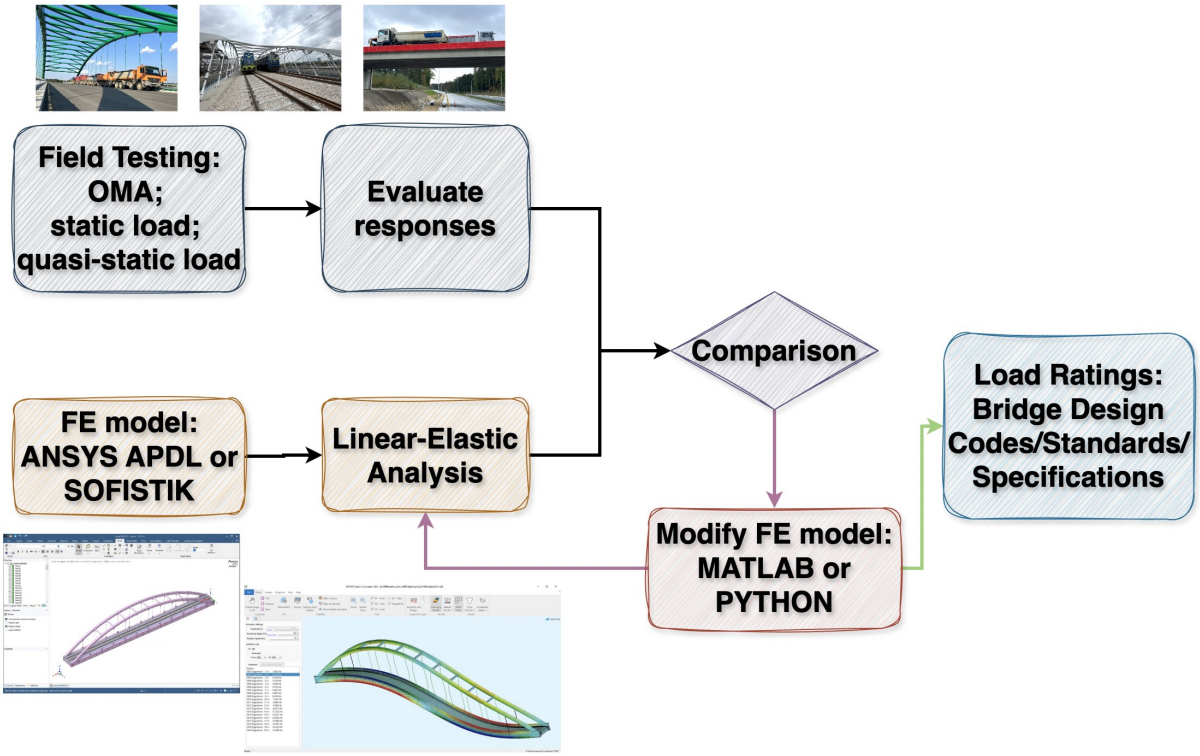

Figure 6.1: The wireless structural testing system (STS-WiFi) for diagnostic load testing in existing bridge structures.

The objective function obtained from the error between the measured responses x_m and the computational responses x_c from the FE modeling, where N represents the number of parameters collected from field measurements.

$$g\,(z) \;=\; \sum_{i=1}^{N} \left(\frac{x_m - x_c}{x_m} \right)^2 \;<\; \text{tolerance} = 10\%. \tag{6.1}$$

6.3 AASHTO bridge specifications

The AASHTO rating and posting load configurations are used to FE model the various truck load cases according to the bridge design standards and compute the ultimate capacity of girders, as shown in Figure 6.2. The rating factors are computed using the equation in the AASHTO manual for the evaluation of bridge structures under load configurations [178]:

$$\mathrm{RF} = \frac{C - A_1\, D}{A_2\, L\, (1 + \mathrm{IM})}, \tag{6.2}$$

where RF is member rating factor, C is structural member capacity (ultimate or allowable, M_n and V_n), D is dead-load (self-weight) effect, L is live-load effect, A_1 is dead-load factor (1.0 for ASD, 1.3 for LFD), A_2 is live-load factor (1.0 for ASD, 2.17 for LFD inventory, 1.3 for LFD operating), IM is live-load impact or dynamic factor (AASHTO or measured), ASD is allowable strength design, LFD is load factor design.

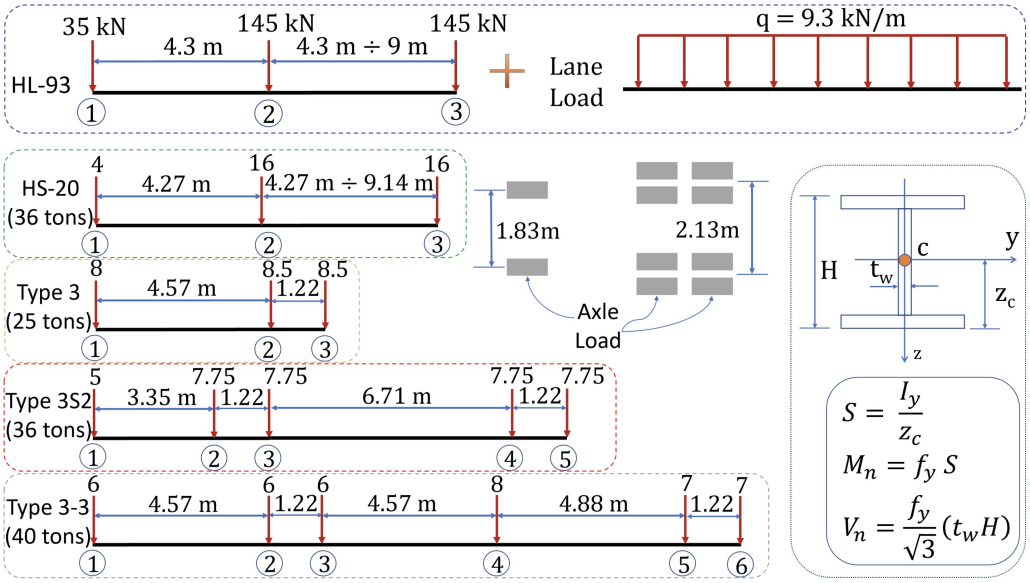

Figure 6.2: Application of load rating procedures using AASHTO load configurations.

For evaluation of a steel member, M_n and V_n are the nominal bending moment capacity and the shear force capacity of the structural members, respectively. In Figure 6.2, H is the section height of I-shaped girders, t_w is web thickness, I_z is the moment of inertia about the z-axis, S is the modulus of section, z_c is the neutral axis (NA) at the center (c) of the cross-section of the I-shaped steel beam. For the steel bridge, f_y is the yield stress limit state of the steel beams (assuming 33 ksi or 227.52 MPa), A_1 is 1.3, A_2 is 2.17 and the impact is 33% according to the bridge design standard. The RF is greater than 1.0, indicating that vehicles can cross the bridge without restriction. When the RF is below 1.0, vehicles should not cross, and the load limit is multiplied by the weight of the truck.

Moreover, the rating factor for moment stresses is calculated as [179]:

$$\mathrm{RF} = \frac{\sigma_{xx}^{C} - \sigma_{xx}^{DL}}{\sigma_{xx}^{LL}\ (1 + \mathrm{IM})}, \tag{6.3}$$

where σ_{xx}^{C} is the allowable stress capacity of structural members in flexure; σ_{xx}^{DL} the maximum flexural stresses due to dead load; σ_{xx}^{LL} is the maximum flexural stresses due to live load; IM is the impact factor with the live load effect (AASHTO or measurement).

The integration approach based on the final calibrated FE model for the load rating of the existing bridges is comprised of four main steps:

- Step 1: Apply the design load standards to the final FE model;
- Step 2: Compute the stress level predictions of the key structural members;
- Step 3: Load rating calculation use the RF equation;
- Step 4: Check the RF $\geq$ 1 for the bridge pass the design loads or RF $<$ 1 fail the legal vehicle loads.

The rating of bridge (RT) in tons for the structural member of the diagnostic load testing, if its RF is less than 1.0 as follows [178]:

$$\mathrm{RT} \ = \ (\mathrm{RF})\ W, \tag{6.4}$$

where W is the weight in tons of the nominal truck load according to design codes and standards.

6.4 Case study 1: FE model updating of RC bridge structure

6.4.1 Structure description and field test procedure

The Vietnamese ThiThac bridge is a four-simple-spans RC beam and deck bridge that has a asphalt pavement layer surface and guardrails. The bridge is located on the old national highway over the saltwater river that flows into ocean water. The lengths of the spans 1, 3 and 4 are 9.1 m, while the length of the span 2 is 8.05 m. The widths of the roadway and the structure are 8.62 m and 9.58 m, respectively. The thickness of the asphalt roadway deck is 5 cm. The thickness of the concrete deck ranges from 6 to 10 cm in center. The ThiThac consists of eight rectangular RC girders with height 0.4 m and width 1.18 m. The girder spacing is 1.2 m.

Static load tests were performed by a two-axle dump truck across the bridge according to three truck paths included centric position, eccentric position on the right and left sides. The truck (78C02978) has a total gross weight of 8.42 tons, a weight of 3.58 tons, and a weight of 4.84 tons in the rear. The distance between the front and rear axles is 5.6 m, while the spacing between two wheels is 1.87 m.

The goal of the instrumentation plan was to measure the static responses of the structural girder members and to record the dynamic behavior of the bridge. The bridge was instrumented with reusable intelligent strain transducers and accelerometers for each span, as shown in Figure 6.3. The structural testing system of this bridge structure in field testing uses the mobile base station with antennas to connect with many four-channel nodes implemented as the different types of weatherproof sensors, including intelligent strain transducers (full Wheatstone bridge with 350 Ω foil gages, ± 4000 με, effective gage length with 76.2 mm); LVDT displacements (± 75 mm); accelerometers (± 5 g). Each four-channel STS-WiFi node can connect to the mobile base station by connecting the wireless network and can communicate wirelessly with the user's laptop. WinSTS software is used to collect field data sets in real time by connecting to the STS-WiFi system with sample rates from 0.1 Hz to 500 Hz (max), as well as automatically zero before the test.

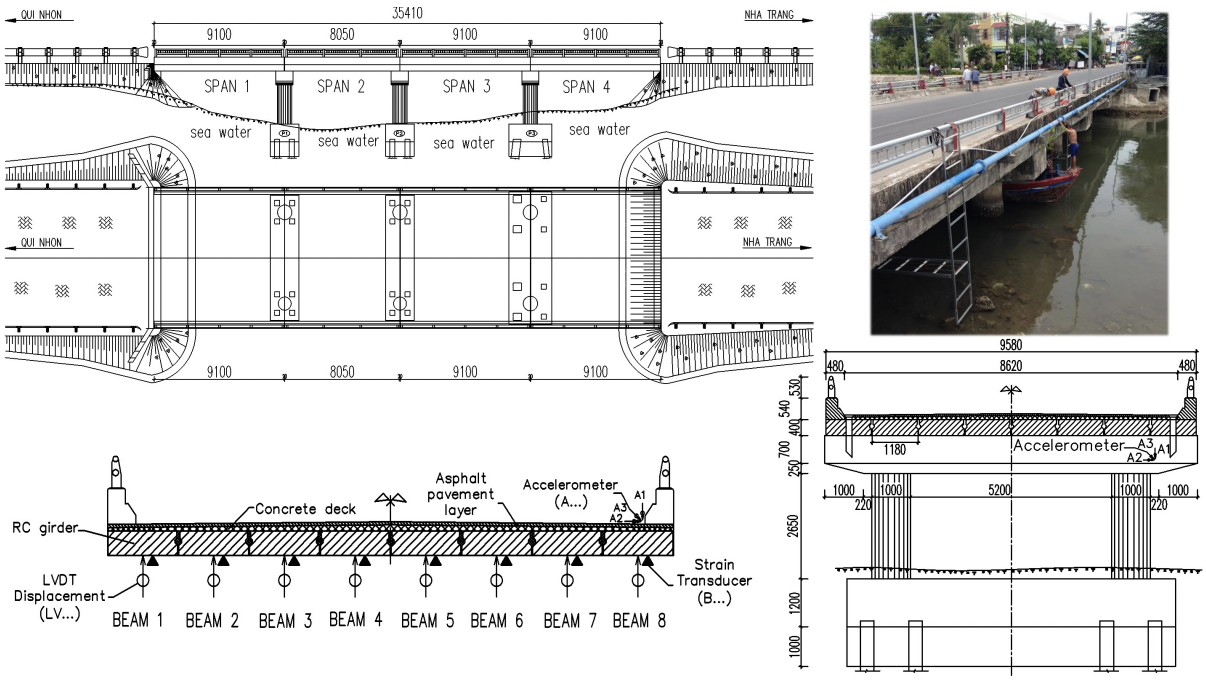

Figure 6.3: Overview of the Vietnamese ThiThac bridge and instrumentation plan [8].

6.4.2 Experimental results of field load testing

The load tests were performed by the single truck applied to the Vietnamese ThiThac RC bridge structure as concentrated vertical centric and eccentric loads. The strain histories of the RC girder members under three static load cases includes a centric load, an eccentric load on the left and right sides of the center line of the bridge, as shown in Figures 6.4 and 6.5, respectively.

The preliminary investigations were conducted directly from the field strain data with conclusions regarding the static behavior of the existing RC bridge. The maximum strains recorded in the longitudinal direction were +3.44 με, +8.13 με and +1.74 με at the mid-span 1 in the cross-sectional member of the girder in load cases 1, 2 and 3, respectively. Maximum tension strains of +17.10 με, +21.42 με and +19.41 με obtained from the girders of the span 2 in various load cases. The maximum measured strains recorded on the beams of the span 3 were +18.95 με, +23.85 με and +18.25 με for each static load case. The largest strains occurring at the midspan 4 of the girders were +20.25 με, +28.28 με and +13.88 με. All strains were multiplied by the Young's modulus of the concrete material to obtain the stresses.

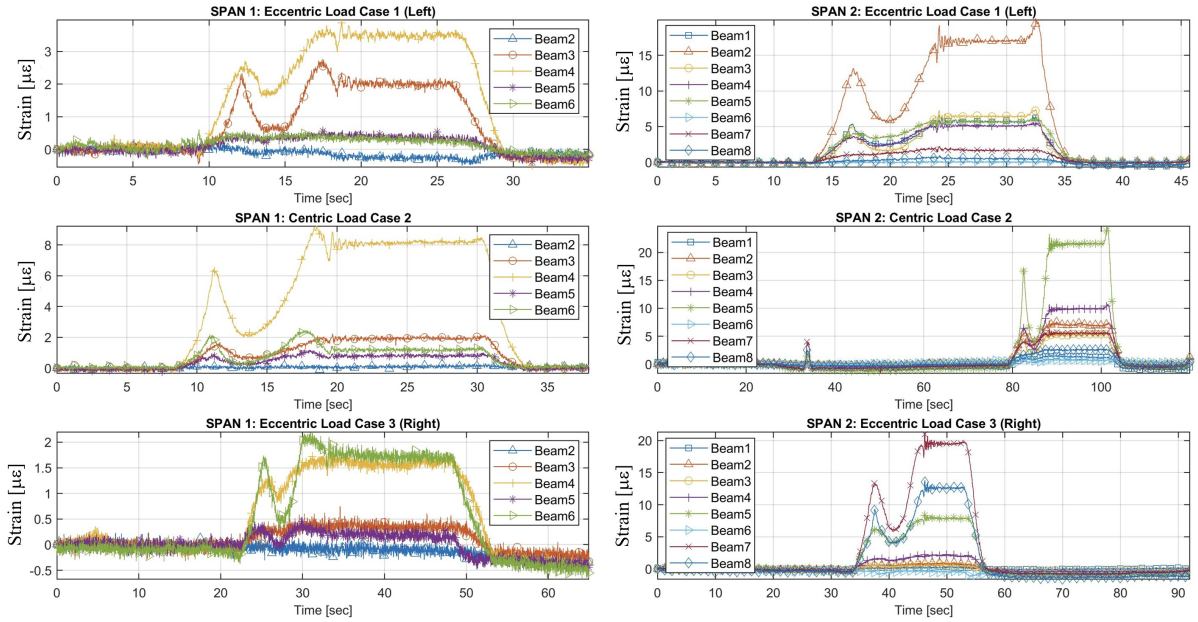

Figure 6.4: The results of measured strain responses for the bridge spans 1 and 2 [8].

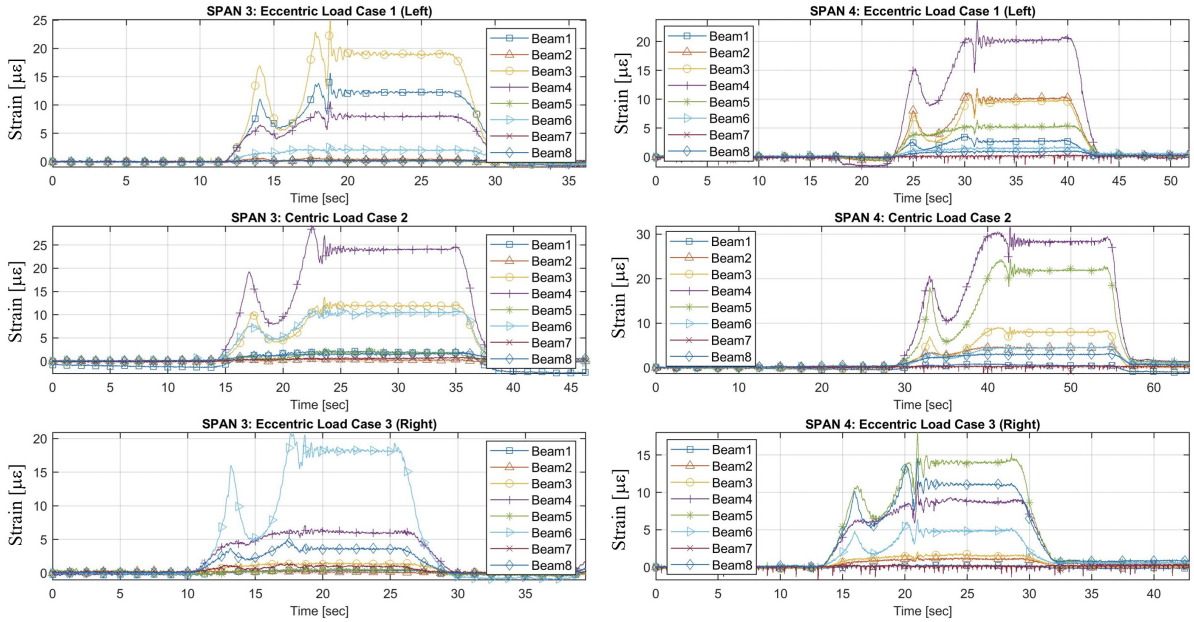

Figure 6.5: The results of experimental strain responses for bridge spans 3 and 4 [8].

6.4.3 FE model updating and analysis

The FE modeling of the Vietnamese ThiThac bridge structure is built in SOFISTIK software. The main structural components of bridge modeling include 2-node frame elements (BEAM) to represent eight rectangular longitudinal girders; 4-node shell elements (QUAD) for the deck and spring elements to simulate elastic supports at bearing locations for boundary conditions, as shown in Figure 6.6. The model is developed so that the configurations of the load testing vehicle are reproduced in the model as the actual test truck on the bridge. The cross-sections of the girders (height h and width b) and the material properties of the concrete are assigned to the various structural elements in the model. Stiffness properties are selected to update the FE model including girder stiffness (E_c and moment of inertia I), deck stiffness (thickness t_d and E_c). Comparison of strain values are made between analytical data and measured results. The initial FE model is updated by modifying the various cross-sectional girders, material properties, and boundary conditions until the results match the measured strain responses in the field testing that the final updated FE model is acceptable, when the average percentage error is minimized to the level of less than 10%. Note that the stress values at the bottom of the girders that relate the installed gauge positions are determined through the neutral axis, the moment of inertia calculations, and the bending moments. All stresses are divided by the elastic modulus of the girders to obtain the strains in micro-strain ($\mu\varepsilon$) which can be used to compare the calculated strains in the updated FE model. The NA locations are determined based on the cross-sectional properties of the rectangular girders and the transformed deck.

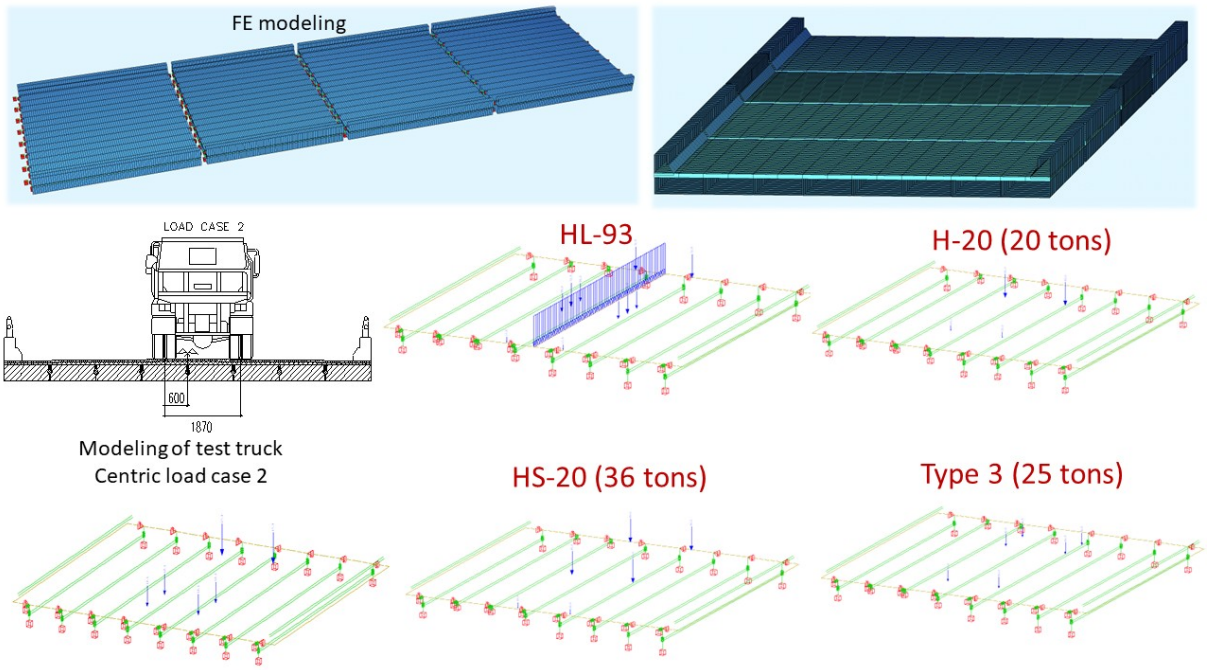

Figure 6.6: FE modeling of the RC bridge structure and modeling of truck configurations [8].

Table 6.1 contains the stiffness properties of the adjustable parameters, the lower and upper limits, and also the initial and final values of the FE model update. The initial concrete elastic modulus (E_c) is 25 GPa, Poisson's ratio is 0.25 and the density is 2500 kg/m^3 assumed for girders, deck slab, and parapets according to the EN 1992-1-1:2004. The initial height and width of the RC girders, and the average thickness (t_d) of the concrete deck slab are based on the design dimensions, for which the cross-sectional groups are defined to assign them to those girder members. The cross-sectional stiffness properties (I_1, I_2, I_3, I_4, I_5, I_6, I_7, I_8) of the RC girders are calibrated in the optimization procedure. Limits in the cross-sectional properties of structural members are increased and decrease from the initial values of the height and width of the RC girder, as in the examples cited here [180].

The strain comparison processing and the structural stiffness update procedure indicated the following results for each span. The concrete elastic modulus of the final calibrated span 1 increases by 10.52%, from 25 GPa to 27.63 GPa, while the spans 2 and 3 decrease by 15.04% and 15.92%, respectively. The elastic modulus of the span 2 climbs to 2.72%, to 25.68 GPa, while the moment values of inertia from the beam 2 to the beam 7 drop considerably. Some exterior beams were not made to calibrate the measured data for the stiffnesses because the sensors were not mounted to these beams and the values were too small. Figures 6.7 to 6.10 display the initial and final values of the parameters of the stiffness properties in the first span of the RC bridge structure.

The variables of the FE model update in the optimization procedure are extracted to plot all pairs of calibrated variables in the correlation coefficient matrix with the corresponding labels with which the lower and upper bounds are illustrated in the diagrams. The results of the stiffness parameters indicated that the calculated data are more on the moment of inertia of the girders than on the concrete elastic modulus of the entire structural span. The optimization process has been carried out by modifying the various height and width values of each girder in the span as independent variables, while the elastic modulus is used to obtain the same parameter for all components of the structure. The correlation coefficients of the stiffness parameters range from -1.0 to +1.0. These values are less than 0.5 indicating the weak linear relationship between two stiffness variables. There are some negative values of the correlation coefficient that have been reflected in the relative movements of two stiffness variables, such as sloping downward or changing in the opposite direction. Some special cases of correlation coefficient matrix close to zero value demonstrated that the two stiffness variables have little to no linear relationship and could be dependent.

Table 6.1: The results of FE model updating for initial and final values of parameters [8].

Stiffness parameters	Initial value	Lowe limit	Upper limit	Final Values			
				Span 1	Span 2	Span 3	Span 4
E_c, [GPa]	25	21	40	27.63	21.24	21.02	25.68
t_d [mm]	100	–	–	–	–	–	–
h [mm]	400	0.15*h	2.5*h	–	–	–	–
b [mm]	1180	0.15*b	2.5*b	–	–	–	–
I_1, [m^4]	6.29e-3	3.18e-6	0.24	12.89e-3	12.23e-3	22.49e-3	6.782e-3
I_2, [m^4]	6.29e-3	3.18e-6	0.24	4.89e-3	70.08e-3	3.97e-3	0.030e-3
I_3, [m^4]	6.29e-3	3.18e-6	0.24	0.75e-3	0.042e-3	4.41e-3	0.123e-3
I_4, [m^4]	6.29e-3	3.18e-6	0.24	25.73e-3	0.006e-3	3.23e-3	0.943e-3
I_5, [m^4]	6.29e-3	3.18e-6	0.24	12.74e-3	0.076e-3	0.92e-3	1.545e-3
I_6, [m^4]	6.29e-3	3.18e-6	0.24	10.79e-3	0.021e-3	2.71e-3	0.607e-3
I_7, [m^4]	6.29e-3	3.18e-6	0.24	29.14e-3	0.850e-3	0.027e-3	1.959e-3
I_8, [m^4]	6.29e-3	3.18e-6	0.24	5.46e-3	0.025e-3	4.53e-3	11.69e-3
Percent Error [%]	–	–	–	0.01	0.21	6.31	7.16
RF (HL93)	–	–	–	0.36	0.05	0.09	0.10
RF (H-20, 20 tons)	–	–	–	1.09	0.12	0.28	0.31
RF (HS-20, 36 tons)	–	–	–	0.94	0.11	0.24	0.26
RF (Type 3, 25 tons)	–	–	–	1.07	0.14	0.30	0.32

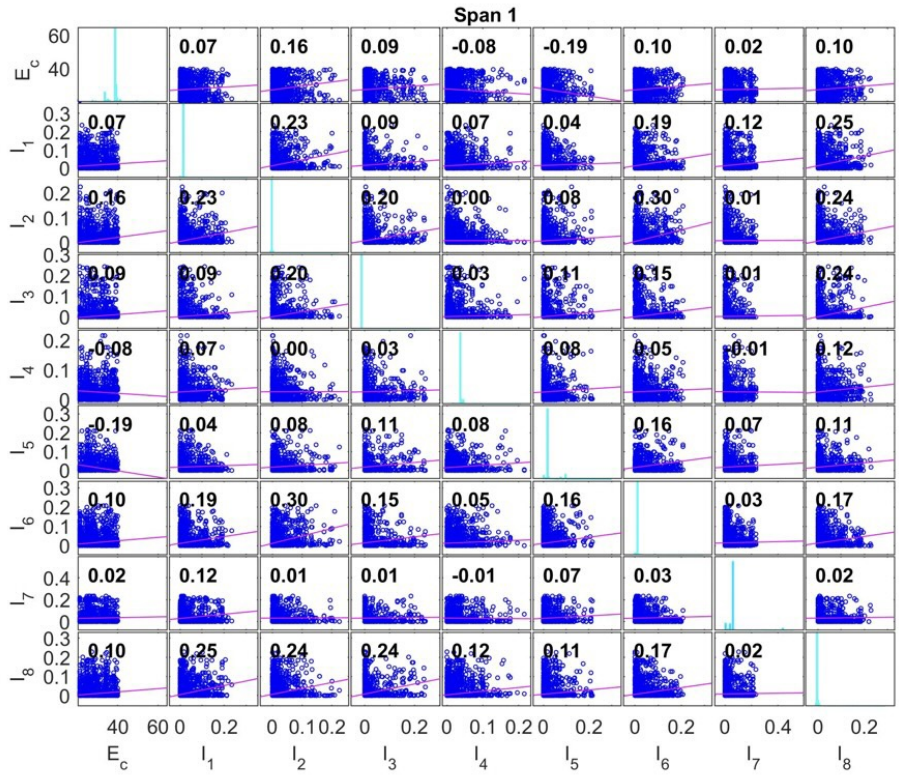

Figure 6.7: The results of the adjustment of the stiffness parameters for the span 1 [8].

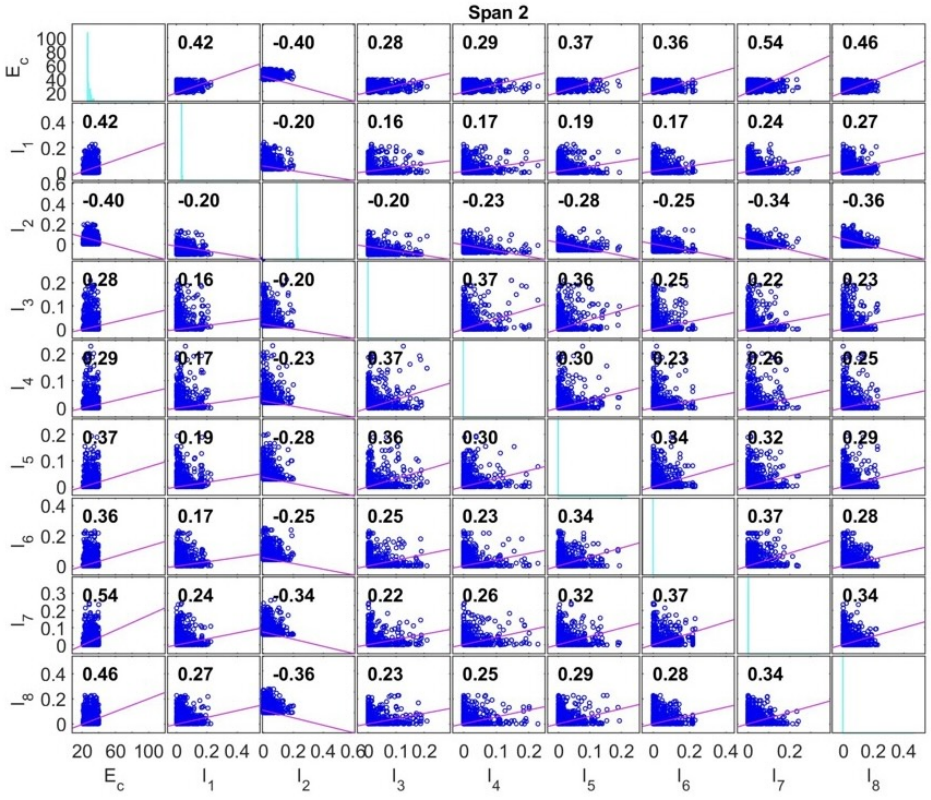

Figure 6.8: The results of the adjustment of the stiffness parameters for the span 2 [8].

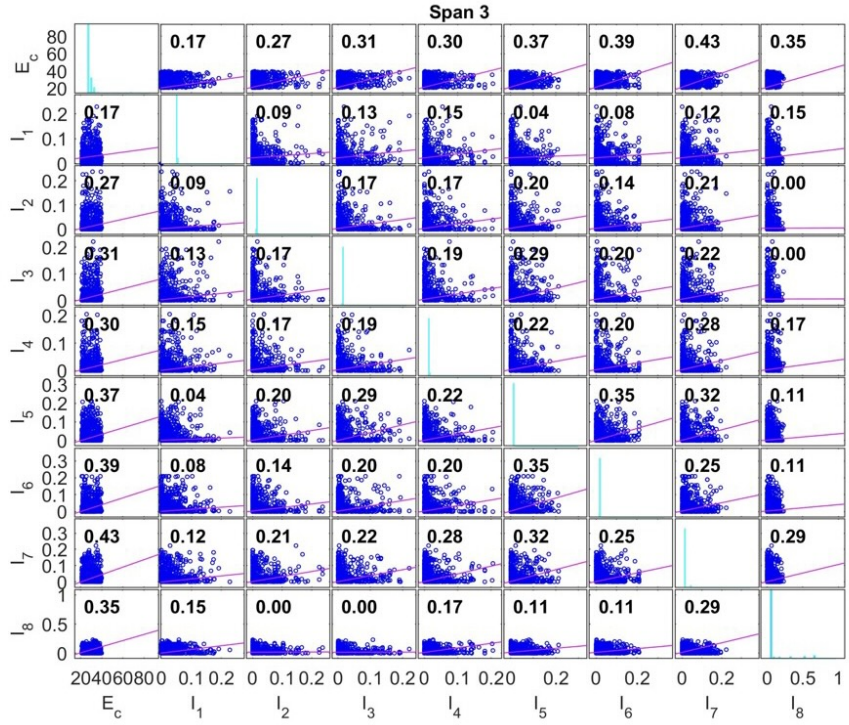

Figure 6.9: The results of the adjustment of the stiffness parameters for the span 3 [8].

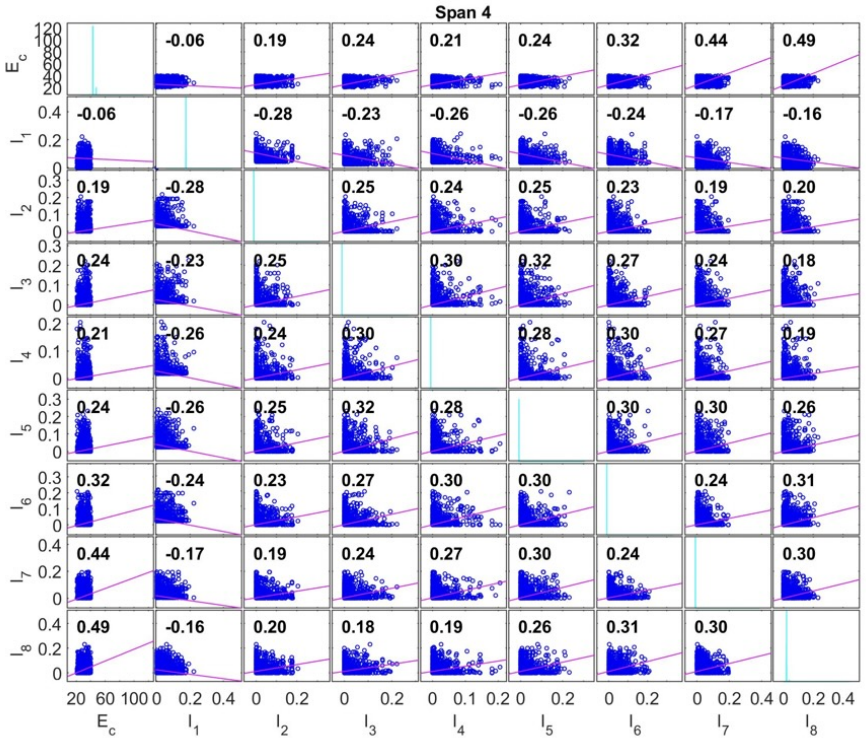

Figure 6.10: The results of the adjustment of the stiffness parameters for the span 4 [8].

Figure 6.11 shows the RF values for each span of the bridge in the update procedures of the FE model, in which the rating factors of the bending stresses of the structural members are calculated by applying the truck load configurations according to the AASHTO standards in the final updated FE models. The spans of the bridge structure are very short spans that could not be applied to all load configurations. Some vehicle load configurations of design standards have been used for the final calibrated FE models, such as HL-93; H-20 (20 tons); HS-20 (36 tons) and Type 3 (25 tons). HL-93 is combined from the truck of 32.5 tons; lane load of 9.3 kN/m and 22 tons of vehicle with two axles so that the RF values of all spans are less than 1.0. The span 2 is the shortest span and has the lowest RF of the entire bridge with the RF value equal to 0.12; 0.11 and 0.14 corresponding to H-20; HS-20 and Type 3, where the loads should decrease the actual capacity of the bridge with 2.40 tons; 3.96 tons and 3.50 tons, respectively. From the load rating results, the spans 3 and 4 have RF values less than 1.0, therefore, these spans are critical for H-20; HS-20 and Type 3 loading. The span 1 was rated as the best of all spans with an RF value of approximately 1.0.

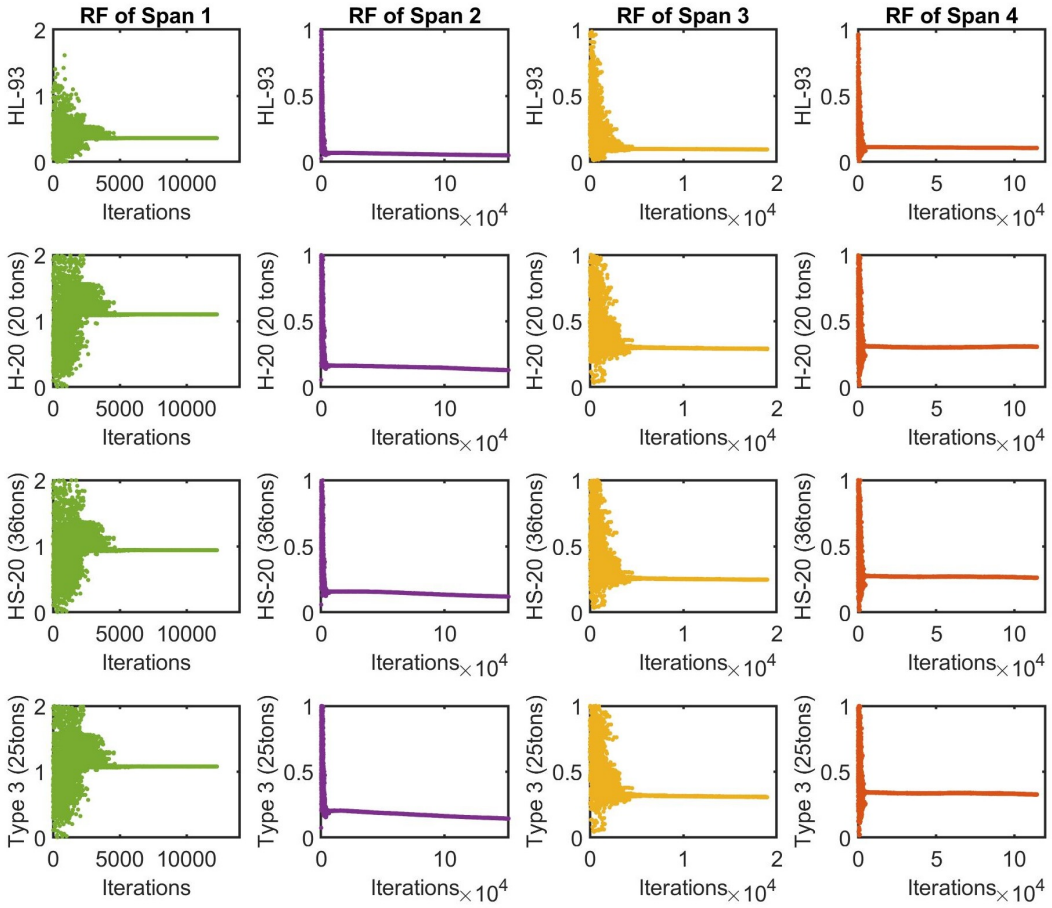

Figure 6.11: RF values of the truck load configurations according to the AASHTO codes [8].

The results of computational strain responses of structural members under the static centric load case 2 that has been used to calibrate the FE model with the measured data in the field testing as shown in Figure 6.12. The numerical comparison of computed and measured strain historical responses has been used to determine the objective function of the average percent error during the calibration procedure. The measured strain records of the spans 1, 2 and 4 are similar to the computed responses, while the strain value of the beam 6 in the span 3 is not similar, and the member stiffnesses should be adjusted more because it could not be well represented. The measured and calculated strain on the beam 4 of the span 1 had the highest strain values of 8.15 με and 8.00 με respectively, with the scale error of 1.84%. The span 2 in which the strains at the beam 5 are 21.67 με of testing and 19.88 με of computing with the error of 8.26%. The error value of the strain on the beam 4 of the span 3 is 2.27% compared to the measured and computed strain with 24.14 με and 23.59 με, respectively. With the span 4, the error of strain at the beam 4 is 5.67% with 28.35 με, respectively, for field strain, and 29.96 με for the FE method.

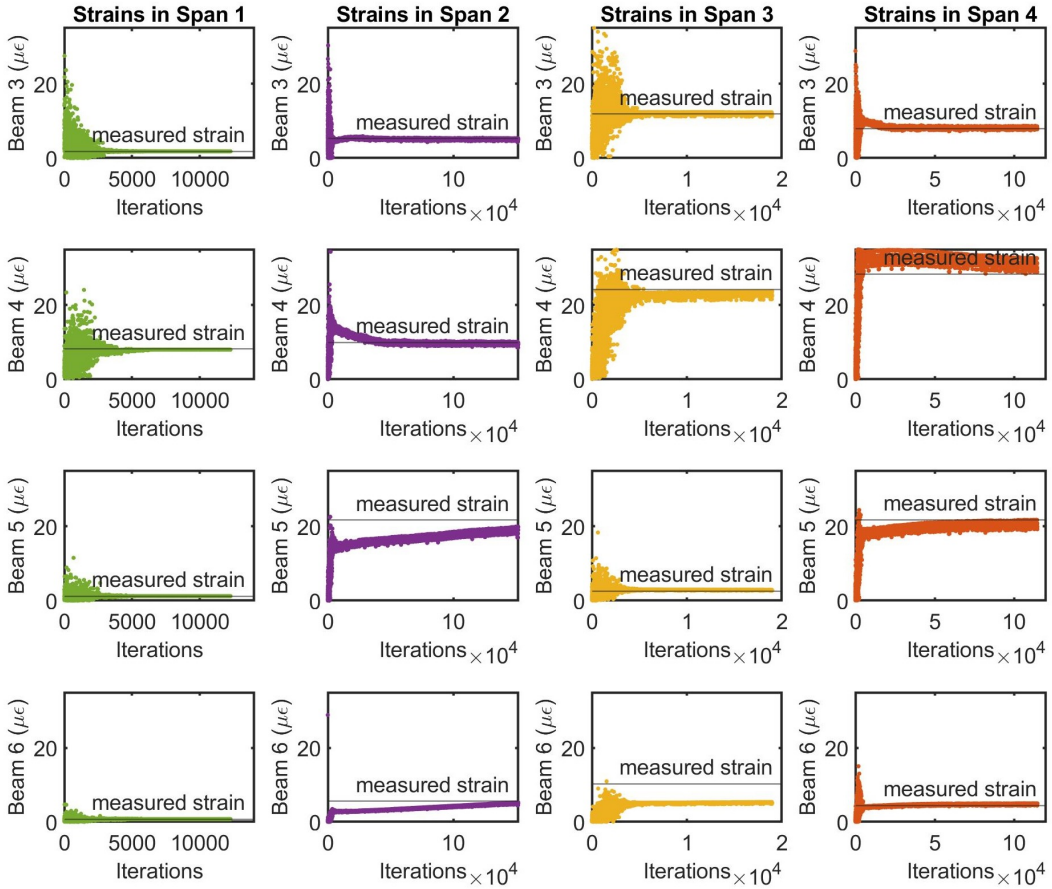

Figure 6.12: The numerical strain responses of the beams 3, 4, 5 and 6 in the bridge spans [8].

Figure 6.13 shows the percentage error of the GA algorithm for the FE model updating scenarios of all structural bridge spans with 12285; 151648; 19004 and 114695 iterations for the span 1, 2, 3 and 4, respectively. The GA algorithm converges fast and has almost the same convergence rate for all spans that start converging after 5000 iterations. The percentage error for the span 1 is 0.01% (lowest), while the span 4 has the error equal to 7.16% (highest). The spans 2 and 3 have error values less than 10% with a percent error of 0.21% and 6.31%, respectively. A good representative model would generally have a percent error value of less than 10%.

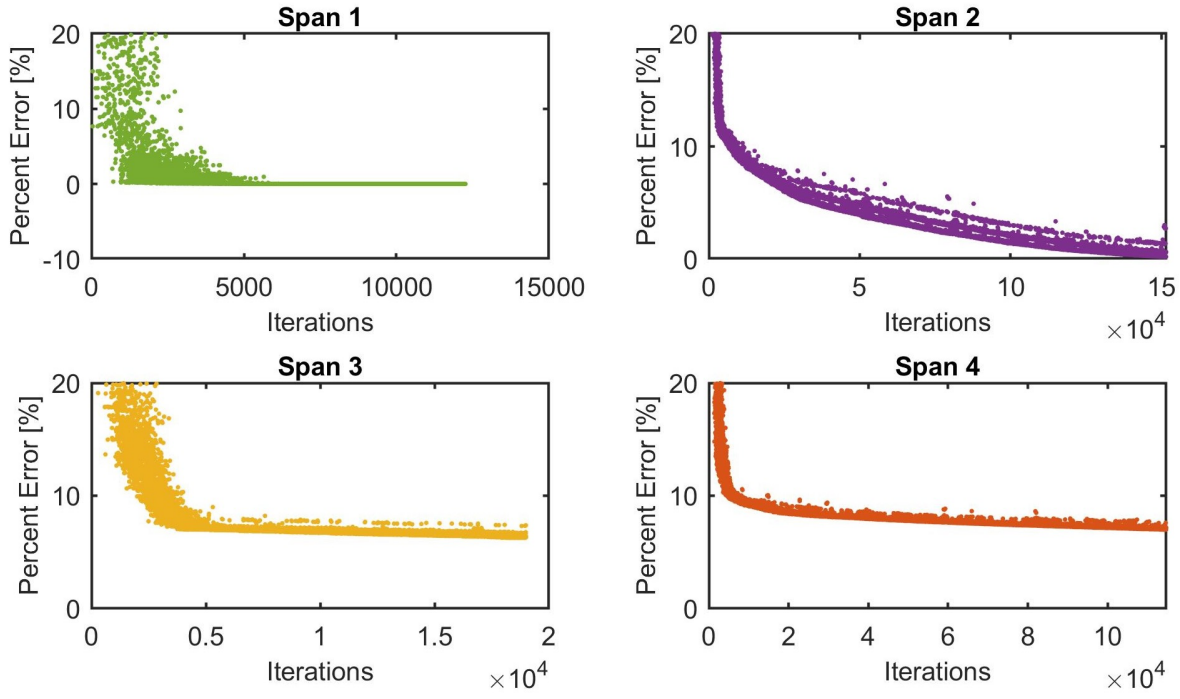

Figure 6.13: The percentage error values using the GA method for updating the FEM modeling of the spans 1, 2, 3 and 4 [8].

6.5 Case study 2: FE model updating of steel-concrete composite bridge

6.5.1 Description of the structure

The Vietnamese Ruri Bridge is located on the main road that connects the provinces of PhuYen and DakLac. The simply supported span is 18 m long and has a skew angle of 60 degrees. The bridge structure consists of seven steel beams (rolled profiles I760) on which a reinforced concrete slab of the deck is placed with a thickness of 15 cm. The beams are connected by five steel crossbars and supported on abutments by steel bearings. Figure 6.14 shows the diagnostic load testing of the existing Ruri bridge and some images in the field. The structural testing procedures in the field include: static load testing with two trucks; dynamic testing with one truck; assessment and evaluation for concrete and steel quality by other devices; scaffoldings for mounting sensors (strain transducers, displacement sensors, and accelerometers).

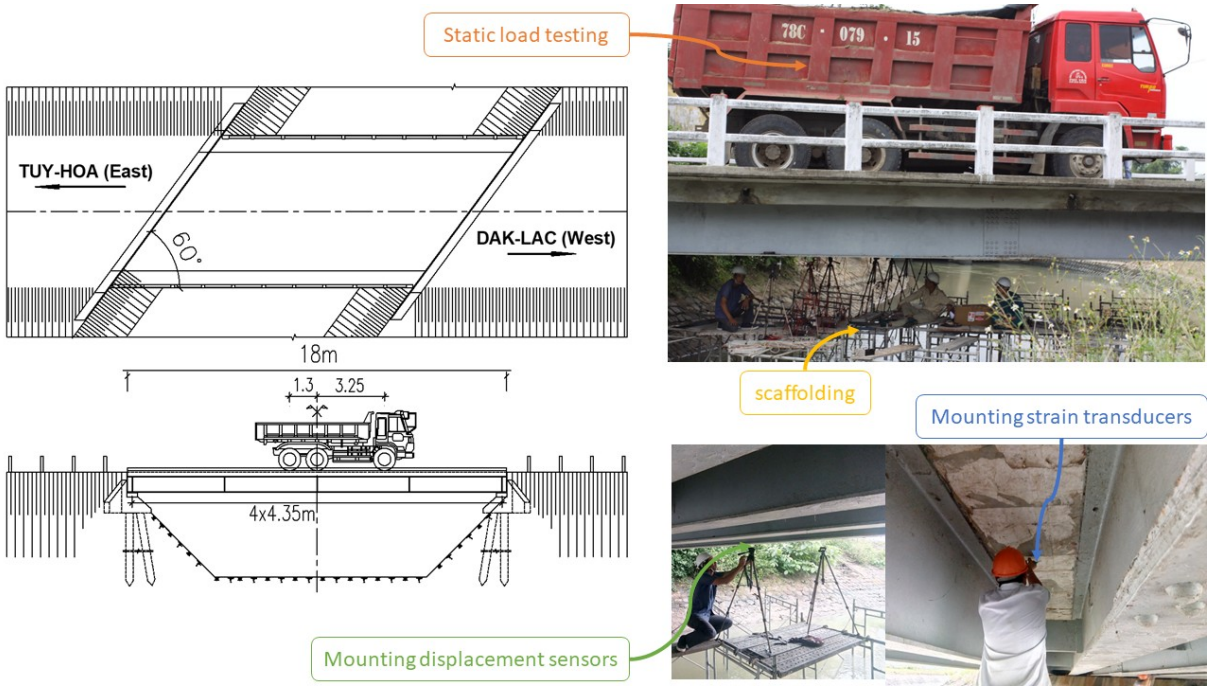

Figure 6.14: Overview of the Vietnamese Ruri bridge [14].

The location and description of the sensors attached to the cross-sectional girders at the midspan are presented in Figure 6.15. LVDT displacement sensors were installed at the bottom of the girders at the midspan and the reusable strain transducers were mounted at the bottom and top of the girders at the midspan, where the measured data was collected according to three static load cases. The accelerometers were located at the middle of the span to record the dynamic behavior of the bridge, while the test truck crossed the bridge at high speed. Intelligent sensors from the SHM system for the structural testing of the bridge were used. In the system, the connector interfaces contain the sensor identification (ID) name and calibration factor within a memory chip inside the sensor connectors. For example, the strain transducer (B3934, B3924, . . .) with "B" means strain sensor; the accelerometer (A2267, A2270, . . .) with "A" means acceleration sensors; the LVDT sensor (LV9804, LV9648, . . .) with "LV" means displacement sensor. The ID name of the sensors is used for the recognition of various types of sensors and can also be used for the database management of sensors by the software automatically.

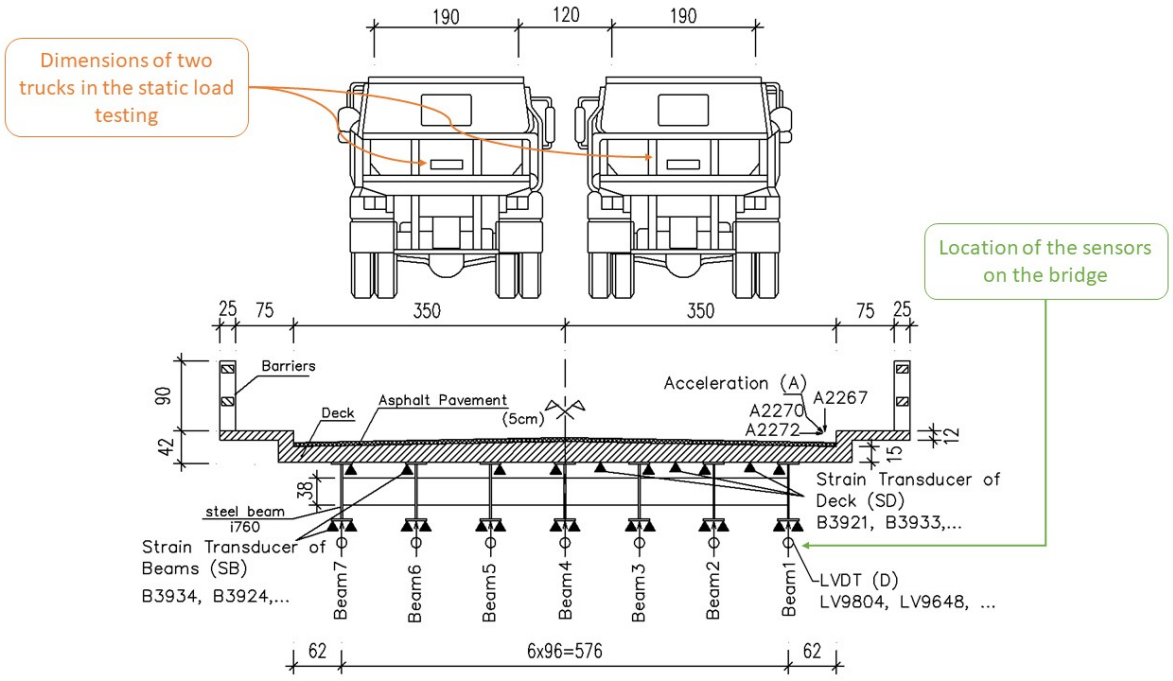

Figure 6.15: Cross-sectional steel girders (in centimeters) and field instrumentation plan [14].

6.5.2 Finite element modeling

The bridge structure was simulated in ANSYS in the form of seven longitudinal beams and five transverse beams which were modeled using the BEAM188 element. The elastic beam element has two nodes with twelve degrees of freedom, including axial, torsional, and bending displacements. A concrete deck slab was modeled using the SHELL181 element, which has four nodes with six degrees of freedom at each node, including displacements along the x, y, and z directions, as well as rotations about the x, y, and z axes. The BEAM188 element is applied to implement the different I-shaped section-cross types in 3-D geometry describing width of flange, flange thickness, web thickness and depth. The FE model of the Ruri Bridge was developed in ANSYS with 3293 nodes and 3964 elements, assuming linear elasticity and ignoring damping effects, with doubly pinned boundary conditions at the ends of the I-shaped steel girders. The results of the modal analysis and natural frequencies of the FE model for the bridge are presented in Figure 6.16. The graph also displays the two-dimensional group of point load cases defined by the FE model, where loads are applied similar to actual load testing and the standard AASHTO rating vehicles. The main purpose of the programming solution with codes and commands written by MAPDL in ANSYS, is to create an own application which can write and read data files after every loop iteration, and then update, and access to database information of the numerical results. MATLAB will support user-friendly interfaces with advanced optimization modules for management of results and parameter files of the FE modeling.

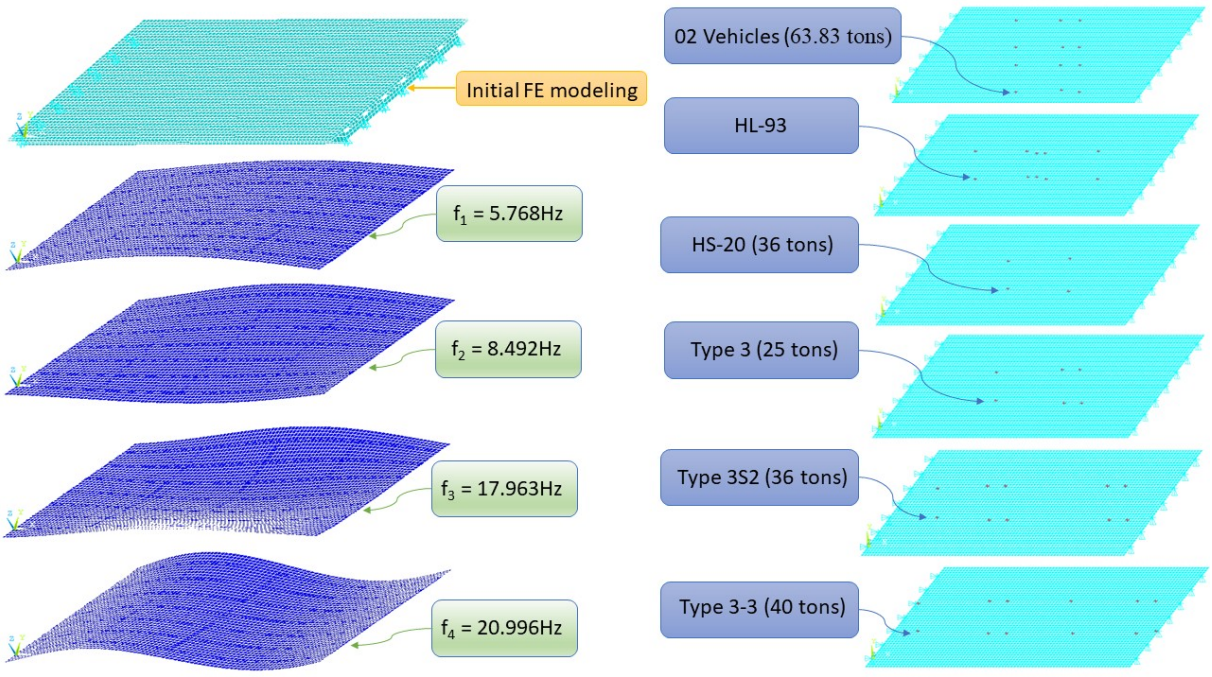

Figure 6.16: The natural vibration modal shapes of the Ruri bridge [14].

6.5.3 Results of the FE model updating

Table 6.2 shows member cross-sections and material properties to be defined for the individual members. Deck elements are defined as concrete material with initial values for material modulus, steel-reinforced concrete and Poisson's ratio. Longitudinal beams are given the same member group having the same I-shaped cross-sections and mechanical properties of structural steel, which are also created to assign for transverse beam elements with the same area of rectangle. The stiffness properties in the initial FE modeling are assigned to the different groups, so they can be changed during the optimization procedure. The variables for various types of beams are set in lower and upper bounds based on steel and concrete standards. Poisson ratios are constant: 0.2 and 0.3 for concrete and steel materials, respectively. Safety barriers and asphalt pavement layers on the concrete bridge deck are not considered in the FE modeling. Dead load includes the self-weight of the structure plus 22.5 kN/m^3 to account for 5 cm of asphalt and railings not defined by the FE model applied during load rating only.

Table 6.2: Parameters of updating FE model for mechanical and section properties [14].

Parameters	Initial values	Lower limit	Upper limit	PSO method	GA method	Ref.
$E_{concrete}$, [GPa]	25	21	40	33.16	32.20	[178], [181], [182], [183], [184]
$\rho_{concrete}$, kg/m^3	2500	2300	2600	2502.60	2378.20	
$t_{thickness\,deck}$, [mm]	150	100	300	133.14	151.91	
E_{Beam1}, [GPa]	210	178.5	220.5	220.35	178.74	
E_{Beam2}, [GPa]				220.50	179.07	
E_{Beam3}, [GPa]				220.50	179.44	
E_{Beam4}, [GPa]				195.68	184.394	
E_{Beam5}, [GPa]				182.268	191.73	
E_{Beam6}, [GPa]				178.50	218.90	
E_{Beam7}, [GPa]				178.50	202.37	
$E_{Tranverse\,Beams}$, [GPa]				203.55	216.45	
ρ_{steel}, kg/m^3	7850	7750	8050	7750	7989.2	
Section dimensions of longitudinal I-shaped steel beams						
Section height, H, [mm]	760	532	912	534.72	540.88	
Flange thickness, t_f, [mm]	30	15	60	60	37.61	
α, ratio	0.35	0.25	0.7	0.25	0.42	
β, ratio	0.66	0.5	1.0	0.92	0.57	
Flange width, B, [mm]	270	α.H		133.91	232	
Web thickness, t_w, [mm]	20	$\beta.t_f$		55.47	21.59	
Section dimensions of transverse rectangular steel plate beams						
Height, h, [mm]	380	$H/2$		267.36	270.44	
Thickness, t, [mm]	20	t_w		55.47	21.59	

Table 6.3 contains the initial design and final values of the natural frequencies of the PSO and GA method, and the results of the experimental frequencies. The final analytical frequencies are obtained from calibrated FE modeling based on PSO and GA techniques with 8.12% and 8.18% of the highest errors within 10000 steps, respectively. From the table, one can observe that for the results of updated modal frequencies after 1000 steps, the percent errors are below the level of 10%.

Table 6.3: Natural frequencies (Hz) [14].

Methods		First mode	Second mode	Third mode	Fourth mode.
Measured Frequencies (Hz)		2.66	4.29	9.38	12.19
Natural Frequencies (Hz)		2.705 (-1.69%)	4.363 (-1.70%)	9.275 (1.11%)	11.920 (2.21%)
Damping (%)		2.7	1.6	2.7	0.2
1000 steps	PSO	2.545 (4.31%)	4.251 (0.90%)	10.191 (-8.64%)	11.154 (8.50%)
	GA	2.526 (5.01%)	4.409 (-2.78%)	10.161 (-8.32%)	11.336 (7.00%)
10000 steps	PSO	2.547 (4.23%)	4.339 (-1.14%)	10.142 (-8.12%)	11.331 (7.04%)
	GA	2.547 (4.22%)	4.361 (-1.66%)	10.148 (-8.18%)	11.340 (6.97%)

Figure 6.17 shows the results of the normal probability distribution of uncertain parameters for updating the FE model obtained from the PSO and GA optimization methods. The graphs are an effective way to verify the calibrated parameters corresponding to an approximation of the Gaussian distribution, which can be used to monitor the tracking stiffness parameters of the FE model updating every step that occurs in the optimization procedure. Sensitivity-based analysis is implemented in the form of 16 vectors of uncertainty parameters of the real bridge structure in the PSO and GA approach after 10000 generated samples. Furthermore, the concrete deck increased from 25 GPa to 33.16 GPa in the PSO method and 32.20 GPa in the GA method, indicating that the reinforced concrete structure behaves normally throughout the entire structure of the interface between the slab and the beams. By modifying the master and slave variables in the model, the calibrated height of the longitudinal I-shaped steel beam decreased from 760 mm of the initial FE modeling calculated from the PSO and GA method to 534.72 mm and 540.88 mm, respectively.

Figure 6.18 presents the graphs of the total percent error with the number of iterations, the natural frequencies of the updated FE modeling, and the results of the moment and shear forces RF for steel structural members under various live-load cases and dead-load using the updated FE model. The values of the PSO method fluctuated significantly, while the variables of the GA method remained stable after 4000 steps. The plots show in tracking important changes of the entire optimization processing taking place step by step, where it could monitor structural health using key RF information to predict load limits. In the RF equation above, dead-load and live load effects were computed from the updated FE modeling at the cross-sections with maximum bending moment and the shear force diagram corresponding to the structural members. From the final updated FE model, the maximum numerical deflections below 63.83 tons of two trucks were 27.48 mm and 25.65 mm from the PSO and GA methods, respectively. The minimum RF of moment in the PSO method was 1.11 for the HL93 load case and the RF in the GA method was 1.27 for the HL93 load case, while the RFs of other load cases were greater than 1.0. The structural members of this bridge have the RFs for shear force much greater than 1.0.

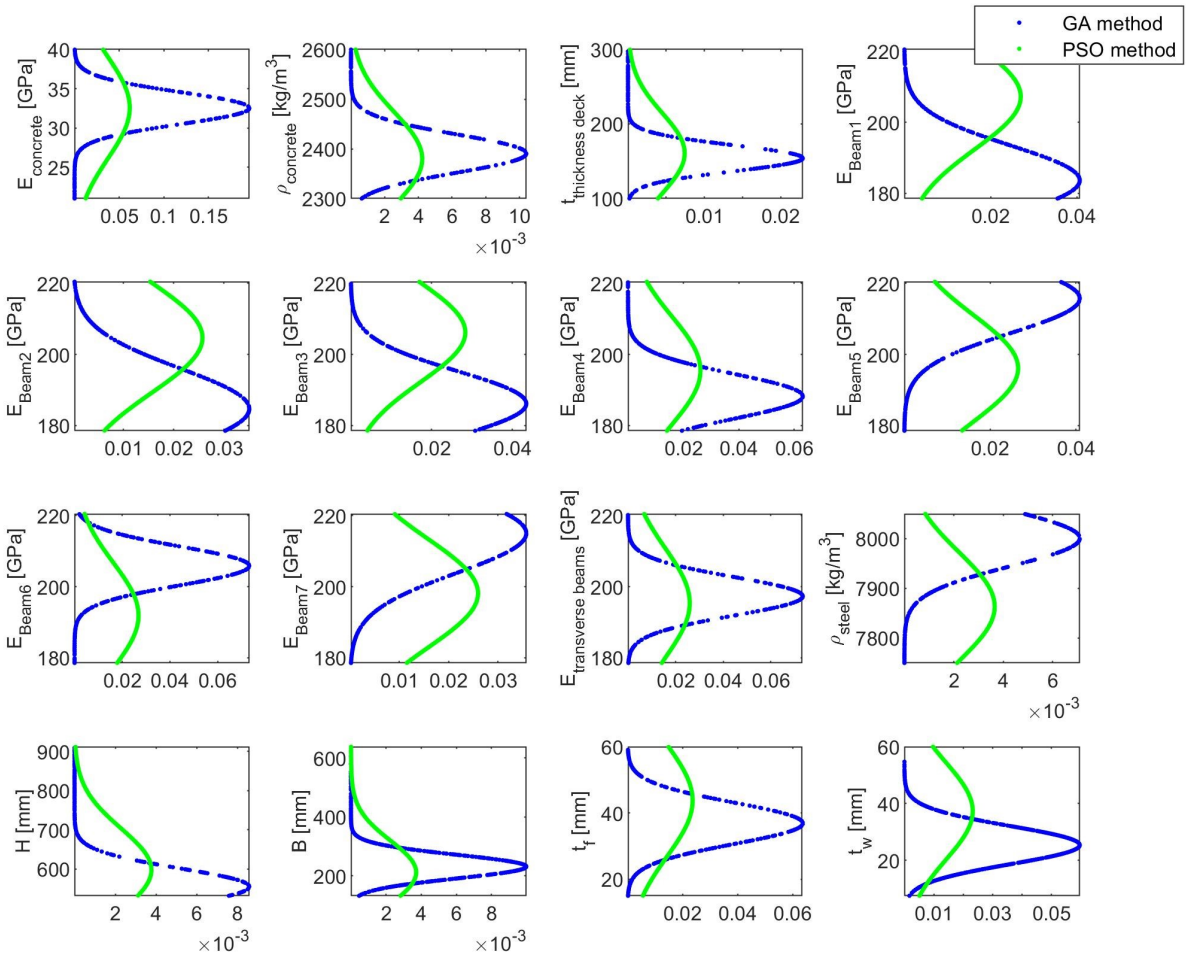

Figure 6.17: Results of the probability Gaussian distribution of 16 parameters [14].

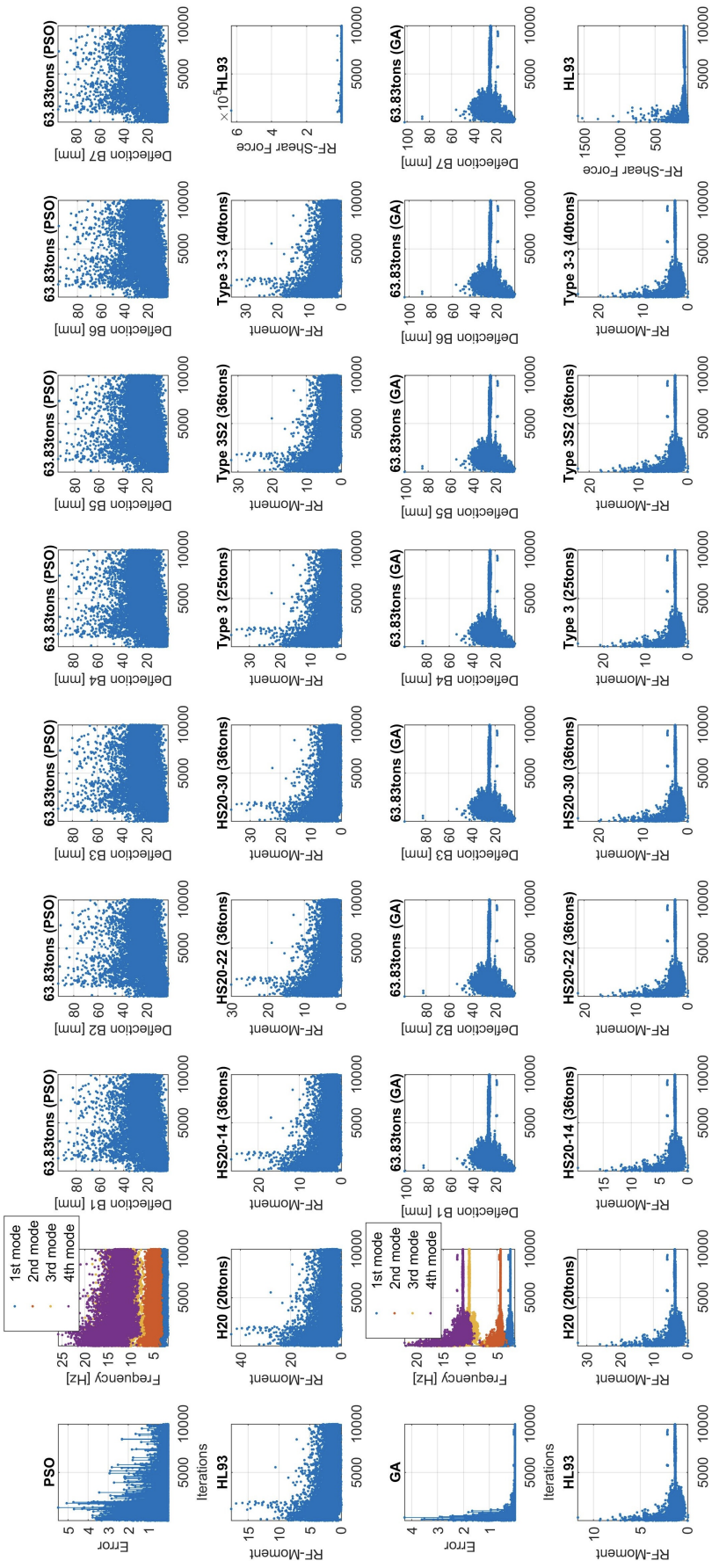

Figure 6.18: Total percent errors and numerical results of calibrated FE model [14].

6.6 Concluding remarks

In this chapter, the FE model updating of the existing bridges was developed to obtain field-calibrated models that could accurately represent the actual responses of the bridge structures and could also apply any truck load configurations to calculate realistic load ratings according to the AASHTO design standards. The most important conclusions made from the final updated FE models of the existing bridge structures based on the field truck load testing are drawn as follows:

- The proposed approaches of the FE model updating could be used for different types of bridge structures and even for other large structures by calibrating the stiffness parameters of structural components that compare the measured data in the field testing and the analytical data in the FE modeling to develop the representative model of the actual structure.
- The simplified finite-element analysis of bridge structures was used with the linear behavior assumption.
- The final calibrated FE models were a very accurate representation of the structure. They can reproduce the actual load distributions, which are better than the initial assumed FE models.
- The rating factors for the bridge spans were less than 1.0 indicating that this bridge was considered critical loads to ensure structural safety and serviceability for repair and maintenance.
- Any load configuration according to bridge design codes, standards and specifications could be applied to the adjusted FE models to make stress level predictions as well as being a very useful tool for increased load limits.
- Bridge load testing procedures and load ratings can be completed very quickly, accurately, and reliably. The automated FE model calibration approach can be applied to similar bridges, as well as complex and large railway arch bridges.

Chapter 7

Conclusion and future work

7.1 Conclusion

The purpose of the present work was to study automated FE model updating, advanced signal processing, and machine learning approaches for bridge health monitoring. Field data sets collected from bridge load diagnostic testing and railway bridge health monitoring were analyzed to evaluate bridge health condition through FE model calibration as well as machine learning-assisted structural health assessment. The following conclusions are drawn from the results obtained:

(1) FE model updating plays a crucial role in reproducing numerical data when comparing measured and computed responses, used for load ratings, load limits or permit loads, and overloads of the existing bridges. The final calibrated FE model could be used to determine the allowable load bearing capacity of structural members for the smart alarm system of long-term bridge health monitoring.

(2) Deep learning-integrated applications were developed for the vibration-based SHM system of the railway steel arch bridge. Wavelet-assisted CNN classification models were performed to predict hanger health conditions for the Dębica railway bridge located in Poland. The tension force values of the hangers were calculated from experimental vibration responses and the updated FE model of the heavy railway bridge to label the healthy and overload states on each hanger in CNN classification models. Using trained CNN models, it is possibe to predict hanger health status under various dynamic loading effects based on the measurements from a single accelerometer installed on the bridge span.

(3) Deep learning-based hanger health monitoring using orbit-shaped analysis of the bidirectional vibration sensor was conducted to assess the bending and torsional behavior of hangers under train load events and wind excitation. The use of orbits for hanger condition monitoring could consider the fundamental theory of mechanics and vibration analysis in terms of the similarity of the mechanical behavior of hangers and machinery shafts subject to dynamic loading, including their boundary conditions.

(4) Data-driven bridge health monitoring using ANN and ANFIS algorithms was performed to predict RMS values of Dębica bridge with various train events over a period of nine months from December 2019 to September 2020. The trained ANN and ANFIS models could be implemented in AI-based sensors to predict potential structural problems in bridge structures.

Summarizing the FE model calibration based on the bridge diagnostic load testing was efficiently proven and also applied for the SHM system. The machine learning-assisted SHM application was demonstrated for the existing railway bridge by integrating the updated FE model for reproducibility. The data-driven SHM using the machine learning and deep learning-attention algorithms was established for the railway steel arch bridge. Finally, the proposed innovative solutions would be cutting-edge technologies when machine learning-based algorithms could be implemented into AI-based vibration sensors for the smart alert system and intelligent data management as developed in this study.

7.2 Future research

In the light of the results of the present investigation, it can be seen that many problems exist and some modifications could be made. Therefore, it is recommended that the following work be carried out:

(1) Instead of updating the FE model, the studies were conducted individually for specific cases. It seems that this procedure of updating the FE model for all bridge structures would be implemented in the digital twin platform to continuously and automatically calibrate the cross-sectional stiffness and material properties of the structural members, and then visualize the results of FE analysis.

(2) The physics-informed machine learning was used for the hanger health diagnostic of the railway steel arch bridge. Using physics-informed ML approaches demonstrates the potential and benefits of integrating the FE model updating into machine learning applications.

(3) Due to the limitations of research time, this project was restricted to machine learning-assisted data-driven SHM for railway steel arch bridge as well as automated FE model updating for simple bridges. It is suggested that the useful results would be obtained from similar work on data-driven SHM for complex bridge structures. The proposed machine learning and signal processing algorithms would be integrated into the web-based digital twin platform for data-driven bridge health monitoring, which is built to access IFC-based 3D models for intelligent bridge data management. The installed sensors would be visualized at their respective locations in these 3D models to access data sets and interact with signal charts, graphs, or representations in real time. The smart alert system would be implemented on this SHM platform to predict structural potential problems and signal anomalies.

(4) The proposed wavelet-assisted machine learning techniques should be integrated into the Web-based platform of intelligent data management for the data-driven vibration-based SHM system. Machine learning-based regression models would be developed to predict hanger health status during weather events in real time with a smart alarm system.

(5) It would be worthwhile to develop quantum machine learning algorithms for the data-driven vibration-based SHM of the complex large railway bridge. The advantages and limitations of QML for industrial vibration-based SHM applications could be discussed for potential issues, such as: signal pre-processing; signal noise; signal feature detection and extraction; classification and regression prediction models.

Bibliography

[1] Brett Commander. “Evolution of Bridge Diagnostic Load Testing in the USA”. In: *Frontiers in Built Environment* 5 (May 2019). DOI: 10.3389/fbuil.2019.00057.

[2] Eloi Figueiredo and James Brownjohn. “Three decades of statistical pattern recognition paradigm for SHM of bridges”. In: *Structural Health Monitoring* 21.6 (Mar. 2022), pp. 3018–3054. DOI: 10.1177/14759217221075241.

[3] Jesse D. Sipple and Masoud Sanayei. “Full-Scale Bridge Finite-Element Model Calibration Using Measured Frequency-Response Functions”. In: *Journal of Bridge Engineering* 20.9 (Sept. 2015). ISSN: 1943-5592. DOI: 10.1061/(asce)be.1943-5592.0000705.

[4] Mohammad Reza Saberi, Ali Reza Rahai, Masoud Sanayei, and Richard M. Vogel. “Bridge Fatigue Service-Life Estimation Using Operational Strain Measurements”. In: *Journal of Bridge Engineering* 21.5 (May 2016). DOI: 10.1061/(asce)be.1943-5592.0000860.

[5] Sreenivas Alampalli, Dan M. Frangopol, Jesse Grimson, Marvin W. Halling, David E. Kosnik, Eva O. L. Lantsoght, David Yang, and Y. Edward Zhou. “Bridge Load Testing: State-of-the-Practice”. In: *Journal of Bridge Engineering* 26.3 (Mar. 2021). DOI: 10.1061/(asce)be.1943-5592.0001678.

[6] Masoud Sanayei, John E. Phelps, Jesse D. Sipple, Erin S. Bell, and Brian R. Brenner. “Instrumentation, Nondestructive Testing, and Finite-Element Model Updating for Bridge Evaluation Using Strain Measurements”. In: *Journal of Bridge Engineering* 17.1 (Jan. 2012), pp. 130–138. DOI: 10.1061/(asce)be.1943-5592.0000228.

[7] Erin Santini Bell, Paul J. Lefebvre, Masoud Sanayei, Brian Brenner, Jesse D. Sipple, and Jason Peddle. “Objective Load Rating of a Steel-Girder Bridge Using Structural Modeling and Health Monitoring”. In: *Journal of Structural Engineering* 139.10 (Oct. 2013), pp. 1771–1779. ISSN: 1943-541X. DOI: 10.1061/(asce)st.1943-541x.0000599.

[8] Duc C. Nguyen, Marek Salamak, Andrzej Katunin, and Michael Gerges. "Finite Element Model Updating of RC Bridge Structure with Static Load Testing: A Case Study of Vietnamese ThiThac Bridge in Coastal and Marine Environment". In: *Sensors* 22.22 (Nov. 2022), p. 8884. DOI: 10.3390/s22228884.

[9] Muhammad Fawad, Marek Salamak, Grzegorz Poprawa, Kalman Koris, Marcin Jasinski, Piotr Lazinski, Dawid Piotrowski, Muhammad Hasnain, and Michael Gerges. "Automation of structural health monitoring (SHM) system of a bridge using BIMification approach and BIM-based finite element model development". In: *Scientific Reports* 13.1 (Aug. 2023). DOI: 10.1038/s41598-023-40355-7.

[10] X.X. Cheng and Z.Y. Song. "Modal experiment and model updating for Yingzhou Bridge". In: *Structures* 32 (Aug. 2021), pp. 746–759. DOI: 10.1016/j.istruc.2021.03.025.

[11] Bjørn T. Svendsen, Øyvind W. Petersen, Gunnstein T. Frøseth, and Anders Rønnquist. "Improved finite element model updating of a full-scale steel bridge using sensitivity analysis". In: *Structure and Infrastructure Engineering* 19.3 (July 2021), pp. 315–331. DOI: 10.1080/15732479.2021.1944227.

[12] Siti Shahirah Saidin, Adiza Jamadin, Sakhiah Abdul Kudus, Norliyati Mohd Amin, and Muhamad Azhan Anuar. "An Overview: The Application of Vibration-Based Techniques in Bridge Structural Health Monitoring". In: *International Journal of Concrete Structures and Materials* 16.1 (Dec. 2022). DOI: 10.1186/s40069-022-00557-1.

[13] B. Barros, B. Conde, M. Cabaleiro, and B. Riveiro. "Deterministic and probabilistic-based model updating of aging steel bridges". In: *Structures* 54 (Aug. 2023), pp. 89–105. DOI: 10.1016/j.istruc.2023.05.020.

[14] Duc C. Nguyen, Marek Salamak, Andrzej Katunin, Michael Gerges, and Mohamed Abdel-Maguid. "Finite element model updating of steel-concrete composite bridge: A study case of the Ruri bridge in Vietnam". In: *Archives of Civil Engineering* vol. 69.No 3 (2023), pp. 425–443. DOI: 10.24425/ace.2023.146089.

[15] Gongkang Fu, Frank P. Pezze, and Sreenivas Alampalli. "Diagnostic Load Testing for Bridge Load Rating". In: *Transportation Research Record: Journal of the Transportation Research Board* 1594.1 (Jan. 1997), pp. 125–133. DOI: 10.3141/1594-13.

[16] Mohammad Abedin, Francisco J. De Caso y Basalo, Nafiseh Kiani, Armin B. Mehrabi, and Antonio Nanni. "Bridge load testing and damage evaluation using model updating method". In: *Engineering Structures* 252 (Feb. 2022), p. 113648. DOI: 10.1016/j.engstruct.2021.113648.

[17] Tomasz Płaszczyk, Kamil Korus, Mateusz Uściłowski, and Marek Salamak. "Cyfryzacja procesów utrzymania obiektów infrastruktury". In: *MATERIAŁY BUDOWLANE* 1.6 (June 2021), pp. 52–54. DOI: 10.15199/33.2021.06.04.

[18] Kamil Korus, Marek Salamak, and Marcin Jasiński. "Optimization of geometric parameters of arch bridges using visual programming FEM components and genetic algorithm". In: *Engineering Structures* 241 (Aug. 2021), p. 112465. DOI: 10.1016/j.engstruct.2021.112465.

[19] Manuel Chiachío, María Megía, Juan Chiachío, Juan Fernandez, and María L. Jalón. "Structural digital twin framework: Formulation and technology integration". In: *Automation in Construction* 140 (Aug. 2022), p. 104333. DOI: 10.1016/j.autcon.2022.104333.

[20] Kamil Korus, Marek Salamak, and Jan Winkler. "Digital Twins as the Next Step in the Design and Management of Bridge Structures". In: *Lecture Notes in Civil Engineering*. Springer Nature Switzerland, 2023, pp. 1586–1593. DOI: 10.1007/978-3-031-32511-3_162.

[21] Song Honghong, Yang Gang, Li Haijiang, Zhang Tian, and Jiang Annan. "Digital twin enhanced BIM to shape full life cycle digital transformation for bridge engineering". In: *Automation in Construction* 147 (Mar. 2023), p. 104736. DOI: 10.1016/j.autcon.2022.104736.

[22] Marcin Jasiński, Piotr Łaziński, and Dawid Piotrowski. "The Concept of Creating Digital Twins of Bridges Using Load Tests". In: *Sensors* 23.17 (Aug. 2023), p. 7349. DOI: 10.3390/s23177349.

[23] Statistics Poland. *Intermodal transport in years 2020-2022*. Updated: 30.11.2023. 2023. URL: https://stat.gov.pl/en/topics/transport-and-communications/transport/intermodal-transport-in-years-2020-2022,14,2.html.

[24] Łukasz Filar, Jerzy Kałuża, and Marek Wazowski. "Bridge Load Tests in Poland Today and Tomorrow – The Standard and the New Ways in Measuring and Research to Ensure Transport Safety". In: *Procedia Engineering* 192 (2017), pp. 183–188. ISSN: 1877-7058. DOI: 10.1016/j.proeng.2017.06.032.

[25] Przemysław Kołakowski, Jacek Szelążek, Krzysztof Sekuła, Andrzej Świercz, Krzysztof Mizerski, and Piotr Gutkiewicz. "Structural health monitoring of a railway truss bridge using vibration-based and ultrasonic methods". In: *Smart Materials and Structures* 20.3 (Feb. 2011), p. 035016. ISSN: 1361-665X. DOI: 10.1088/0964-1726/20/3/035016.

[26] Piotr Klikowicz, Marek Salamak, and Grzegorz Poprawa. "Structural Health Monitoring of Urban Structures". In: *Procedia Engineering* 161 (2016), pp. 958–962. DOI: 10.1016/j.proeng.2016.08.833.

[27] Mikołaj Miśkiewicz and Łukasz Pyrzowski. "Load test of new European record holder in span length among extradosed type bridges". In: *E3S Web of Conferences* 63 (2018). Ed. by G. Nykiel, p. 00006. ISSN: 2267-1242. DOI: 10.1051/e3sconf/20186300006.

[28] Joyraj Chakraborty, Andrzej Katunin, Piotr Klikowicz, and Marek Salamak. "Early Crack Detection of Reinforced Concrete Structure Using Embedded Sensors". In: *Sensors* 19.18 (Sept. 2019), p. 3879. DOI: 10.3390/s19183879.

[29] Jan Bień and Mieszko Kużawa. "Dynamic Tests in Bridge Health Monitoring". In: *Studia Geotechnica et Mechanica* 42.4 (June 2020), pp. 291–296. ISSN: 2083-831X. DOI: 10.2478/sgem-2019-0045.

[30] Jacek Kwiatkowski, Wojciech Anigacz, and Damian Beben. "Comparison of Non-Destructive Techniques for Technological Bridge Deflection Testing". In: *Materials* 13.8 (Apr. 2020), p. 1908. ISSN: 1996-1944. DOI: 10.3390/ma13081908.

[31] Jan Biliszczuk, Paweł Hawryszków, and Marco Teichgraeber. "SHM System and a FEM Model-Based Force Analysis Assessment in Stay Cables". In: *Sensors* 21.6 (Mar. 2021), p. 1927. ISSN: 1424-8220. DOI: 10.3390/s21061927.

[32] Pawel Tysiac, Mikolaj Miskiewicz, and Dawid Bruski. "Bridge Non-Destructive Measurements Using a Laser Scanning during Acceptance Testing: Case Study". In: *Materials* 15.23 (Nov. 2022), p. 8533. ISSN: 1996-1944. DOI: 10.3390/ma15238533.

[33] Mateusz Bocian, Nikolaos Nikitas, Maksat Kalybek, Mieszko Kużawa, Paweł Hawryszków, Jan Bień, Jerzy Onysyk, and Jan Biliszczuk. "Dynamic performance verification of the Rędziński Bridge using portable camera-based vibration monitoring systems". In: *Archives of Civil and Mechanical Engineering* 23.1 (Dec. 2022). ISSN: 1644-9665. DOI: 10.1007/s43452-022-00582-7.

[34] Krzysztof Zoltowski, Anna Banas, Mikolaj Binczyk, and Przemyslaw Kalitowski. "Control of the bridge span vibration with high coefficient passive damper. Theoretical consideration and application". In: *Engineering Structures* 254 (Mar. 2022), p. 113781. DOI: 10.1016/j.engstruct.2021.113781.

[35] Nguyen Duc C., Marek Salamak, Andrzej Katunin, Grzegorz Poprawa, Piotr Przystałka, and Mateusz Hypki. "Vibration-based SHM of Dębica railway steel bridge with optimized ANN and ANFIS". In: *Journal of Constructional Steel Research* 215 (Apr. 2024), p. 108505. ISSN: 0143-974X. DOI: 10.1016/j.jcsr.2024.108505.

[36] OpenDevelopment Vietnam. *Infrastructure*. Updated: 08.10.2022. 2022. URL: https://vietnam.opendevelopmentmekong.net/vi/topics/infrastructure/.

[37] Department of international trade. *VIETNAM INFRASTRUCTURE*. Updated: 5.2019. 2019. URL: https://www.ukabc.org.uk/wp-content/uploads/2019/07/Infrastructure-Update-May-2019.pdf.

[38] Grzegorz Świt, Aleksandra Krampikowska, and Minh Chinh Luong. "A prototype system for acoustic emission-based structural health monitoring of My Thuan bridge". In: *2016 Prognostics and System Health Management Conference (PHM-Chengdu)*. 2016, pp. 1–6. DOI: 10.1109/PHM.2016.7819877.

[39] Luong Minh Chinh. "The Inadequacies of the Existing Structural Health Monitoring Systems for Cable Stayed Bridges in Vietnam". In: *CIGOS 2019, Innovation for Sustainable Infrastructure*. Springer Singapore, Oct. 2019, pp. 215–220. ISBN: 9789811508028. DOI: 10.1007/978-981-15-0802-8_31. URL: http://dx.doi.org/10.1007/978-981-15-0802-8_31.

[40] Thanh Q Nguyen, Tuan Anh Nguyen, and Thuy T Nguyen. "PSD characteristics for the random vibration signals used in bridge structural health monitoring in Vietnam based on a multi-sensor system". In: *International Journal of Distributed Sensor Networks* 18.9 (Sept. 2022), p. 155013292211251. ISSN: 1550-1477. DOI: 10.1177/15501329221125110.

[41] Toan Pham-Bao, Nhi Ngo-Kieu, Luan Vuong-Cong, and Tam Nguyen-Nhat. "Energy dissipation-based material deterioration assessment using random decrement technique and convolutional neural network: A case study of Saigon bridge in Ho Chi Minh City, Vietnam". In: *Structural Control and Health Monitoring* 29.7 (Mar. 2022). ISSN: 1545-2263. DOI: 10.1002/stc.2956.

[42] Toan Pham-Bao, Tam Nguyen-Nhat, and Nhi Ngo-Kieu. "A novel approach to investigate the mechanical properties of the material for bridge health monitoring using convolutional neural network". In: *Structure and Infrastructure Engineering* (Sept. 2022), pp. 1–21. ISSN: 1744-8980. DOI: 10.1080/15732479.2022.2127792.

[43] An Huynh-Thai, Toan Pham-Bao, Hung Nguyen-Quoc, and Luan Vuong-Cong. "Evaluating Damping Model Applied for Cable Tension of Cable-Stayed Bridge". In: *Lecture Notes in Civil Engineering*. Springer Nature Singapore, Aug. 2023, pp. 623–629. ISBN: 9789819923458. DOI: 10.1007/978-981-99-2345-8_63. URL: http://dx.doi.org/10.1007/978-981-99-2345-8_63.

[44] Lan Nguyen and Hung Huy Pham. "Health Monitoring System for Long Span Bridges Across the Han River in Da Nang City, Vietnam". In: *Structural Health Monitoring and Engineering Structures*. Springer Singapore, 2021, pp. 381–397. ISBN: 9789811609459. DOI: 10.1007/978-981-16-0945-9_31. URL: http://dx.doi.org/10.1007/978-981-16-0945-9_31.

[45] Hua-Peng Chen and Yi-Qing Ni. *Structural Health Monitoring of Large Civil Engineering Structures*. Wiley, Feb. 2018. DOI: 10.1002/9781119166641.

[46] B. H. J. Pushpakumara and G. A. Thusitha. "Development of a Structural Health Monitoring Tool for Underwater Concrete Structures". In: *Journal of Construction Engineering and Management* 147.10 (Oct. 2021). DOI: 10.1061/(asce)co.1943-7862.0002163.

[47] Arman Malekloo, Ekin Ozer, Mohammad AlHamaydeh, and Mark Girolami. "Machine learning and structural health monitoring overview with emerging technology and high-dimensional data source highlights". In: *Structural Health Monitoring* 21.4 (Aug. 2021), pp. 1906–1955. DOI: 10.1177/14759217211036880.

[48] Mohammad AlHamaydeh and Nour Ghazal Aswad. "Structural Health Monitoring Techniques and Technologies for Large-Scale Structures: Challenges, Limitations, and Recommendations". In: *Practice Periodical on Structural Design and Construction* 27.3 (Aug. 2022). DOI: 10.1061/(asce)sc.1943-5576.0000703.

[49] Zhiguo He, Wentao Li, Hadi Salehi, Hao Zhang, Haiyi Zhou, and Pengcheng Jiao. "Integrated structural health monitoring in bridge engineering". In: *Automation in Construction* 136 (Apr. 2022), p. 104168. DOI: 10.1016/j.autcon.2022.104168.

[50] Ge-Wei Chen, Piotr Omenzetter, and Sherif Beskhyroun. "Operational modal analysis of an eleven-span concrete bridge subjected to weak ambient excitations". In: *Engineering Structures* 151 (Nov. 2017), pp. 839–860. ISSN: 0141-0296. DOI: 10.1016/j.engstruct.2017.08.066.

[51] Dimitrios Anastasopoulos, Guido De Roeck, and Edwin P.B. Reynders. "One-year operational modal analysis of a steel bridge from high-resolution macrostrain monitoring: Influence of temperature vs. retrofitting". In: *Mechanical Systems and Signal*

Processing 161 (Dec. 2021), p. 107951. ISSN: 0888-3270. DOI: 10.1016/j.ymssp.2021.107951.

[52] Enrique García-Macías, Antonello Ruccolo, Mariano Angelo Zanini, Carlo Pellegrino, Carmelo Gentile, Filippo Ubertini, and Paolo Mannella. "P3P: a software suite for autonomous SHM of bridge networks". In: *Journal of Civil Structural Health Monitoring* 13.8 (Nov. 2022), pp. 1577–1594. ISSN: 2190-5479. DOI: 10.1007/s13349-022-00653-6.

[53] Bjørn T. Svendsen, Ole Øiseth, Gunnstein T. Frøseth, and Anders Rønnquist. "A hybrid structural health monitoring approach for damage detection in steel bridges under simulated environmental conditions using numerical and experimental data". In: *Structural Health Monitoring* 22.1 (May 2022), pp. 540–561. ISSN: 1741-3168. DOI: 10.1177/14759217221098998.

[54] Siti Shahirah Saidin, Sakhiah Abdul Kudus, Adiza Jamadin, Muhamad Azhan Anuar, Norliyati Mohd Amin, Atikah Bt Zakaria Ya, and Kunitomo Sugiura. "Vibration-based approach for structural health monitoring of ultra-high-performance concrete bridge". In: *Case Studies in Construction Materials* 18 (July 2023), e01752. ISSN: 2214-5095. DOI: 10.1016/j.cscm.2022.e01752.

[55] Samten Wangchuk, Dionysius M. Siringoringo, and Yozo Fujino. "Modal analysis and tension estimation of stay cables using noncontact vision-based motion magnification method". In: *Structural Control and Health Monitoring* 29.7 (Mar. 2022). ISSN: 1545-2263. DOI: 10.1002/stc.2957.

[56] Nguyen Duc C., Marek Salamak, Andrzej Katunin, and Grzegorz Poprawa. "Finite Element Model Updating of Steel Bridge Structure Using Vibration-Based Structural Health Monitoring System: A Case Study of Railway Steel Arch Bridge in Poland". In: *Experimental Vibration Analysis for Civil Engineering Structures*. Ed. by Maria Pina Limongelli, Pier Francesco Giordano, Said Quqa, Carmelo Gentile, and Alfredo Cigada. Vol. 433. Cham: Springer Nature Switzerland, 2023, pp. 371–380. ISBN: 978-3-031-39117-0. DOI: 10.1007/978-3-031-39117-0_38.

[57] Matteo Vagnoli and Rasa Remenyte-Prescott. "An automatic bridge damage diagnostics method using empirical mode decomposition based health indicators and neuro-fuzzy classification". In: *Structural Control and Health Monitoring* 29.10 (June 2022). DOI: 10.1002/stc.3027.

[58] Sunjoong Kim and Taeyong Kim. "Machine-learning-based prediction of vortex-induced vibration in long-span bridges using limited information". In: *Engineering Structures* 266 (Sept. 2022), p. 114551. ISSN: 0141-0296. DOI: 10.1016/j.engstruct.2022.114551.

[59] Xiao-Wei Ye, Zhen Sun, and Jun Lu. "Prediction and early warning of wind-induced girder and tower vibration in cable-stayed bridges with machine learning-based approach". In: *Engineering Structures* 275 (Jan. 2023), p. 115261. ISSN: 0141-0296. DOI: 10.1016/j.engstruct.2022.115261.

[60] W.L. Bayissa, N. Haritos, and S. Thelandersson. "Vibration-based structural damage identification using wavelet transform". In: *Mechanical Systems and Signal Processing* 22.5 (July 2008), pp. 1194–1215. ISSN: 0888-3270. DOI: 10.1016/j.ymssp.2007.11.001.

[61] Yu Chongchong, Zhang Jia, Jia Shuo, Yang Yang, and Tu Xuyan. "On vibration signals analysis in Bridge Healthy Monitoring system using wavelet transform". In: *2008 27th Chinese Control Conference*. 2008, pp. 209–213. DOI: 10.1109/CHICC.2008.4605029.

[62] Xiang-jun Chen, Zhan-feng Gao, Yue-e Ma, and Qiang Guo. "Application of Wavelet Analysis in Vibration Signal Processing of Bridge Structure". In: *2010 International Conference on Measuring Technology and Mechatronics Automation*. Vol. 1. 2010, pp. 671–674. DOI: 10.1109/ICMTMA.2010.95.

[63] D. Hester and A. González. "A wavelet-based damage detection algorithm based on bridge acceleration response to a vehicle". In: *Mechanical Systems and Signal Processing* 28 (Apr. 2012), pp. 145–166. ISSN: 0888-3270. DOI: 10.1016/j.ymssp.2011.06.007.

[64] J. V. Araujo dos Santos, A. Katunin, and H. Lopes. "Vibration-Based Damage Identification Using Wavelet Transform and a Numerical Model of Shearography". In: *International Journal of Structural Stability and Dynamics* 19.04 (Apr. 2019), p. 1950038. ISSN: 1793-6764. DOI: 10.1142/s021945541950038x.

[65] Yuanfeng Xia, Jian Pang, Liang Yang, Qin Zhao, and Xianwu Yang. "Study on vibration response and orbits of misaligned rigid rotors connected by hexangular flexible coupling". In: *Applied Acoustics* 155 (Dec. 2019), pp. 286–296. ISSN: 0003-682X. DOI: 10.1016/j.apacoust.2019.05.022.

[66] Mingjin Zhang, Xu Huang, Yongle Li, Hao Sun, Jingyu Zhang, and Bin Huang. "Improved Continuous Wavelet Transform for Modal Parameter Identification of Long-Span Bridges". In: *Shock and Vibration* 2020 (Jan. 2020), pp. 1–16. ISSN: 1875-9203. DOI: 10.1155/2020/4360184.

[67] Emrah Erduran, Fredrik Marøy Pettersen, Semih Gonen, and Albert Lau. "Identification of Vibration Frequencies of Railway Bridges from Train-Mounted Sensors Using Wavelet Transformation". In: *Sensors* 23.3 (Jan. 2023), p. 1191. ISSN: 1424-8220. DOI: 10.3390/s23031191.

[68] Jun S. Lee, Hyun Min Kim, Sung Il Kim, and Hyun Min Lee. "Evaluation of structural integrity of railway bridge using acceleration data and semi-supervised learning approach". In: *Engineering Structures* 239 (July 2021), p. 112330. ISSN: 0141-0296. DOI: 10.1016/j.engstruct.2021.112330.

[69] Pasquale Santaniello and Paolo Russo. "Bridge Damage Identification Using Deep Neural Networks on Time–Frequency Signals Representation". In: *Sensors* 23.13 (July 2023), p. 6152. DOI: 10.3390/s23136152.

[70] Hessam Amanollah, Arghavan Asghari, Mohammadreza Mashayekhi, and Seyed Mehdi Zahrai. "Damage detection of structures based on wavelet analysis using improved AlexNet". In: *Structures* 56 (Oct. 2023), p. 105019. ISSN: 2352-0124. DOI: 10.1016/j.istruc.2023.105019.

[71] Vicente J. Bolós and Rafael Benítez. "The Wavelet Scalogram in the Study of Time Series". In: *SEMA SIMAI Springer Series*. Springer International Publishing, 2014, pp. 147–154. ISBN: 9783319069531. DOI: 10.1007/978-3-319-06953-1_15.

[72] Rafael S. Salles and Paulo F. Ribeiro. "The use of deep learning and 2-D wavelet scalograms for power quality disturbances classification". In: *Electric Power Systems Research* 214 (Jan. 2023), p. 108834. ISSN: 0378-7796. DOI: 10.1016/j.epsr.2022.108834.

[73] Ahmed Silik, Mohammad Noori, Wael A. Altabey, and Ramin Ghiasi. "Selecting optimum levels of wavelet multi-resolution analysis for time-varying signals in structural health monitoring". In: *Structural Control and Health Monitoring* 28.8 (May 2021). ISSN: 1545-2263. DOI: 10.1002/stc.2762.

[74] Hongbing Li, Wenzhi Zhao, Hong Cao, Fengchang Yao, and Longyi Shao. "Measures of scale based on the wavelet scalogram with applications to seismic attenuation". In: *GEOPHYSICS* 71.5 (Sept. 2006), pp. V111–V118. ISSN: 1942-2156. DOI: 10.1190/1.2211529.

[75] Z. PENG, F. CHU, and Y. HE. “VIBRATION SIGNAL ANALYSIS AND FEATURE EXTRACTION BASED ON REASSIGNED WAVELET SCALOGRAM”. In: *Journal of Sound and Vibration* 253.5 (June 2002), pp. 1087–1100. ISSN: 0022-460X. DOI: 10.1006/jsvi.2001.4085.

[76] Duc C. Nguyen, Marek Salamak, and Andrzej Katunin. “Application of low-cost web-based wireless structural health monitoring RASP systems for bridge structures”. In: *Young Science Beyond Borders*. 2023, p. 24. ISBN: 978-83-66847-73-6.

[77] Stphane Mallat. *A Wavelet Tour of Signal Processing, Third Edition: The Sparse Way*. Elsevier, 2009. ISBN: 9780123743701. DOI: 10.1016/b978-0-12-374370-1.x0001-8.

[78] Foad Shiri and Behnam Mohammadi-ivatloo. “Identification of inter-area oscillations using wavelet transform and phasor measurement unit data”. In: *International Transactions on Electrical Energy Systems* 25.11 (Oct. 2014), pp. 2831–2846. DOI: 10.1002/etep.1994.

[79] Jonathan M. Lilly. “Element analysis: a wavelet-based method for analysing time-localized events in noisy time series”. In: *Proceedings of the Royal Society A: Mathematical, Physical and Engineering Sciences* 473.2200 (Apr. 2017), p. 20160776. DOI: 10.1098/rspa.2016.0776.

[80] Andrzej Katunin. “Damage identification in composite plates using two-dimensional B-spline wavelets”. In: *Mechanical Systems and Signal Processing* 25.8 (Nov. 2011), pp. 3153–3167. ISSN: 0888-3270. DOI: 10.1016/j.ymssp.2011.05.015.

[81] J. M. Lilly and S. C. Olhede. “Generalized Morse Wavelets as a Superfamily of Analytic Wavelets”. In: *IEEE Transactions on Signal Processing* 60.11 (Nov. 2012), pp. 6036–6041. DOI: 10.1109/tsp.2012.2210890.

[82] Erick Axel Martinez-Rios, Rogelio Bustamante-Bello, Sergio Navarro-Tuch, and Hector Perez-Meana. “Applications of the Generalized Morse Wavelets: A Review”. In: *IEEE Access* 11 (2023), pp. 667–688. DOI: 10.1109/access.2022.3232729.

[83] J.M. Lilly and S.C. Olhede. “Higher-Order Properties of Analytic Wavelets”. In: *IEEE Transactions on Signal Processing* 57.1 (Jan. 2009), pp. 146–160. DOI: 10.1109/tsp.2008.2007607.

[84] Shyh-Jier Huang, Cheng-Tao Hsieh, and Ching-Lien Huang. “Application of Morlet wavelets to supervise power system disturbances”. In: *IEEE Transactions on Power Delivery* 14.1 (1999), pp. 235–243. DOI: 10.1109/61.736728.

[85] Hui Li. "Complex Morlet wavelet amplitude and phase map based bearing fault diagnosis". In: *2010 8th World Congress on Intelligent Control and Automation*. 2010, pp. 6923–6926. DOI: 10.1109/WCICA.2010.5554232.

[86] Lin Li, Haiyan Cai, and Qingtang Jiang. "Adaptive synchrosqueezing transform with a time-varying parameter for non-stationary signal separation". In: *Applied and Computational Harmonic Analysis* 49.3 (Nov. 2020), pp. 1075–1106. DOI: 10.1016/j.acha.2019.06.002.

[87] Rafia Nishat Toma, Farzana Haque Toma, and Jong-Myon Kim. "Comparative Analysis of Continuous Wavelet Transforms on Vibration signal in Bearing Fault Diagnosis of Induction Motor". In: *2021 International Conference on Electronics, Communications and Information Technology (ICECIT)*. 2021, pp. 1–4. DOI: 10.1109/ICECIT54077.2021.9641199.

[88] Mariette Awad and Rahul Khanna. "Deep Neural Networks". In: *Efficient Learning Machines*. Apress, 2015, pp. 127–147. DOI: 10.1007/978-1-4302-5990-9_7.

[89] Iqbal H. Sarker. "Deep Learning: A Comprehensive Overview on Techniques, Taxonomy, Applications and Research Directions". In: *SN Computer Science* 2.6 (Aug. 2021). DOI: 10.1007/s42979-021-00815-1.

[90] Xu Han, Huoyue Xiang, Yongle Li, and Yichao Wang. "Predictions of vertical train-bridge response using artificial neural network-based surrogate model". In: *Advances in Structural Engineering* 22.12 (May 2019), pp. 2712–2723. DOI: 10.1177/1369433219849809.

[91] Zaharah Allah Bukhsh, Irina Stipanovic, Aaqib Saeed, and Andre G. Doree. "Maintenance intervention predictions using entity-embedding neural networks". In: *Automation in Construction* 116 (Aug. 2020), p. 103202. DOI: 10.1016/j.autcon.2020.103202.

[92] Pengyong Miao. "Prediction-Based Maintenance of Existing Bridges Using Neural Network and Sensitivity Analysis". In: *Advances in Civil Engineering* 2021 (July 2021). Ed. by Pengfei Liu, pp. 1–17. DOI: 10.1155/2021/4598337.

[93] Essam Althaqafi and Eddie Chou. "Developing Bridge Deterioration Models Using an Artificial Neural Network". In: *Infrastructures* 7.8 (July 2022), p. 101. DOI: 10.3390/infrastructures7080101.

[94] Osval Antonio Montesinos López, Abelardo Montesinos López, and Jose Crossa. "Fundamentals of Artificial Neural Networks and Deep Learning". In: *Multivariate Statistical Machine Learning Methods for Genomic Prediction*. Springer International Publishing, 2022, pp. 379–425. DOI: 10.1007/978-3-030-89010-0_10.

[95] Shuling Hu, Wei Wang, and Yongchang Lu. "Explainable machine learning models for probabilistic buckling stress prediction of steel shear panel dampers". In: *Engineering Structures* 288 (Aug. 2023), p. 116235. ISSN: 0141-0296. DOI: 10.1016/j.engstruct.2023.116235.

[96] Tarun Kumar Gupta and Khalid Raza. "Optimization of ANN Architecture: A Review on Nature-Inspired Techniques". In: *Machine Learning in Bio-Signal Analysis and Diagnostic Imaging*. Elsevier, 2019, pp. 159–182. DOI: 10.1016/b978-0-12-816086-2.00007-2.

[97] Imran Shafi, Jamil Ahmad, Syed Ismail Shah, and Faisal M Kashif. "Impact of Varying Neurons and Hidden Layers in Neural Network Architecture for a Time Frequency Application". In: *2006 IEEE International Multitopic Conference*. IEEE, Dec. 2006, pp. 188–193. DOI: 10.1109/inmic.2006.358160.

[98] Kanendra Naidu, Mohd Syukri Ali, Ab Halim Abu Bakar, Chia Kwang Tan, Hamzah Arof, and Hazlie Mokhlis. "Optimized artificial neural network to improve the accuracy of estimated fault impedances and distances for underground distribution system". In: *PLOS ONE* 15.1 (Jan. 2020). Ed. by Paweł Pławiak, e0227494. DOI: 10.1371/journal.pone.0227494.

[99] Marcio Carvalho and Teresa B. Ludermir. "Particle Swarm Optimization of Neural Network Architectures and Weights". In: *7th International Conference on Hybrid Intelligent Systems (HIS 2007)*. IEEE, Sept. 2007, pp. 336–339. DOI: 10.1109/his.2007.45.

[100] Lydia Bouzar-Benlabiod, Stuart H. Rubin, and Amel Benaida. "Optimizing Deep Neural Network Architectures: an overview". In: *2021 IEEE 22nd International Conference on Information Reuse and Integration for Data Science (IRI)*. IEEE, Aug. 2021, pp. 25–32. DOI: 10.1109/iri51335.2021.00010.

[101] Razan Jamous, Hosam ALRahhal, and Mohamed El-Darieby. "Neural Network Architecture Selection Using Particle Swarm Optimization Technique". In: *Applied Artificial Intelligence* 35.15 (Nov. 2021), pp. 1219–1236. DOI: 10.1080/08839514.2021.1972251.

[102] Alan J Thomas, Miltos Petridis, Simon D Walters, Saeed Malekshahi Gheytassi, and Robert E Morgan. "On Predicting the Optimal Number of Hidden Nodes". In: *2015 International Conference on Computational Science and Computational Intelligence (CSCI)*. IEEE, Dec. 2015, pp. 565–570. DOI: 10.1109/csci.2015.33.

[103] Radosław Winiczenko, Krzysztof Górnicki, Agnieszka Kaleta, and Monika Janaszek-Mańkowska. "Optimisation of ANN topology for predicting the rehydrated apple cubes colour change using RSM and GA". In: *Neural Computing and Applications* 30.6 (Dec. 2016), pp. 1795–1809. DOI: 10.1007/s00521-016-2801-y.

[104] Hai-Bang Ly, May Huu Nguyen, and Binh Thai Pham. "Metaheuristic optimization of Levenberg–Marquardt-based artificial neural network using particle swarm optimization for prediction of foamed concrete compressive strength". In: *Neural Computing and Applications* 33.24 (Aug. 2021), pp. 17331–17351. DOI: 10.1007/s00521-021-06321-y.

[105] Tuan Anh Pham, Van Quan Tran, and Huong-Lan Thi Vu. "Evolution of Deep Neural Network Architecture Using Particle Swarm Optimization to Improve the Performance in Determining the Friction Angle of Soil". In: *Mathematical Problems in Engineering* 2021 (May 2021). Ed. by Venkatesan Rajinikanth, pp. 1–17. DOI: 10.1155/2021/5570945.

[106] Donald W. Marquardt. "An Algorithm for Least-Squares Estimation of Nonlinear Parameters". In: *Journal of the Society for Industrial and Applied Mathematics* 11.2 (June 1963), pp. 431–441. DOI: 10.1137/0111030.

[107] M.T. Hagan and M.B. Menhaj. "Training feedforward networks with the Marquardt algorithm". In: *IEEE Transactions on Neural Networks* 5.6 (1994), pp. 989–993. DOI: 10.1109/72.329697.

[108] Nazmul Siddique and Hojjat Adeli. *Computational Intelligence*. John Wiley & Sons Ltd, May 2013. DOI: 10.1002/9781118534823.

[109] Sk. F. Ali and A. Ramaswamy. "Benchmark Control Problem for Highway Bridge Based on FLC". In: *Structures Congress 2006*. American Society of Civil Engineers, Oct. 2006, pp. 1–8. DOI: 10.1061/40889(201)91.

[110] Ying-Ming Wang and Taha M.S. Elhag. "An adaptive neuro-fuzzy inference system for bridge risk assessment". In: *Expert Systems with Applications* 34.4 (2008), pp. 3099–3106. ISSN: 0957-4174. DOI: 10.1016/j.eswa.2007.06.026.

[111] Ashraf A. A. Beshr and Fawzi H. Zarzoura. “Using artificial neural networks for GNSS observations analysis and displacement prediction of suspension highway bridge”. In: *Innovative Infrastructure Solutions* 6.2 (Mar. 2021). DOI: 10.1007/s41062-021-00458-4.

[112] James C. Bezdek. *Pattern Recognition with Fuzzy Objective Function Algorithms*. Springer US, 1981. DOI: 10.1007/978-1-4757-0450-1.

[113] Leo Breiman. “Random Forests”. In: *Machine Learning* 45.1 (Oct. 2001), pp. 5–32. ISSN: 1573-0565. DOI: 10.1023/A:1010933404324.

[114] Leo Breiman. “Bagging predictors”. In: *Machine Learning* 24.2 (Aug. 1996), pp. 123–140. DOI: 10.1007/bf00058655.

[115] Ulrike Grömping. “Variable Importance Assessment in Regression: Linear Regression versus Random Forest”. In: *The American Statistician* 63.4 (Nov. 2009), pp. 308–319. DOI: 10.1198/tast.2009.08199.

[116] Kellie J. Archer and Ryan V. Kimes. “Empirical characterization of random forest variable importance measures”. In: *Computational Statistics & Data Analysis* 52.4 (Jan. 2008), pp. 2249–2260. DOI: 10.1016/j.csda.2007.08.015.

[117] Wei-Yin Loh. “Classification and regression trees”. In: *WIREs Data Mining and Knowledge Discovery* 1.1 (Jan. 2011), pp. 14–23. DOI: 10.1002/widm.8.

[118] Leo Breiman, Jerome H. Friedman, Richard A. Olshen, and Charles J. Stone. *Classification And Regression Trees*. Routledge, Oct. 2017. DOI: 10.1201/9781315139470.

[119] Mohammad Amin Morid, Olivia R. Liu Sheng, Kensaku Kawamoto, and Samir Abdelrahman. “Learning hidden patterns from patient multivariate time series data using convolutional neural networks: A case study of healthcare cost prediction”. In: *Journal of Biomedical Informatics* 111 (Nov. 2020), p. 103565. DOI: 10.1016/j.jbi.2020.103565.

[120] Ashesh Chattopadhyay, Pedram Hassanzadeh, and Saba Pasha. “Predicting clustered weather patterns: A test case for applications of convolutional neural networks to spatio-temporal climate data”. In: *Scientific Reports* 10.1 (Jan. 2020). DOI: 10.1038/s41598-020-57897-9.

[121] Laith Alzubaidi, Jinglan Zhang, Amjad J. Humaidi, Ayad Al-Dujaili, Ye Duan, Omran Al-Shamma, J. Santamaría, Mohammed A. Fadhel, Muthana Al-Amidie, and Laith Farhan. "Review of deep learning: concepts, CNN architectures, challenges, applications, future directions". In: *Journal of Big Data* 8.1 (Mar. 2021). DOI: 10.1186/s40537-021-00444-8.

[122] Zewen Li, Fan Liu, Wenjie Yang, Shouheng Peng, and Jun Zhou. "A Survey of Convolutional Neural Networks: Analysis, Applications, and Prospects". In: *IEEE Transactions on Neural Networks and Learning Systems* 33.12 (Dec. 2022), pp. 6999–7019. DOI: 10.1109/tnnls.2021.3084827.

[123] Osama Abdeljaber, Onur Avci, Serkan Kiranyaz, Moncef Gabbouj, and Daniel J. Inman. "Real-time vibration-based structural damage detection using one-dimensional convolutional neural networks". In: *Journal of Sound and Vibration* 388 (Feb. 2017), pp. 154–170. DOI: 10.1016/j.jsv.2016.10.043.

[124] Ruhua Wang, Jun Li, Chencho, Senjian An, Hong Hao, Wanquan Liu, and Ling Li. "Densely connected convolutional networks for vibration based structural damage identification". In: *Engineering Structures* 245 (Oct. 2021), p. 112871. DOI: 10.1016/j.engstruct.2021.112871.

[125] Osama Alazzawi and Dansheng Wang. "A novel structural damage identification method based on the acceleration responses under ambient vibration and an optimized deep residual algorithm". In: *Structural Health Monitoring* 21.6 (Jan. 2022), pp. 2587–2617. DOI: 10.1177/14759217211065009.

[126] Christian Szegedy, Wei Liu, Yangqing Jia, Pierre Sermanet, Scott Reed, Dragomir Anguelov, Dumitru Erhan, Vincent Vanhoucke, and Andrew Rabinovich. "Going deeper with convolutions". In: *2015 IEEE Conference on Computer Vision and Pattern Recognition (CVPR)*. 2015, pp. 1–9. DOI: 10.1109/CVPR.2015.7298594.

[127] Shuying Liu and Weihong Deng. "Very deep convolutional neural network based image classification using small training sample size". In: *2015 3rd IAPR Asian Conference on Pattern Recognition (ACPR)*. 2015, pp. 730–734. DOI: 10.1109/ACPR.2015.7486599.

[128] Alex Krizhevsky, Ilya Sutskever, and Geoffrey E. Hinton. "ImageNet classification with deep convolutional neural networks". In: *Communications of the ACM* 60.6 (May 2017), pp. 84–90. DOI: 10.1145/3065386.

[129] Gao Huang, Zhuang Liu, Laurens Van Der Maaten, and Kilian Q. Weinberger. "Densely Connected Convolutional Networks". In: *2017 IEEE Conference on Computer Vision and Pattern Recognition (CVPR)*. 2017, pp. 2261–2269. DOI: 10.1109/CVPR.2017.243.

[130] Donya Hajializadeh. "Deep learning-based indirect bridge damage identification system". In: *Structural Health Monitoring* 22.2 (May 2022), pp. 897–912. DOI: 10.1177/14759217221087147.

[131] Pauline Ong, Yean Keong Tan, Kee Huong Lai, and Chee Kiong Sia. "A deep convolutional neural network for vibration-based health-monitoring of rotating machinery". In: *Decision Analytics Journal* 7 (June 2023), p. 100219. ISSN: 2772-6622. DOI: 10.1016/j.dajour.2023.100219.

[132] Ali Mirzazade, Cosmin Popescu, Jaime Gonzalez-Libreros, Thomas Blanksvärd, Björn Täljsten, and Gabriel Sas. "Semi-autonomous inspection for concrete structures using digital models and a hybrid approach based on deep learning and photogrammetry". In: *Journal of Civil Structural Health Monitoring* 13.8 (Jan. 2023), pp. 1633–1652. ISSN: 2190-5479. DOI: 10.1007/s13349-023-00680-x.

[133] Myungyon Kim, Joon Ha Jung, Jin Uk Ko, Hyeon Bae Kong, Jinwook Lee, and Byeng Dong Youn. "Direct Connection-Based Convolutional Neural Network (DC-CNN) for Fault Diagnosis of Rotor Systems". In: *IEEE Access* 8 (2020), pp. 172043–172056. ISSN: 2169-3536. DOI: 10.1109/access.2020.3024544.

[134] Sheng Shen, Hao Lu, Mohammadkazem Sadoughi, Chao Hu, Venkat Nemani, Adam Thelen, Keith Webster, Matthew Darr, Jeff Sidon, and Shawn Kenny. "A physics-informed deep learning approach for bearing fault detection". In: *Engineering Applications of Artificial Intelligence* 103 (Aug. 2021), p. 104295. ISSN: 0952-1976. DOI: 10.1016/j.engappai.2021.104295.

[135] Sadeq Kord, Touraj Taghikhany, and Mohammad Akbari. "A novel spatiotemporal 3D CNN framework with multi-task learning for efficient structural damage detection". In: *Structural Health Monitoring* (Nov. 2023). ISSN: 1741-3168. DOI: 10.1177/14759217231206178.

[136] Maikel Kerkhof, Lichao Wu, Guilherme Perin, and Stjepan Picek. "No (good) loss no gain: systematic evaluation of loss functions in deep learning-based side-channel analysis". In: *Journal of Cryptographic Engineering* 13.3 (May 2023), pp. 311–324. ISSN: 2190-8516. DOI: 10.1007/s13389-023-00320-6.

[137] Ruihua Liang, Weifeng Liu, Sakdirat Kaewunruen, Hougui Zhang, and Zongzhen Wu. "Classification of External Vibration Sources through Data-Driven Models Using Hybrid CNNs and LSTMs". In: *Structural Control and Health Monitoring* 2023 (Mar. 2023). Ed. by Fabio Casciati, pp. 1–18. ISSN: 1545-2255. DOI: 10.1155/2023/1900447.

[138] Jake Lever, Martin Krzywinski, and Naomi Altman. "Classification evaluation". In: *Nature Methods* 13.8 (July 2016), pp. 603–604. DOI: 10.1038/nmeth.3945.

[139] Peter Flach. "Performance Evaluation in Machine Learning: The Good, the Bad, the Ugly, and the Way Forward". In: *Proceedings of the AAAI Conference on Artificial Intelligence* 33.01 (July 2019), pp. 9808–9814. DOI: 10.1609/aaai.v33i01.33019808.

[140] Wentao Zhang, Ting Zhang, Guohua Cui, and Ying Pan. "Intelligent Machine Fault Diagnosis Using Convolutional Neural Networks and Transfer Learning". In: *IEEE Access* 10 (2022), pp. 50959–50973. ISSN: 2169-3536. DOI: 10.1109/access.2022.3173444.

[141] Steven A. Hicks, Inga Strümke, Vajira Thambawita, Malek Hammou, Michael A. Riegler, Pål Halvorsen, and Sravanthi Parasa. "On evaluation metrics for medical applications of artificial intelligence". In: *Scientific Reports* 12.1 (Apr. 2022). DOI: 10.1038/s41598-022-09954-8.

[142] Fangyu Liu, Zhoujing Ye, and Linbing Wang. "Deep transfer learning-based vehicle classification by asphalt pavement vibration". In: *Construction and Building Materials* 342 (Aug. 2022), p. 127997. ISSN: 0950-0618. DOI: 10.1016/j.conbuildmat.2022.127997.

[143] Saeid Talaei, Xinqun Zhu, Jianchun Li, Yang Yu, and Tommy H.T. Chan. "Transfer learning based bridge damage detection: Leveraging time-frequency features". In: *Structures* 57 (Nov. 2023), p. 105052. ISSN: 2352-0124. DOI: 10.1016/j.istruc.2023.105052.

[144] D G Altman and J M Bland. "Statistics Notes: Diagnostic tests 1: sensitivity and specificity". In: *BMJ* 308.6943 (June 1994), pp. 1552–1552. DOI: 10.1136/bmj.308.6943.1552.

[145] Krishna Garkal, Dr. N.B. Chaphalkar, and Dr. Sayali Sandbhor. "Bridge Construction Cost Prediction using Multiple Linear Regression". In: *International Journal of Innovative Technology and Exploring Engineering* 8.9 (July 2019), pp. 3115–3121. ISSN: 2278-3075. DOI: 10.35940/ijitee.i8916.078919.

[146] Dario Fernandez Castellon, Aksel Fenerci, and Ole Øiseth. "A comparative study of wind-induced dynamic response models of long-span bridges using artificial neural networks, support vector regression and buffeting theory". In: *Journal of Wind Engineering and Industrial Aerodynamics* 209 (Feb. 2021), p. 104484. DOI: 10.1016/j.jweia.2020.104484.

[147] Weiying Fan, Yao Chen, Jiaqiang Li, Yue Sun, Jian Feng, Hany Hassanin, and Pooya Sareh. "Machine learning applied to the design and inspection of reinforced concrete bridges: Resilient methods and emerging applications". In: *Structures* 33 (Oct. 2021), pp. 3954–3963. DOI: 10.1016/j.istruc.2021.06.110.

[148] Miljan Kovačević, Nenad Ivanišević, Dragan Stević, Ljiljana Milić Marković, Borko Bulajić, Ljubo Marković, and Nikola Gvozdović. "Decision-Support System for Estimating Resource Consumption in Bridge Construction Based on Machine Learning". In: *Axioms* 12.1 (Dec. 2022), p. 19. DOI: 10.3390/axioms12010019.

[149] Roman Trach, Victor Moshynskyi, Denys Chernyshev, Oleksandr Borysyuk, Yuliia Trach, Pavlo Striletskyi, and Volodymyr Tyvoniuk. "Modeling the Quantitative Assessment of the Condition of Bridge Components Made of Reinforced Concrete Using ANN". In: *Sustainability* 14.23 (Nov. 2022), p. 15779. DOI: 10.3390/su142315779.

[150] Huong-Giang Thi Hoang, Thuy-Anh Nguyen, Hoang-Long Nguyen, and Hai-Bang Ly. "Neural network approach for GO-modified asphalt properties estimation". In: *Case Studies in Construction Materials* 17 (Dec. 2022), e01617. DOI: 10.1016/j.cscm.2022.e01617.

[151] Van Quan Tran, Hai-Van Thi Mai, Thuy-Anh Nguyen, and Hai-Bang Ly. "Assessment of different machine learning techniques in predicting the compressive strength of self-compacting concrete". In: *Frontiers of Structural and Civil Engineering* 16.7 (July 2022), pp. 928–945. DOI: 10.1007/s11709-022-0837-x.

[152] Hai-Van Thi Mai, May Huu Nguyen, Son Hoang Trinh, and Hai-Bang Ly. "Toward improved prediction of recycled brick aggregate concrete compressive strength by designing ensemble machine learning models". In: *Construction and Building Materials* 369 (Mar. 2023), p. 130613. DOI: 10.1016/j.conbuildmat.2023.130613.

[153] K. W. Penrose, A. G. Nelson, and A. G. Fisher. "GENERALIZED BODY COMPOSITION PREDICTION EQUATION FOR MEN USING SIMPLE MEASUREMENT TECHNIQUES". In: *Medicine and Science in Sports and Exercise* 17.2 (Apr. 1985), p. 189. DOI: 10.1249/00005768-198504000-00037.

[154] Jörg Henseler, Christian M. Ringle, and Rudolf R. Sinkovics. "The use of partial least squares path modeling in international marketing". In: *Advances in International Marketing*. Emerald Group Publishing Limited, Jan. 2009, pp. 277–319. DOI: 10.1108/s1474-7979(2009)0000020014.

[155] Joe F. Hair, Christian M. Ringle, and Marko Sarstedt. "PLS-SEM: Indeed a Silver Bullet". In: *Journal of Marketing Theory and Practice* 19.2 (Apr. 2011), pp. 139–152. DOI: 10.2753/mtp1069-6679190202.

[156] Davide Chicco, Matthijs J. Warrens, and Giuseppe Jurman. "The coefficient of determination R-squared is more informative than SMAPE, MAE, MAPE, MSE and RMSE in regression analysis evaluation". In: *PeerJ Computer Science* 7 (July 2021), e623. DOI: 10.7717/peerj-cs.623.

[157] Juan José Montaño Moreno, Alfonso Palmer Pol, and Albert Sesé Abad. "Using the R-MAPE index as a resistant measure of forecast accuracy". In: *Psicothema* 25.4 (Nov. 2013), pp. 500–506. DOI: 10.7334/psicothema2013.23.

[158] Chompoonoot Kasemset, Nisachon Sae-Haew, and Apichat Sopadang. "Multiple Regression Model for Forecasting Quantity of Supply of Off-season Longan". In: *Chiang Mai University Journal of Natural Sciences* 13.3 (2014). DOI: 10.12982/cmujns.2014.0044.

[159] J.E. Nash and J.V. Sutcliffe. "River flow forecasting through conceptual models part I — A discussion of principles". In: *Journal of Hydrology* 10.3 (Apr. 1970), pp. 282–290. DOI: 10.1016/0022-1694(70)90255-6.

[160] D. N. Moriasi, J. G. Arnold, M. W. Van Liew, R. L. Bingner, R. D. Harmel, and T. L. Veith. "Model Evaluation Guidelines for Systematic Quantification of Accuracy in Watershed Simulations". In: *Transactions of the ASABE* 50.3 (2007), pp. 885–900. DOI: 10.13031/2013.23153.

[161] Nagireddy Masthan Reddy, Subbarayan Saravanan, and Devanantham Abijith. "Streamflow simulation using conceptual and neural network models in the Hemavathi sub-watershed, India". In: *Geosystems and Geoenvironment* 2.2 (May 2023), p. 100153. DOI: 10.1016/j.geogeo.2022.100153.

[162] Charles Gyamfi, Julius Ndambuki, and Ramadhan Salim. "Hydrological Responses to Land Use/Cover Changes in the Olifants Basin, South Africa". In: *Water* 8.12 (Dec. 2016), p. 588. DOI: 10.3390/w8120588.

[163] S. Verma, S. K. Mishra, and R. K. Verma. "Improved runoff curve numbers for a large number of watersheds of the USA". In: *Hydrological Sciences Journal* 65.16 (Nov. 2020), pp. 2658–2668. DOI: 10.1080/02626667.2020.1832676.

[164] You-Wu Wang, Yi-Qing Ni, and Su-Mei Wang. "Structural health monitoring of railway bridges using innovative sensing technologies and machine learning algorithms: a concise review". In: *Intelligent Transportation Infrastructure* 1 (2022). DOI: 10.1093/iti/liac009.

[165] Wen-Hwa Wu, Chien-Chou Chen, Arief Kusbiantoro, and Gwolong Lai. "Finite element model of a cable-stayed bridge updated with vibration measurements and its application to investigate the variation of modal frequencies in monitoring". In: *Structure and Infrastructure Engineering* (Oct. 2022), pp. 1–11. DOI: 10.1080/15732479.2022.2132517.

[166] Selcuk Bas, Chuan-Zhi Dong, Nurdan M. Apaydin, Alper Ilki, and F. Necati Catbas. "Hanger replacement influence on seismic response of suspension bridges: Implementation to the Bosphorus Bridge subjected to multi-support excitation". In: *Earthquake Engineering and Structural Dynamics* 49.14 (July 2020), pp. 1496–1518. ISSN: 1096-9845. DOI: 10.1002/eqe.3314.

[167] Hrishikesh D. Vinod. "Matrix Algebra Topics in Statistics and Economics Using R". In: *Handbook of Statistics*. Elsevier, 2014, pp. 143–176. DOI: 10.1016/b978-0-444-63431-3.00004-8.

[168] Patrick Schober, Christa Boer, and Lothar A. Schwarte. "Correlation Coefficients". In: *Anesthesia & Analgesia* 126.5 (May 2018), pp. 1763–1768. DOI: 10.1213/ane.0000000000002864.

[169] Lokeswara Reddy Poreddy, Manoj Kumar Pathapadu, Chereddy Navyatha, Jayaprakash Vemuri, and Rajaram Chenna. "Correlation analysis between ground motion parameters and seismic damage of buildings for near-field ground motions". In: *Natural Hazards Research* 2.3 (Sept. 2022), pp. 202–209. DOI: 10.1016/j.nhres.2022.08.002.

[170] BS EN. "PN-EN 1997-2: 2003, Eurocode 1: Actions on structures-Part 2: Traffic loads on bridges". In: *ICS*. 1991, pp. 93–040.

[171] Cezary Kraśkiewicz, Rafał Michalczyk, Karol Brzeziński, and Monika Płudowska. "Finite Element Modelling and Design Procedures for Verifications of Trackbed Structure". In: *Procedia Engineering* 111 (2015). XXIV R-S-P seminar, Theoretical Foundation of Civil Engineering (24RSP) (TFoCE 2015), pp. 462–469. ISSN: 1877-7058. DOI: 10.1016/j.proeng.2015.07.117.

[172] Haedong Jeong, Seungtae Park, Sunhee Woo, and Seungchul Lee. "Rotating Machinery Diagnostics Using Deep Learning on Orbit Plot Images". In: *Procedia Manufacturing* 5 (2016), pp. 1107–1118. ISSN: 2351-9789. DOI: 10.1016/j.promfg.2016.08.083.

[173] P. Pennacchi and A. Vania. "Diagnosis and Model Based Identification of a Coupling Misalignment". In: *Shock and Vibration* 12.4 (2005), pp. 293–308. ISSN: 1875-9203. DOI: 10.1155/2005/607319.

[174] Jie Wu, Quansheng Yan, Shiping Huang, Chao Zou, Jintu Zhong, and Weifeng Wang. "Finite Element Model Updating in Bridge Structures Using Kriging Model and Latin Hypercube Sampling Method". In: *Advances in Civil Engineering* 2018 (Dec. 2018), pp. 1–11. DOI: 10.1155/2018/8980756.

[175] Md Asjad Mokhtar, Ashish Kamalakar Darpe, and Kshitij Gupta. "Investigations on bending-torsional vibrations of rotor during rotor-stator rub using Lagrange multiplier method". In: *Journal of Sound and Vibration* 401 (Aug. 2017), pp. 94–113. ISSN: 0022-460X. DOI: 10.1016/j.jsv.2017.03.026.

[176] Akile Neşe Halilbeşe, Cong Zhang, and Osman Azmi Özsoysal. "Effect of Coupled Torsional and Transverse Vibrations of the Marine Propulsion Shaft System". In: *Journal of Marine Science and Application* 20.2 (June 2021), pp. 201–212. ISSN: 1993-5048. DOI: 10.1007/s11804-021-00205-2.

[177] Pingchao Yu, Li Hou, Ke Jiang, Zihan Jiang, and Xuanjun Tao. "Dynamic modeling and nonlinear analysis for lateral-torsional coupling vibration in an unbalanced rotor system". In: *Applied Mathematical Modelling* 126 (Feb. 2024), pp. 439–456. ISSN: 0307-904X. DOI: 10.1016/j.apm.2023.11.005.

[178] American Association of State Highway and Transportation Officials. *The manual for bridge evaluation*. 2018.

[179] American Association of State Highway and Transportation Officials. *LRFD Bridge design specifications*. 2014.

[180] Parisa Asadollahi, Yong Huang, and Jian Li. "Bayesian Finite Element Model Updating and Assessment of Cable-Stayed Bridges Using Wireless Sensor Data". In: *Sensors* 18.9 (Sept. 2018), p. 3057. DOI: 10.3390/s18093057.

[181] Claudio Bernuzzi and Benedetto Cordova. *Structural Steel Design to Eurocode 3 and AISC Specifications*. Wiley, Feb. 2016. DOI: 10.1002/9781118631201.

[182] Chris R. Hendy and Roger P. Johnson. *Designers' Guide to EN 1994-2 Eurocode 4: Design of Steel and Composite Structures*. Thomas Telford Publishing, 2006. DOI: 10.1680/dgte4.31616.

[183] Paweł Szeptyński and Leszek Mikulski. “Preliminary optimization technique in the design of steel girders according to Eurocode 3”. In: *Archives of Civil Engineering* vol. 69.No 1 (2023), pp. 71–89. DOI: 10.24425/ace.2023.144160.

[184] Bin Huang and Wen-Fu Zhang. “Overall buckling performance of high strength steel welded I-sections under combined axial compression and bending”. In: *Archives of Civil Engineering* vol. 68.No 3 (2022), pp. 369–384. DOI: 10.24425/ace.2022.141891.

Index

Appendix A

ANN and ANFIS regression models in MATLAB

A.1 ANFIS regression models

```
%%%%%%%% Main of ANFIS %%%%%%%%
% Author: Nguyen Cong Duc
% Email in Poland until September 2024: cong.nguyen@polsl.pl
% Email in Viet Nam: nguyencongduc@muce.edu.vn
clc;
clear;
close all;
% Results of Evaluation Metrics
Output_Metrics = fopen('Metrics_ANFIS.txt','w+');
% Results of Parameters of ANFIS
Output_Parameters = fopen('Parameters_ANFIS.txt','w+');
% Data sets of RMS accelerations
dataset = xlsread('RMS_Deck_Hangers.xlsx');
% Design data for input, output (targets), train and test
Inputs = dataset(:,:);
Targets = dataset(:,:);
TrainInputs = Inputs(:,:);
TrainTargets = Targets(:,:);
TestInputs = Inputs(:,:);
TestTargets = Targets(:,:);
```

```
% ANFIS Structure for Training
PARAMS = [200; 0; 0.01; 0.9;  1.1];
fun = ANFIS_Models(PARAMS, TrainInputs, TrainTargets,...
      TestInputs, TestTargets,...
      Inputs, Targets,...
      Output_Parameters, Output_Metrics);
%%%%%%%%%%%%%%%%%%%%%%%%%%%%%
function Error = ANFIS_Models(PARAMS, TrainInputs, TrainTargets,...
              TestInputs, TestTargets,...
              Inputs, Targets,...
              Output_Parameters, Output_Metrics)
% Setting the Parameters of FIS Generation Methods
nCluster = 15;
Exponent = 2;
MaxIt = 200;
MinImprovment = 1e-5;
DisplayInfo = true;
opt = genfisOptions('FCMClustering','NumClusters', nCluster,..
    'Exponent', Exponent,...
    'MaxNumIteration', MaxIt, 'MinImprovement',...
    MinImprovment, 'Verbose', DisplayInfo);
fis=genfis(TrainInputs,TrainTargets,opt);
% Training ANFIS Structure
MaxEpoch = PARAMS(1);
ErrorGoal = PARAMS(2);
InitialStepSize = PARAMS(3);
StepSizeDecreaseRate = PARAMS(4);
StepSizeIncreaseRate = PARAMS(5);
TrainOptions = [MaxEpoch ...
              ErrorGoal ...
              InitialStepSize ...
              StepSizeDecreaseRate ...
              StepSizeIncreaseRate];
DisplayInfo=true;
DisplayError=true;
DisplayStepSize=true;
```

```
DisplayFinalResult=true;
DisplayOptions=[DisplayInfo ...
                DisplayError ...
                DisplayStepSize ...
                DisplayFinalResult];
OptimizationMethod=1;
% 0: Backpropagation
% 1: Hybrid
fis = anfis([TrainInputs TrainTargets],fis,...
          TrainOptions,DisplayOptions,[],OptimizationMethod);

% Apply trained ANFIS to predict new data
Outputs = evalfis(fis,Inputs);
TrainOutputs = evalfis(fis,TrainInputs);
TestOutputs = evalfis(fis,TestInputs);

% Calculate Errors and Metrics
TrainErrors = TrainTargets-TrainOutputs;
TrainMSE = mean(TrainErrors.^2);
TrainRMSE = sqrt(TrainMSE);
TrainErrorMean = mean(TrainErrors);
TrainErrorSTD = std(TrainErrors);
TrainMAE = mae(TrainErrors);
TrainMAPE = mean(abs(TrainErrors)./TrainTargets)*100;
TrainNSE = 1-(sum((TrainOutputs-TrainTargets).^2)...
         /sum((TrainTargets-mean(TrainTargets)).^2))

TestErrors = TestTargets-TestOutputs;
TestMSE = mean(TestErrors.^2);
TestRMSE = sqrt(TestMSE);
TestErrorMean = mean(TestErrors);
TestErrorSTD = std(TestErrors);
TestMAE = mae(TestErrors);
TestMAPE = mean(abs(TestErrors)./TestTargets)*100;
TestNSE = 1-(sum((TestOutputs-TestTargets).^2)...
          /sum((TestTargets-mean(TestTargets)).^2))
```

```
93
94  R_Train = corrcoef(TrainTargets,TrainOutputs);
95  R_Train = R_Train(2,1);
96  R2_Train = corr(TrainTargets,TrainOutputs).^2;
97  R2_Test = corr(TestTargets,TestOutputs).^2;
98  R_Test = corrcoef(TestTargets,TestOutputs);
99  R_Test = R_Test(2,1);
100 Error = TestRMSE + TrainRMSE
101
102 % Print results of training and testing of regression models
103 fprintf(Output_Metrics,'%10.4f\t%10.4f\t%10.4f\t%10.4f\t...',...
104         Error,R2_Train, R2_Test,...
105         R_Train, R_Test, TrainRMSE, TestRMSE,...
106         TrainMAE, TestMAE, TrainMAPE, TestMAPE,...
107         TrainNSE, TestNSE, TrainMSE, TestMSE,...
108         TrainErrorMean, TestErrorMean,...
109         TrainErrorSTD, TestErrorSTD);
110 fprintf(Output_Metrics,'\n');
111
112 fprintf(Output_Parameters,'%d\t%10.4f\t%10.4f\t%10.4f\t%10.4f',...
113 MaxEpoch, ErrorGoal, InitialStepSize,...
114 StepSizeDecreaseRate, StepSizeIncreaseRate);
115 fprintf(Output_Parameters,'\n');
116
117 % Save the results
118 NTrain = size(TrainOutputs,1);
119 NTest  = size(TestOutputs,1);
120 NAll   = size(Outputs,1);
121
122 Results_Test  = fopen('output_TestANN.txt' ,'w+');
123 Results_Train = fopen('output_TrainANN.txt' ,'w+');
124 Results_All   = fopen('output_AllANN.txt' ,'w+');
125
126 for i = 1:NTrain
127     fprintf(Results_Train,'%10.4f\t%10.4f',...
128     TrainTargets(i), TrainOutputs(i));
```

```
129     fprintf(Results_Train,'\n');
130 end
131 
132 for i = 1:NTest
133     fprintf(Results_Test,'%10.4f\t%10.4f',...
134     TestTargets(i), TestOutputs(i));
135     fprintf(Results_Test,'\n');
136 end
137 
138 for i = 1:NAll
139     fprintf(Results_All,'%10.4f\t%10.4f',...
140     Targets(i), Outputs(i));
141     fprintf(Results_All,'\n');
142 end
143 
144 end
145 % End function of ANFIS_Models
```

A.2 Optimized ANN regression models

```
%%%%%%% Main of optimized ANN %%%%%%%%
% Author: Nguyen Cong Duc
% Email in Poland until September 2024: cong.nguyen@polsl.pl
% Email in Viet Nam: nguyencongduc@muce.edu.vn
clc;
clear;
close all;
% Data sets of RMS accelerations
dataset = xlsread('RMS_Deck_Hangers.xlsx');
% Design data for input, output (targets), train and test
Inputs = dataset(:,:);
Targets = dataset(:,:);
TrainInputs=Inputs(:,:);
TrainTargets=Targets(:,:);
TestInputs=Inputs(:,:);
TestTargets=Targets(:,:);

i = 3; % number of layers
files_metrics(i) = "output_metrics"+num2str(i)+ ".txt";
files_layers(i) = "output_layers"+num2str(i)+ ".txt";
Output_Metrics(i) = fopen(files_metrics(i),'w+');
Nvars_Layers(i) = fopen(files_layers(i),'w+');
NLayers = i;

Error = @(z)OptimizedANN(z, TrainInputs,TrainTargets,...
        TestInputs,TestTargets,...
        Inputs, Targets, Output_Metrics(i),...
        Nvars_Layers(i), NLayers);

lb = 1*ones(1,i); % lower limits: the number of hidden neurons
ub = 30*ones(1,i); % upper limits: the number of hidden neurons
Varsinteger = linspace(1, i, i);
nvars = i;
options = optimoptions("gamultiobj")
```

```
[x,fval] = gamultiobj(Error,nvars,[],[],[],...
        [],lb,ub,[], Varsinteger, options);

%%%%%%%%% Function of ANN_Models %%%%%%%%%
function Error = OptimizedANN(NNeurons, TrainInputs,...
                TrainTargets, TestInputs, TestTargets,...
                Inputs, Targets,...
                Output_Metrics, Nvars_Layers, NLayers)
net = newff(TrainInputs,TrainTargets,NNeutrons,...
      {'tansig', , ,}); % Noted: tansig for nonlinear issues

% Train network
net.trainparam.epochs=200;
net = train(net,TrainInputs,TrainTargets);
Outputs = sim(net,Inputs');
TrainOutputs = sim(net,TrainInputs);
TestOutputs = sim(net,TestInputs);

% Calculate Metrics
TrainErrors = TrainTargets-TrainOutputs;
TrainMSE = mean(TrainErrors.^2);
TrainRMSE = sqrt(TrainMSE);
TrainErrorMean = mean(TrainErrors);
TrainErrorSTD = std(TrainErrors);
TrainMAE = mae(TrainErrors);
TrainMAPE = mean(abs(TrainErrors)./TrainTargets)*100;
TrainNSE = 1-(sum((TrainOutputs-TrainTargets).^2)...
/sum((TrainTargets-mean(TrainTargets)).^2))

TestErrors = TestTargets-TestOutputs;
TestMSE = mean(TestErrors.^2);
TestRMSE = sqrt(TestMSE);
TestErrorMean = mean(TestErrors);
TestErrorSTD = std(TestErrors);
TestMAE = mae(TestErrors);
TestMAPE = mean(abs(TestErrors)./TestTargets)*100;
```

```
71 TestNSE = 1-(sum((TestOutputs-TestTargets).^2)...
72 /sum((TestTargets-mean(TestTargets)).^2))
73
74 R_Train = corrcoef(TrainTargets', TrainOutputs');
75 R_Train = R_Train(2,1)
76 R2_Train = corr(TrainTargets', TrainOutputs').^2
77 R2_Test = corr(TestTargets', TestOutputs').^2
78 R_Test = corrcoef(TestTargets', TestOutputs');
79 R_Test = R_Test(2,1)
80 Error = (TestRMSE+TrainRMSE)
81
82 % Print results of evaluation metrics of ANN models
83 fprintf(Output_Metrics,'%10.4f\t%10.4f\t%10.4f\t...\n',...
84       Error, R2_Train, R2_Test,...
85       R_Train, R_Test, TrainRMSE, TestRMSE,...
86       TrainMAE, TestMAE, TrainMAPE, TestMAPE,...
87       TrainNSE, TestNSE, TrainMSE, TestMSE, ...
88       TrainErrorMean, TestErrorMean,...
89       TrainErrorSTD, TestErrorSTD);
90
91 % Print results of the number of hidden layers with neurons
92 for i =1:NLayers
93     fprintf(Nvars_Layers,'%d', NNeurons(i));
94     fprintf(Nvars_Layers,'\t');
95 end
96 fprintf(Nvars_Layers,'\n');
97
98 end
```

Appendix B

Wavelet assisted CNN models in MATLAB

B.1 Wavelet-integrated CNN classification models

```
%%%% Wavelet-based CNN classification models %%%%
% Author: Nguyen Cong Duc
% Email in Poland until September 2024: cong.nguyen@polsl.pl
% Email in Viet Nam: nguyencongduc@muce.edu.vn
% Entering command ">experimentManager" used the outputs of
% this "Experiment_setup" function
% to call and edit the trainNetwork function
function [imdsTrain,layers,options] = Experiment_setup(params)
% Load Training Data
imdsTrain=imageDatastore("...\Folder_Wavelet_Images",...
        "IncludeSubfolders", true,"LabelSource","foldernames");
[imdsTrain,imdsValidation]=splitEachLabel(imdsTrain,0.7,...
                            "randomized");

% Define Network Architecture
numClasses = 2; % The number of labels
inputSize = [224 224 3]; % Size of wavelet-based images
augimdsTrain = augmentedImageDatastore(inputSize(1:2),imdsTrain);
augimdsValidation = augmentedImageDatastore(inputSize(1:2), ...
    imdsValidation);
net = googlenet;
layers = layerGraph(net);
```

```
newLearnableLayer = fullyConnectedLayer(numClasses, ...
    'Name','new_fc', ...
    'WeightLearnRateFactor',10, ...
    'BiasLearnRateFactor',10);
layers = replaceLayer(layers,'loss3-classifier',newLearnableLayer);
newClassLayer = classificationLayer('Name','new_classoutput');
layers = replaceLayer(layers,'output',newClassLayer);

% Specify Training Options
options = trainingOptions('adam', ...
    'MaxEpochs', 30, ...
    'Shuffle','every-epoch',...
    'MiniBatchSize',128, ...
    'ValidationData',augimdsValidation, ...
    'InitialLearnRate',0.001,...
    'ValidationFrequency',50);
end
```

B.2 Wavelet-integrated CNN regression models

```
%%%% Wavelet-based CNN Regression models %%%%
% Author: Nguyen Cong Duc
% Email in Poland until September 2024: cong.nguyen@polsl.pl
% Email in Viet Nam: nguyencongduc@muce.edu.vn
% Create File: "Wavelet_images.txt"
% Begining of File
% D:\...\RZp-2019_12_13_00_04_15.png    53.73
% D:\...\RZp-2019_12_13_01_58_09.png    52.8
% D:\...\RZp-2019_12_13_03_30_14.png    56.99
% D:\...\RZp-2019_12_13_05_14_15.png    46.95
% D:\...\RZp-2019_12_13_05_23_13.png    53.86
% D:\...\RZp-2019_12_13_05_40_11.png    49.66
% D:\...\RZp-2019_12_13_05_54_59.png    42.26
% D:\...\RZp-2019_12_13_05_58_16.png    46.71
% D:\...\RZp-2019_12_13_06_02_24.png    53.7
% D:\...\RZp-2019_12_13_06_36_18.png    46.73
% D:\...\RZp-2019_12_13_06_37_03.png    54.59
% D:\...\RZp-2019_12_13_06_43_46.png    53.67
% D:\...\RZp-2019_12_13_07_07_18.png    52.94
% D:\...\RZp-2019_12_13_07_15_34.png    49
% ....
% Ending of file
%%%%%%%%%%%%%%
clc, clearvars, close all
Whanger = readtable('Wavelet_images.txt','Delimiter','tab');

address_images= Whanger{:,1};
responses_sensors = Whanger{:,2};
images_responses = table(address_images, responses_sensors);
imds = imageDatastore(images_responses{:,1});

%%% Convert images into 4D array for input
images4DArray = readall(imds);
numofImages = numel(images4DArray);
```

```
[h,w,c] = size(images4DArray{1});
Xinput = zeros(h,w,c, numofImages);
for i=1:numofImages
    Xinput(:,:,:,i) = im2double(images4DArray{i});
end

%%% Data for output
Youtput = double(images_responses{:,2});

shuffledIndices = randperm(numofImages);
% Use 70% of the images for training.
numTrain = round(0.70 * numofImages);
trainingIdx = shuffledIndices(1:numTrain);
% Use 30% of the images for validation
valIdx = shuffledIndices(numTrain+1:end);

% All data sets
Alldata = Xinput(:,:,:,:);
YAll =  Youtput(:);

% Training data sets
XTrain = Xinput(:,:,:,trainingIdx);
YTrain = Youtput(trainingIdx);

% Testing data sets
XValidation = Xinput(:,:,:,valIdx);
YValidation = Youtput(valIdx);

% Run GoogLeNet architecture
net = googlenet;
layers = layerGraph(net);
layers = replaceLayer(layers,'data',...
         imageInputLayer([224 224 3],'Name','input'));
layers = replaceLayer(layers,'loss3-classifier',...
         fullyConnectedLayer(1));
layers = removeLayers(layers, 'output');
```

```
71 layers = replaceLayer(layers, 'prob',regressionLayer);
72
73 % Set up Parameters of GoogLeNet architecture
74 options = trainingOptions('adam', ...
75     'MaxEpochs',30, ...
76     'Plots','training-progress', ...
77     'ValidationFrequency',50, ...
78     'ValidationData',{XValidation,YValidation}, ...
79     'InitialLearnRate',0.001,...
80     'Verbose',false);
81
82 net = trainNetwork(XTrain,YTrain, layers,options);
83
84 % Print results
85 YPredictedTest = predict(net,XValidation);
86 YYTest = table(YValidation, YPredictedTest);
87 writetable(YYTest,'Output_Test.txt','Delimiter','tab',...
88            'WriteVariableNames', false)
89
90 YPredictedTrain = predict(net,XTrain);
91 YYTrain = table(YTrain, YPredictedTrain);
92 writetable(YYTrain,'Output_Train.txt','Delimiter','tab',...
93            'WriteVariableNames', false)
94
95 YPredictedAll = predict(net,Alldata);
96 YYAll = table(YAll, YPredictedAll);
97 writetable(YYAll,'Output_Alldata.txt','Delimiter','tab',...
98            'WriteVariableNames', false)
99 end
```

Appendix C

FE model updating in MATLAB/PYTHON and ANSYS/SOFISTIK

C.1 Interfacing MATLAB with ANSYS for FE model updating of Vietnamese bridges

```
%%%%%%%% Main of MATLAB and ANSYS %%%%%%%%
% Author: Nguyen Cong Duc
% Email in Poland until September 2024: cong.nguyen@polsl.pl
% Email in Viet Nam: nguyencongduc@muce.edu.vn
updated_variables = fopen('output_updated_variables.txt','w+');
responses_FEM = fopen('output_FEMresponses.txt','w+');
error = fopen('output_error.txt','w+');

% Input of FE modeling of bridge
inputFile = 'inputFEM.txt';

% Output temporary file (macro) of ANSYS APDL
outputFile = 'outputFEM.txt';

% Link and Path of ANSYS software
ansys_path= '"C:\Program Files\...\ansys\bin\winx64\MAPDL.exe"';

```

```
% Experimental structural responses
measured_responses = [, , , ];

% Objective Function with parameters
error = @(x)objectiveFunction(x, measured_responses,...
       inputFile, outputFile, updated_variables,...
       responses_FEM, error, ansys_path);

% Parameters/Variables with lower and upper limits
lb = [, , , ]; % lower limits
ub = [, , , ]; % upper limits
nvars =  ;     % the number of variables to update

% PSO method
options = optimoptions('particleswarm', 'SwarmSize', 1000,...
'HybridFcn',@fmincon);
[xn,fvaln,exitflagn,outputn] = particleswarm(error,nvars,...
                              lb,ub,options);
% GA method
options = optimoptions('ga');
[xn,fvaln,exitflagn,outputn] = ga(error,nvars,[],[],[],[],...
                               lb,ub,[],[],options);

fclose(updated_variables);
fclose(responses_FEM);
fclose(error);

%%%%%%%%%%%%% objective Function %%%%%%%%%%%%%
function error = objectiveFunction(measured_responses,...
       inputFile, outputFile, updated_variables,...
       responses_FEM, error, ansys_path)

Nm = length(measured_responses); % size of measured responses
d = length(updated_variables);  % size of parameters

% FEM from ANSYS APDL
```

```
54 computed_responses = updated_parameters(updated_variables,....
55                      inputFile, outputFile, ansys_path);
56
57 % Error between measurement and computation
58 for i =1:Nm
59     err(i) = ((measured_responses(i)-...
60     computed_responses(i))/measured_responses(i)).^2;
61 end
62 err =sum(err)
63
64 % Print updated variables of FE model
65 fprintf(updated_variables,'%10.5f   \n',...
66     [ , , , ]);
67 % Print structural responses from FE model in ANSYS software
68 fprintf(responses_FEM,'%10.5f   \n', [ , , , ]);
69 % Print error
70 fprintf(error,'%10.10f\n', err);
71
72 end
73
74 %%%%%%%%%%%%%% Editing new file to input ANSYS APDL %%%%%%%%%%%
75 function [computed_responses] = updated_parameters(...
76        updated_variables, inputFile,...
77        outputFile, ansys_path)
78
79 % For exmples, define parameters in new file in ANSYS APDL
80 Ec = updated_variables(1);
81 rhoc = updated_variables(2);
82 Es = updated_variables(3);
83 rhos = updated_variables(3);
84 numlines =    ; %Number of lines in the input file
85
86 % Clear output file
87 [fileID] = fopen(outputFile,'w');
88 fclose(fileID);
89
```

```
% Open and change 'Input File'
fileID = fopen(inputFile,'r');
for i=1:numlines
    tline = fgetl(fileID);
    Inp{i} = tline;
end
fclose(fileID);
Inp = Inp';

% For exmples, editing new file
Inp{ } = sprintf('Ec = %10.5f',Ec);
Inp{ } = sprintf('rhoc = %10.5f',rhoc);
Inp{ } = sprintf('Es = %10.5f', Es);
Inp{ } = sprintf('rhos = %10.5f', rhos);
fileID = fopen(inputFile,'w');
for i = 1:numel(Inp)
    fprintf(fileID,'%s\n', Inp{i});
end
fclose(fileID);

% Run ANSYS APDL / MAPDL
RunAnsysMAPDL(inputFile, ansys_path);

% Read results of computed responses from ANSYS software
Results_ANSYS = readtable(char(outputFile),'Delimiter','\t',...
                'ReadVariableNames',false);
df = str2num(char(Results_ANSYS{:,1}));
computed_responses = df;
end
```

```
!%%%%%%% Input of FE modeling of bridge
! inputFile = 'inputFEM.txt';
/CWD,'D:\FEModelUpdating'
/CLEAR
Ec = 25
rhoc = 2500
```

```
Es = 210
rhos = 7850
/prep7
K,1, 0,    0, 0
K,2, 4.35,  0, 0
K,3, 8.7,  0, 0
K,4, 13.05, 0, 0
K,5, 17.4,   0, 0
....
SOLVE
FINISH
/post1
...
*CFOPEN,outputFEM,txt,,
*VWRITE,PF(1,1),PF(1,2),PF(1,3),PF(1,4),PF(1,5),PF(1,6),PF(1,7)
(7(' ',E20.10))
*CFCLOS
```

C.2 Connecting MATLAB with SOFISTIK for FE model updating of Vietnamese bridges

```
%%%%%% Main of MATLAB and SOFISTIK %%%%%%%%
% Author: Nguyen Cong Duc
% Email in Poland until September 2024: cong.nguyen@polsl.pl
% Email in Viet Nam: nguyencongduc@muce.edu.vn

inputFile = 'input_FEM.dat';
outputerror = 'output_error.csv';
updated_variables = fopen('updated_variables.txt','w+');
updated_errors = fopen('updated_errors.txt','w+');

% Link and Path of SOFISTIK software
sofistik_path = "C:\Program Files\SOFiSTiK\*\sps.exe";

error = @(x)objectiveFunction(x, inputFile, outputerror,...
      sofistik_path, updated_variables, updated_errors);

% Parameters/Variables with lower and upper limits
lb = [, , , ]; % lower limits
ub = [, , , ]; % upper limits
nvars =  ;     % the number of variables to update

% PSO method
options = optimoptions('particleswarm');
[xn,fvaln,exitflagn,outputn] = particleswarm(error,nvars,...
                              lb,ub,options);
% GA method
options = optimoptions('ga');
[xn,fvaln,exitflagn,outputn] = ga(error,nvars,[],[],[],[],...
                               lb,ub,[],[],options);

end
%%%%%% Function to run and control SOFISTIK %%%%%%%%
```

```
function RunSOFISTIK(inputFile, sofistik_path)
cmd = sprintf('"%s" %s', sofistik_path, inputFile);
system(cmd);
end
```

```
!%%%%% FE model in SOFISTIK %%%%%%%%
! "input_FEM.dat"
! FE modeling of Bridge
#DEFINE Ec = 30
#DEFINE Es = 210
....
! Create text with error values for the objective function
let#err ((measured_responses - computed_responses)/...
measured_responses)^2
<TEXT,FILE=+output_error.csv>
#(#err,8.5),
</TEXT>
...
```

C.3 Integrating SOFISTIK and PYTHON for Dębica bridge FE model updating

```
#### Main of FE model updating: PYTHON and SOFISTIK ####
#### FE model of Railway steel arch brigde in Poland ####
# Author: Nguyen Cong Duc
# Email in Poland until September 2024: cong.nguyen@polsl.pl
# Email in Viet Nam: nguyencongduc@muce.edu.vn

import pandas as pd
import sys, subprocess
import numpy as np
import os
import pygad

#Update new parameters
def replace_lines(file_name, Es, rhos,  Ec, rhoc):
    with open(file_name) as file:
        lines = file.readlines()
    lines[6-1]= '#DEFINE Es='+str(Es)+"\n"
    lines[7-1]= '#DEFINE rhos='+str(rhos)+"\n"
    lines[8-1]= '#DEFINE Ec='+str(Ec)+"\n"
    lines[9-1]= '#DEFINE rhoc='+str(rhoc)+"\n"
    return lines

#Define the FE model
def FEMmodelUpdating(Es, rhos, Ec, rhoc):
    # replace file of FEM
    file_name = 'BridgeFEModeling.dat'
    lines = replace_lines(file_name, Es, rhos, Ec, rhoc)
    with open(file_name, "w") as file:
        for line in lines:
            file.write(line)
    #run SOFISTIK
    sofistik_path = '..../sps.exe'
```

```
33      subprocess.run([sofistik_path, file_name])
34      #read resutls
35      fc = pd.read_csv('outputupdating.csv', header=None)
36      #Numerical frequencies
37      fc1 = fc.values[0][0]    fc2 = fc.values[0][1]
38      fc3 = fc.values[0][2]    fc4 = fc.values[0][3]
39      #Error
40      error = fc.values[0][4]
41      return fc1, fc2, fc3, fc4, error
42
43 #Experimental frequencies
44 #fm1 = 2.0; fm2 = 2.95
45 #fm3 = 4.37; fm4 = 4.94
46 #Define the cost function
47 def fitness_function(x, y):
48      Es = x[0]
49      rhos = x[1]
50      Ec = x[2]
51      rhoc = x[3]
52      fem = FEMmodelUpdating(Es, rhos, Ec, rhoc)
53      fc= [fem[0], fem[1], fem[2], fem[3]]
54      error = fem[5]
55      fitness =  error
56      return fitness
57
58 # Set lower and upper variables for material properties
59 sa = 0.80 # lower
60 sb = 1.20 # upper or higher
61 gene_space = [{'low': 210*sa,   'high': 210*sb},
62               {'low': 7850*sa, 'high': 7850*sb},
63               {'low': 35*sa,   'high': 35*sb},
64               {'low': 2500*sa, 'high': 2500*sb}]
65
66 # Set parameters for optimization procedure
67 num_genes = 4
68 num_generations = 100
```

```
num_parents_mating = 5
sol_per_pop = 10
mutation_percent_genes = 10
mutation_type=None

# Run optimization process
ga_instance = pygad.GA(num_generations=num_generations,
            num_parents_mating=num_parents_mating,
            fitness_func=fitness_function,
            sol_per_pop=sol_per_pop,
            num_genes=num_genes,
            gene_space=gene_space,
            gene_type=[float, float, float, float],
            mutation_percent_genes=mutation_percent_genes,)
```

C.4 SOFISTIK FE modeling of Dębica bridge in Poland

```
! File of FE model: 'BridgeFEModeling.dat'
! Info Bridge: Debica Railway Steel Arch Bridge in Poland
! Author: Nguyen Cong Duc
! Email in Poland until September 2024: cong.nguyen@polsl.pl
! Email in Viet Nam: nguyencongduc@muce.edu.vn
#DEFINE Es=210    ! Elastic modulus of steel
#DEFINE rhos=7850 ! Density of steel
#DEFINE Ec=35     ! Elastic modulus of concrete
#DEFINE rhoc=2500 ! Density of concrete
...
...
...
!#!Chapter vibration analysis
+prog dyna urs:5
head natural frequencies
eige neig 20 type lanc lc 1001
...

!#!Chapter  results
+PROG TEMPLATE urs:6
HEAD Result Summary
let#pi 3.1415926535
let#nmodes 20

! Experimental natural frequencies from OMA
let#f1 2.0
let#f2 2.95
let#f3 4.37
let#f4 4.94

! Calculate numerical natural frequencies
loop#i #nmodes
@KEY 012 1001+#i
sto#omega(#i)  @(7)
```

```
let#fc(#i)    #omega(#i)/(2*#pi)
endloop

! Calculate error between measured and computed frequencies
let#error (ABS((#f1-#fc(1))/#f1)+ABS((#f2-#fc(4))/#f2)+ABS((#f3-#fc(6))/#f3

! Save file for frequencies after each step
<TEXT,FILE=+outputupdating.csv>
#(#fc(1),8.2), #(#fc(4),8.2), #(#fc(6),8.2),
#(#fc(7),8.2), #(#error,8.4)
</TEXT>

! Save file for all optimized parameters, frequenices and error
<TEXT,FILE=+outputdebica_parameters.csv>
$(Es), $(rhos), $(Ec), $(rhoc), #(#fc(1),8.2), #(#fc(4),8.2),
#(#fc(6),8.2), #(#fc(7),8.2), #(#error*100,8.2)
</TEXT>
...
```

NGUYEN CONG DUC

DOI: 0000-0002-3393-0197

E-mail : cong.nguyen@polsl.pl

Mobile : +48 739 537 650

A. Publications in the PhD thesis

A.1. Journal Articles

[1] **Duc C. Nguyen**, Marek Salamak, Andrzej Katunin, and Michael Gerges. "Finite Element Model Updating of RC Bridge Structure with Static Load Testing: A Case Study of Vietnamese ThiThac Bridge in Coastal and Marine Environment". In: *Sensors* 22.22 (2022). ISSN: 1424-8220. DOI: 10.3390/s22228884.

[2] **Duc C. Nguyen**, Marek Salamak, Andrzej Katunin, Grzegorz Poprawa, Piotr Przystałka, and Mateusz Hypki. "Vibration-based SHM of Dębica railway steel bridge with optimized ANN and ANFIS". In: *Journal of Constructional Steel Research* 215 (Apr. 2024), p. 108505. ISSN: 0143-974X. DOI: 10.1016/j.jcsr.2024.108505.

[3] **Duc C. Nguyen**, Marek Salamak, Andrzej Katunin, Michael Gerges, and Mohamed Abdel-Maguid. "Finite element model updating of steel-concrete composite bridge: A study case of the Ruri bridge in Vietnam". In: *Archives of Civil Engineering* vol. 69.No 3 (2023), pp. 425–443. DOI: 10.24425/ace.2023.146089.

A.2. Conference in Proceedings

[1] **Duc C. Nguyen**, Marek Salamak, Andrzej Katunin, and Grzegorz Poprawa. "Finite Element Model Updating of Steel Bridge Structure Using Vibration-Based Structural Health Monitoring System: A Case Study of Railway Steel Arch Bridge in Poland". In: *Experimental Vibration Analysis for Civil Engineering Structures*. Ed. by Maria Pina Limongelli, Pier Francesco Giordano, Said Quqa, Carmelo Gentile, and Alfredo Cigada. Vol. 433. Cham: Springer Nature Switzerland, 2023, pp. 371–380. ISBN: 978-3-031-39117-0. DOI: 10.1007/978-3-031-39117-0_38.

[2] **Duc C. Nguyen**, Marek Salamak, and Andrzej Katunin. "Finite element model updating of bridge structure using field structural testing: a case study of RC bridge". In: *4th International Conference on Health Monitoring of Civil & Maritime Structures. HeaMES 2023. Proceedings.12-13*. 2023, pp. 5–11. ISBN: 978-1-7394385-0-0.

[3] **Duc C. Nguyen**, Marek Salamak, and Andrzej Katunin. "Application of low-cost web-based wireless structural health monitoring RASP systems for bridge structures". In: *Young Science Beyond Borders*. 2023, p. 24. ISBN: 978-83-66847-73-6.

[4] **Duc C. Nguyen**, Marek Salamak, and Andrzej Katunin. “FE model updating using load test and Genetic Algorithm: A case study of Vietnamese SuoiMon Bridge with precast girders”. In: *13th Central European Congress on Concrete Engineering, fib CEB-FIP Poland and infraTEAM, Zakopane*. 2022. ISBN: 978-83-938649-7-3.

B. Other Publications

[1] Phuc Tran Van, Vu Le Hoang, **Duc Nguyen Cong**, and Tien Pham Ngoc. “Determination of Collapse Load of Engineering Structures using Iterative Node-based Smoothed Finite Element Analysis Method”. In: *IOP Conference Series: Materials Science and Engineering* 869.7 (June 2020), p. 072002. DOI: 10.1088/1757-899x/869/7/072002.

[2] L H Vu, **N C Duc**, L V Dong, D L Truong, N M T Anh, H Q Hung, and P V Hue. “Load Rating and Buckling of Circular Concrete-Filled Steel Tube (CFST): Simulation and Experiment”. In: *IOP Conference Series: Materials Science and Engineering* 371 (June 2018), p. 012032. DOI: 10.1088/1757-899x/371/1/012032.

[3] **Nguyen Cong Duc**, Huynh Quoc Hung, Phan Cong Ban, Tran Van Mot, Nguyen Cong Minh, Pham Bao Toan, and Ngo Kieu Nhi. “Low-Cost Vibration Measurement for Behavior of Small-Scale Steel Modeling using MEMS, Raspberry Pi-3 and Arduino Mega 2560”. In: *Proceedings of the XIV National Conference on Solid Mechanics,Vietnam Association of Mechanics and Tran Dai Nghia University (Ho Chi Minh City)* (July 2018).

[4] Huynh Quoc Hung, Le Van Dong, Tran Han Van, and **Duc Cong Nguyen**. “Technology approach for manufacturing of soil-cement bricks in rural countrysides of Vietnam”. In: *Vietnam Journal of Construction - Ministry of Construction Vietnam* (Sept. 2018).

[5] **Nguyen Cong Duc**, Huynh Quoc Hung, Tran Van Han, Tran Van Mot, Nguyen Cong Minh, Pham Bao Toan, and Ngo Kieu Nhi. “Development and Application of Structural Health Monitoring using Low-Cost MEMS and Arduino Nano Microcontroller Board”. In: *Vietnam Journal of Construction - Ministry of Construction Vietnam* (Sept. 2018).

[6] Dang Ngoc Tan, Pham Hoang Dung, Tran Van Mot, **Nguyen Cong Duc**, and Huynh Quoc Hung. “Experimental and Computational Approach on the Vibration Responses of GFRP Concrete Panels under Dynamic Forces”. In: *Vietnam Journal of Construction - Ministry of Construction Vietnam* (Dec. 2017).

[7] Huynh Quoc Hung, **Nguyen Cong Duc**, and Nguyen Minh Tuan Anh. “Bending behaviour of concrete beams reinforced with MMFX steel preventing the corrosion”. In: *Vietnam Journal of Construction - Ministry of Construction Vietnam* (Dec. 2017).

[8] **Nguyen Cong Duc**, Tran Van Mot, Nguyen Cong Minh, Pham Trung Thanh, and Quincy Nguyen. “Cracks and Joints Sealing and Filling Technologies in Portland Cement Concrete Pavements of Airports, Highways and Habors using Mastic Sealants”. In: *Vietnam Journal of Construction - Ministry of Construction Vietnam* (Dec. 2017).

[9] Nguyen Cong Minh, Tran Van Mot, Phan Cong Ban, and **Nguyen Cong Duc**. “Experimental investigation on the vibration characteristics of sandwich composite beam and panel under harmonic load using accelerometers and displacement sensors”. In: *Proceedings of the Vietnam national scientific conference on composite materials: Mechanics, Technology and Application, The Vietnam Society of Solid Mechanics (VSSM)* (July 2016).

[10] **Nguyen Cong Duc**, Tran Van Mot, Duong Le Truong, and Phan Cong Ban. “An experimental investigation of the displacement response on acceleration signal of single-span steel beam”. In: *VNU-HCM “Science and Technology Development” Journal* (Mar. 2015). URL: https://vjol.info.vn/index.php/JSTD/article/view/23458.

[11] **Nguyen Cong Duc**, Huynh Quoc Hung, Pham Bao Toan, and Ngo Kieu Nhi. “Optimization of Strain-Sensor Positions on Calibrated Finite-Element Modeling of Real Simple-Span Bridge using Principal Component Analysis”. In: *Conference of the 10th National Conference on Mechanics and 8th National Congress of The National Association for Mechanics at the Military Technical Academy(MTA) in Ha Noi capital Viet Nam* (Sept. 2017).

C. Reviewing for Journals

- From 2020-present: Journal of Structures (Q1)
- From 2019-present: Journal of Engineering Structures (Q1)
- From 2023-present: Journal of Shock and Vibration (Q3)
- From 2024-present: Journal of Scientific Reports (Q1)

D. Fundings, Awards & Scholarships

- 2020 - 2021: Polish language and culture course at Crakow University of Technology in Krakow city funded by the NAWA - Polish Government as part of bilateral agreements and cooperation with Vietnamese Government, under the grant No. PPN/FRC/2020/1/00034.
- 2020 and 2021 - 2024: PhD Scholarship at the Silesian University of Technology from the NAWA implements programs of academic exchange for students and scientists as part of bilateral agreements and cooperation with Vietnamese Government, under the grant No. BPN/FRC/2021/1/00048.
- 2020 - 2024: The Vietnamese Government's Grant No. 3416/QĐ-BGDĐT 04/11/2020; 4534/QĐ-BGDĐT 30/11/2021; Nr145/21-NG-LHS 21/6/2021.
- 6^{th} February 2023 (RN2.5610.5.2.2023): The pro-quality funding of Rector of Silesian University of Technology for publications in TOP10, under the grant No. 08/IDUB/2019/94.
- 1^{st} March 2023 (RN2.5610.14.35.2023): The pro-quality funding of Rector of Silesian University of Technology for publications in collaboration with foreign scientific author, under the SUT Rector's grant No. 08/IDUB/2019/94.
- 23^{th} October 2023 (RN2.5610.14.469.2023): The pro-quality funding of Rector of Silesian University of Technology for publications in collaboration with foreign scientific author, under the grant No. 08/IDUB/2019/94.
- 23^{th} April 2024 (RN2.5610.14.282.2024): The pro-quality funding of Rector of Silesian University of Technology for publications in collaboration with scientific discipline of mechanical engineering, under the grant No. 08/IDUB/2019/94.